1

TiO_2 Nanoparticles: Properties and Applications

Ozioma U. Akakuru[1], Zubair M. Iqbal[1,2], and Aiguo Wu[1]*

[1] Cixi Institute of Biomedical Engineering, CAS Key Laboratory of Magnetic Materials and Devices, & Key Laboratory of Additive Manufacturing Materials of Zhejiang Province, Ningbo Institute of Materials Technology and Engineering, Chinese Academy of Sciences, No. 1219 Zhongguan West Road, Ningbo 315201, P.R. China
[2] School of Materials Science and Engineering, Zhejiang Sci-Tech University, No.2 Road of Xiasha, Hangzhou, 310018, P.R. China

CHAPTER MENU

1.1 Introduction

The important discovery of ultraviolet (UV) light-mediated water splitting on titanium dioxide (TiO_2) surface by Fujishima and Honda [1] has promoted immense research on other applications of TiO_2 nanoparticles, particularly in nanobiotechnology and nanomedicine [2]. Undoubtedly, the past few decades have witnessed an exponential growth in nanoscience and nanotechnology research activities [3–5]. Nanoparticles have gained immense interest for both academic and industrial applications owing to the fact that the use of these nanoparticles with other materials has improved scientific discoveries and breakthroughs [6]. These advances have been aided by the fact that new chemical and physical properties of materials emerge on reduction of their sizes to the nanometer range and varying their shapes [7]. It has been reported that the specific surface area and the ratio of the surface to the volume of nanomaterials dramatically increase as their sizes decrease [8]. Interestingly, high surface area, a consequence of small particle size, is of benefit to TiO_2 nanoparticles, as the surface area-dependent interaction/reaction of TiO_2 nanoparticles devices and those of the contact media basically occurs at the surfaces or interfaces [7].

*Corresponding author: zubair@nimte.ac.cn, zubair@zstu.edu.cn

TiO_2 Nanoparticles: Applications in Nanobiotechnology and Nanomedicine,
First Edition. Edited by Aiguo Wu and Wenzhi Ren.

Interestingly, TiO_2 nanoparticles have been extensively studied owing to their low production costs, mechanical and chemical stabilities, thin film transparency, bio- and chemical inertness, hydrophilicity, high light conversion efficiency, and corrosion resistance [9, 10]. Based on these exceptional properties, TiO_2 nanoparticles have vast array of applications that include nanomedicine, nanobiotechnology, solar and electrochemical cells, wastewater treatment, food, soil remediation, gas sensing, cosmetics, plastics, paint and paper productions, hydrogen fuel generation, antiseptics and antibacterial compositions, self-cleaning devices, and printing inks [10, 11]. Extensive research has been recently conducted on the nanomedical application of TiO_2 nanoparticles in the domains of cancer therapy and imaging. These recent progresses in nanomedicine do not only depend on the TiO_2 nanoparticles themselves but also on their functionalization with other inorganic or organic compounds [12]. Specifically, TiO_2 nanoparticles combined with magnetic nanoparticles have been used as magnetic resonance imaging (MRI) contrast agents and inorganic photosensitizers for photodynamic therapy [13], nanocarriers in chemotherapy [12], and in the recently discovered hydrogenated black TiO_2 nanoparticles as efficient cancer photothermal therapeutic agents [14]. Their cancer therapeutic efficacy has been linked to their good biocompatibility, low cytotoxicity, and unique photocatalytic properties [15].

Some researchers recently opined that there are many other new applications for TiO_2 that are either under way or presently in pilot production [16]. These new applications may be uncovered sooner than expected, due to the US FDA approval of TiO_2 to be freely incorporated into numerous domestic products (dental pastes, non-parenteral medicines, tablets, and oral capsules), thereby dramatically increasing the production and availability of TiO_2 for various applications [17]. This chapter will therefore discuss the properties, synthesis, and applications of TiO_2 nanoparticles with respect to nanobiotechnology and nanomedicine.

1.2 Properties of TiO_2 Nanoparticles

The fascinating properties of TiO_2 nanoparticles have dramatically enhanced their applications in various aspects [18, 19]. For instance, their high light-conversion efficiencies have been exploited for the fabrication of energy devices [20]. Their chemical stability, thin film transparency, and low production costs are responsible for their utility as photocatalysts for various environmental remediation strategies such as wastewater treatment, air pollution, and soil viability improvement [9]. Recently, TiO_2 nanoparticles were applied for cancer photothermal therapy (PTT), exploiting their non-radiative recombination ability [14]. In the following subsections, specific properties of TiO_2 nanoparticles will be discussed in more detail.

1.2.1 Crystal Properties

Nanocrystalline TiO_2 exists in three major polymorphic forms, which include rutile, anatase, and brookite, based on the conditions of fabrication and post

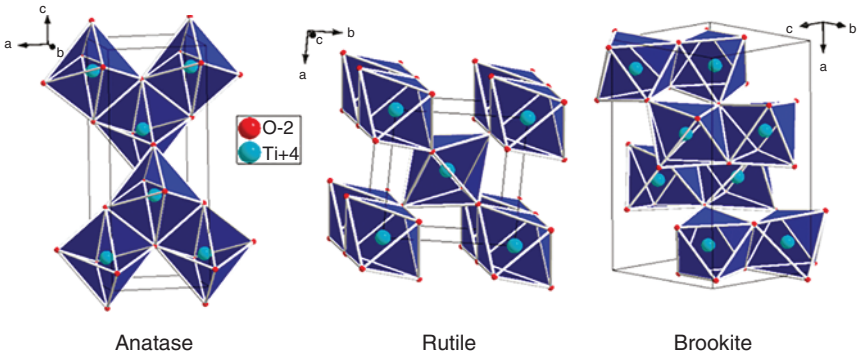

Figure 1.1 The crystal structures of anatase, rutile, brookite TiO_2 phases. Source: Adapted with permission from Dambournet et al. 2010 [27]. Copyright American Chemical Society.

fabrication heat treatment [21]. The fourth polymorphic form TiO_2(B) is quite uncommon [22]. Aside these four polymorphs, some researchers have reported the successful synthesis of two high-pressure phases from that of rutile: the TiO_2(II) that has the PbO_2-like structure [23] and the TiO_2(H) that structure looks more like a hollandite [24].

Both the anatase and rutile phases possess tetragonal crystal structures even though they do not belong to the same phase groups, while brookite has an orthorhombic structure and the uncommon TiO_2(B) phase is monoclinic [22, 25, 26]. As shown in Figure 1.1, the distortion of anatase phase octahedral structure is slightly larger than that of rutile [27]. It has been reported that even though the rutile phase is less stable than the anatase phase at 0 K, corresponding energy difference between these phases is rather small (about 2–10 kJ/mol). With respect to solar cell application, anatase phase TiO_2 is chosen over other phases as a result of its low density, high electron mobility, and low dielectric constant [22]. It is also attractive that in an anatase crystal, the reactivity of its (101) facets is much lower than that of its (001) facets [28].

As a consequence of the anatase phase low density, it easily undergoes transition to the rutile phase at high temperatures (usually around 450–1200 °C) [29]. This observed transformation is not only temperature dependent but is also affected by some other factors such as dopant concentration, initial phase, and particle size [30]. It has also been observed that both the brookite and anatase phases usually transform to the rutile phase at pre-determined particle sizes, wherein the rutile phase gains higher stability against the anatase phase at particles sizes that are greater than 14 nm [31]. Additionally, it has been reported that whenever the rutile phase is formed, it grows quicker in comparison to the anatase phase [22]. The crystal properties of TiO_2 are summarized in Table 1.1.

1.2.2 Optical Properties

The extensive use of TiO_2 nanoparticles in optical devices are attributed to their excellent mechanical durability, high transparency in the visible region, and chemical stability in aqueous medium [18]. Several other structural parameters

Table 1.1 The crystal properties of TiO_2 [20–22].

Properties	Anatase	Rutile	Brookite
Crystal structure	Tetragonal	Tetragonal	Orthorhombic
Density (g/cm^2)	3.894	4.250	4.120
Space group	$I4_1/amd$	$P4_2/mnm$	Pbca
Molecule (cell)	2	2	4
Lattice constant (Å)	$a = 3.784$ $b = 9.515$	$a = 4.594$ $b = 2.959$	$a = 9.184$ $b = 5.447$ $c = 5.154$
Ti—O bond length (Å)	1.937(4) 1.965(2)	1.949(4) 1.980(2)	1.87–2.04
O—Ti—O bond angle	77.7° 92.6°	81.2° 90.0°	77.0°–105.0°
Volume/molecule ($Å^3$)	34.061	31.216	32.172

such as phase composition, band gap, crystalline quality, size distribution, morphology, porosity, and particle size have been reported to influence the optical activities of TiO_2 nanoparticles [32]. Remarkably, decreasing the particle size of TiO_2 nanoparticles from 200 nm to smaller materials of about 10 nm or less changes the optical properties of these nanoparticles from opaque to transparent in the visible region of the light spectrum and subsequently to intriguing UV light blockers [33].

In pure TiO_2, the anatase phase shows superior catalytic ability and electron mobility than either the rutile or brookite phases, a property that is beneficial for photovoltaic and photocatalytic applications [20, 34]. The increased photoreactivity of the anatase phase has been linked to its low oxygen adsorption capacity, increased hydroxylation degree, and slightly higher Fermi level [20]. On the other hand, the rutile phase exhibits high refractive index and high optical absorptivity, which are responsible for its application in optical communication devices such as modulators, switches, and isolators [34].

On exposure of TiO_2 nanoparticles to UV light, the electrons in their valence bands (VB) gain energy and as such undergo excitation to corresponding conduction bands (CBs), thus generating holes (h^+) on those VBs (Figure 1.2). At this instance, the excited electrons (e^-) are purely in 3d states, and due to dissimilar parity, the probability for e^- transition is reduced, with attendant decrease in the e^-/h^+ recombination [22]. In this respect, the anatase phase is regarded as the active photocatalytic component that is also attributable to its chemical properties and the generation of charge carriers (e^- and h^+) that arise from its ability to absorb UV light, which is in correspondence with its band gap [35]. The rutile phase is generally regarded as a poor photocatalyst, due to the fact that the bulk recombination of h^+ and e^- takes place, whereby only the h^+ that are quite near to the surface are withheld and subsequently undergo surface transfer by the upward band bending [36]. These h^+ subsequently interact with the

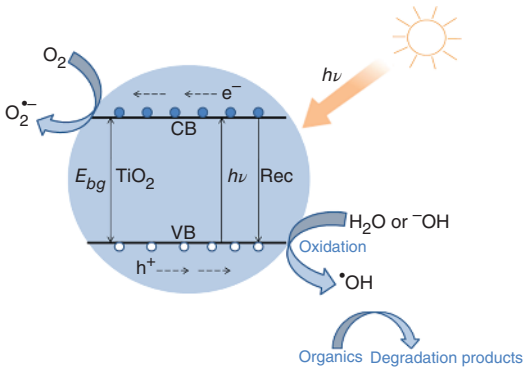

Figure 1.2 Illustration of the general mechanism of TiO_2 in solar photocatalysis process.

molecules of H_2O, thereby forming hydroxyl radicals ($OH^\bullet$) that in synergy with the h^+ effectively oxidize the organic compounds in their vicinity on the surface of the particles [35]. Also, the e^- in the CB interact with air molecular oxygen following a reduction reaction process, thereby producing superoxide radical anions ($O_2^{\bullet-}$) [36].

It is worthy of note that the charge couple (e^-/h^+) redox potential of an ideal photocatalyst is expected to fall within the domain of its band gap [37]. Additionally, the reduction activity of photoelectrons is determined by existence of energy level on the bottom of the CB of the photocatalyst, while the oxidation activity of photogenerated h^+ is a function of the energy level on top of the photocatalyst VB [22]. Based on these properties, TiO_2 nanoparticles are considered as near-ideal photocatalysts as their h^+ are redox selective and strongly oxidized, dramatically increasing more research into nano-sized TiO_2-based photocatalysts [37].

1.2.3 Electrochemical Properties

The chemical and physical properties of nano-TiO_2 are altered by their inherent electronic structure, size, shape, surface properties, and organization [38]. The electronic properties of TiO_2 nanoparticles have been reported as huge contributors to their particle- and crystal-size distributions [33]. TiO_2 in its pure form is a wide band gap n-type semiconductor that possesses indirect energy band gaps of the rutile, anatase, and brookite phases of 3.02, 3.2, and 2.96 eV, respectively [29, 39, 40]. It has also been reported that rutile Fermi level is lower than the anatase by ~0.1 eV [20]. Additionally, anatase has a smaller electron effective mass than rutile, resulting to an increase in mobility for the charge carriers in anatase, a characteristic that is highly favorable for optoelectronic devices production [20]. The TiO_2 CB consists of 3d orbitals of titanium, whereas its VB has 2p oxygen orbitals that form hybrids alongside 3d titanium orbitals [22].

The lattice oxygen sites in TiO_2 are very important with respect to the observed superhydrophilicity of TiO_2 nanoparticles, originating from the chemical conformation changes of their surfaces [41]. This is because some amounts of the trapped h^+ on the lattice sites of oxygen might interact with the TiO_2 specifically, thereby weakening the oxygen ions and lattice titanium bonds. As a consequence, H_2O molecules can interrupt these bonds resulting in the generation of new -OH

groups. These singly linked -OH groups are thermodynamically unstable and possess high surface energy, which leads to the generation of TiO_2 surface with superhydrophilicity [36, 41].

One of the observed disadvantages for the use of TiO_2 nanoparticles in photoelectrochemical devices is the large density of states that are involved in e^-/h^+ recombination and electron transfer reactions at the electrolyte–oxide interface, if located in the band gap [42]. On the other hand, this is an advantage for the adsorption of redox-active compounds on the surfaces of TiO_2 nanoparticles that is of special interest in dental implant applications [43]. For instance, serum proteins such as fibrinogen are reportedly chemisorbed by an electron transfer process on the surface of TiO_2 nanoparticles [42]. It was demonstrated that the electronic behavior of the TiO_2 nanoparticles affects the thrombogenicity of the fibrinogen due to the semiconducting property of fibrinogen, which is crucial in the blood coagulation pathway. It then follows that an alteration in the Fermi energy placement and/or band size of the TiO_2 nanoparticles could trigger a change in the adsorption and subsequent decomposition of the protein, since the band structure of the fibrinogen fits into that of the TiO_2 nanoparticles [42].

1.3 Synthesis of TiO_2 Nanoparticles

Numerous types of TiO_2 nanoparticles have been synthesized in the form of nanotubes, nanofibers, nanosheets, nanorods, and interconnected architectures [36, 44, 45]. The regularly employed synthesis methods are the hydrothermal, sol–gel, solvothermal, vapor deposition, oxidation, and the thermal decomposition methods. Other methods that have been used for the successful synthesis of various forms of TiO_2 nanoparticles include but not limited to sol, electrodeposition, sonochemical and microwave-assisted, and micelle and inverse micellar methods. For instance, in the micellar synthetic strategy, TiO_2 nanoparticles were prepared via the tetraisopropyl titanate hydrolysis in the presence of sodium bis (2-ethylhexyl) sulfosuccinate reverse micelles to obtain nanoparticles whose average size ranged from 20 to 200 nm [21]. Based on the micellar water pool, various TiO_2 phases were produced, wherein large pools afforded anatase and small pools afforded the amorphous nanoparticles. In the following subsections, some commonly used strategies for synthesizing TiO_2 nanoparticles are discussed in more detail.

1.3.1 The Hydrothermal Method

The hydrothermal synthetic method is usually conducted in steel pressure vessels, i.e. autoclaves with the Teflon liners under regulated pressure and temperature. This temperature can be increased from the boiling point of water up to saturation vapor pressure, but the pressure produced is also dependent on the amount of added solution [7]. Hydrothermal method has therefore been utilized by many researchers for the synthesis of TiO_2 nanoparticles [46–48]. In this regard, Dawson et al. synthesized TiO_2 nanoparticles by the hydrothermal method, wherein

they subjected various compositions and particle sizes of TiO_2 mixed powders to hydrothermal reaction in the presence of NaOH [49]. At 140 °C, trititanate nanotubes easily formed from the anatase phase of the starting material and at 170 °C, trititanate belts and plates formed from the rutile phase component. Increasing the reaction time to seven days exclusively converted all the TiO_2 to trititanate nanoplates and belts, without the formation of nanotubes. Hitherto, there is no clear description of the structure of TiO_2 nanotubes but researchers have assumed the existence of hydrogen titanate where the tubes are separated by hydrogen ions [2].

In a related experiment, pure rutile nanotubes with average diameters less than 20 nm were synthesized from rutile–anatase TiO_2 particles using the hydrothermal method in NaOH water–ethanol solution [50]. It was observed that the structure and morphology of the products depended on the type of alcohol, as well as the alcohol–water ratio. This was explained by the variation in optoelectronic behaviors of the rutile nanotubes and raw TiO_2. The hydrothermal method was also used to synthesize titanate nanotubes for the degradation of Acid Red 18 [51]. These researchers further calcined the nanotubes at various temperatures (400–700 °C) and observed that the nanotubes calcined at 600 °C were most active toward the Acid Red 18 decomposition. It was reported that the mechanism for the formation of TiO_2 nanotubes involved multilayered nanosheet wrapping, rather than the wrapping or scrolling of single-layered nanosheets, which is usually accompanied by the crystallization of successive layers [52]. Nano-sized TiO_2 has also been synthesized from commercial TiO_2 on a fluorine-doped tin oxide (FTO) substrate as shown in Figure 1.3a [53]. The reaction was carried out for 24 hours at 135 °C in a solution of NaOH, resulting in TiO_2 nanotubes with average diameter of 10–12 nm (Figure 1.3b,c).

In another study, nano-TiO_2 were obtained from titanium (IV) alkoxide in an acidified water–ethanol solution [47]. The dropwise addition of titanium tetraisopropoxide (TTIP) into the water–ethanol solution at pH 0.7, followed by a four hour reaction at 240 °C, yielded the TiO_2 nanoparticles dominated by the anatase phase. It was observed that tuning the solvent system and the Ti precursor was able to control the size of the as-synthesized nanoparticles to about 7–25 nm. Nanowires of TiO_2 have also been obtained by the hydrothermal method using white TiO_2 powders in 10–15 M NaOH at temperatures of about 150–200 °C without stirring in an autoclave for 24–72 hours [54]. Zhang and Gao treated $TiCl_4$ solution with an acid or organic salt for 12 hours at 33–423 °C to obtain TiO_2 nanorods [55]. They also reported that a change in the surfactant or the solvent composition could affect the morphology of the synthesized nanorods. The hydrothermal method was also employed by Chong et al. to synthesized TiO_2 nanofibers with average thickness of 40–100 nm [56]. The hydrothermal synthetic method was conducted in the presence of NaOH and an ion-exchange post-synthesis in a solution of HCl. Specifically, the researchers reacted 3 g anatase TiO_2 in 10 M NaOH (80 ml), followed by autoclaving for 48 hours at 180 °C in a poly-tetrafluoroethylene container. They obtained a sodium titanate nanofiber precipitate that underwent H^+ exchange and calcination for three hours at 700 °C to obtain the TiO_2 nanofibers.

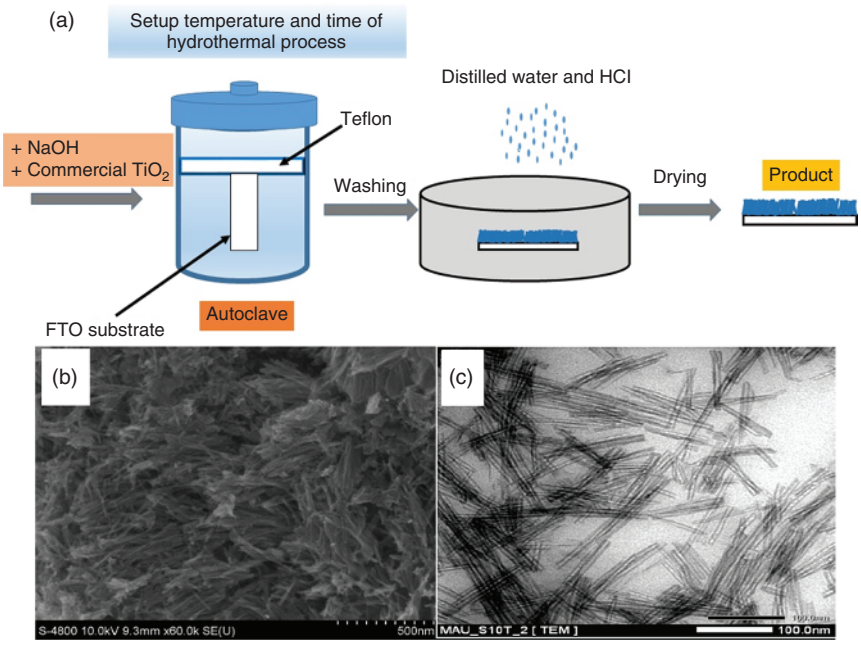

Figure 1.3 (a) Illustration of the synthesis process of TiO_2 nanotubes on an FTO substrate via the hydrothermal method, (b) field emission scanning electron microscopy (FESEM), and (c) transmission electron microscopy (TEM) images of the synthesized TiO_2 nanotubes. Source: Reprinted with permission from Viet et al. 2016 [53]. Copyright AIMS Press.

1.3.2 Sol–Gel Method

The sol–gel synthetic strategy is generally employed to synthesize crystalline or amorphous structures of organic or inorganic materials that offers the advantage of obtaining better purity and homogeneity of the synthesized nanoparticles at low temperatures [45]. Utilizing the sol–gel strategy, nano-TiO_2 were synthesized following hydrolysis of a TiO_2 precursor as shown in Figure 1.4 [57]. This usually proceeds by acid-mediated titanium (IV) alkoxide hydrolysis, which is followed by a condensation reaction [7]. The formation of the chains of Ti–O–Ti has been reportedly encouraged by slow hydrolysis rates, high amount of titanium (IV) alkoxide, and small amount of water [58, 59]. On the other hand, it is possible to obtain different shapes and sizes of anatase TiO_2 nanoparticles with high crystallinity by the tetramethylammonium hydroxide-mediated titanium (IV) alkoxide polycondensation [58]. Typically, the titanium (IV) alkoxide could be complemented with NaOH and an alcohol at 2 °C and heated for 13 days at 50–60 °C or six hours at an elevated temperature (90–100 °C). For the purpose of improving the crystal nature of the as-synthesized nanoparticle, a secondary heat treatment (175 and 200 °C) in an autoclave can be performed [7]. Furthermore, for the avoidance of agglomeration during the crystallization process of the nanoparticles, a prolonged heat treatment can be performed at temperatures below 100 °C [58].

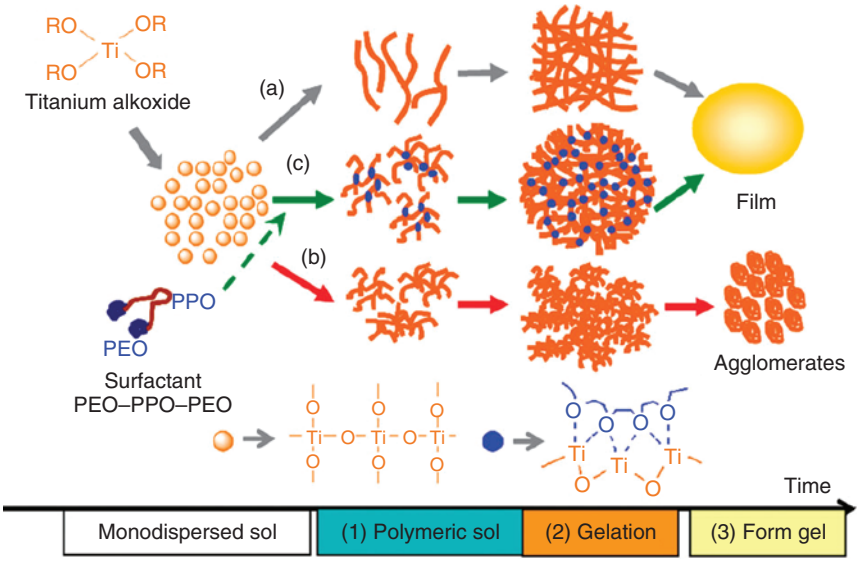

Figure 1.4 Illustrating the sol–gel synthetic mechanism in the presence of an (a) acid, (b) base, and (c) P123-templated, basic condition in dimethylformamide. Source: Adapted with permission from Cao et al. 2011 [57]. Copyright The Royal Society of Chemistry.

Although the sol–gel method has been regarded as a conventionally accepted method for the synthesis of TiO_2 nanoparticles, several disadvantages of this method has inevitably caused researchers to explore other synthesis strategies. Among these disadvantages is the fact that the calcination process obviously causes the grain growth and low specific surface area and induces phase transformations [60]. Additionally, comparatively poor crystallinity and particle size uniformity often characterize the synthesized nanoparticles [32]. These drawbacks notwithstanding, some researchers have successfully applied this strategy for the synthesis of TiO_2 nanoparticles for practical applications. For instance, TiO_2 nanorods were successfully prepared by sol–gel synthetic strategy by dipping porous anodic alumina membrane (denoted as AAM) template in a boiled sol of TiO_2, accompanied with the usual procedures of drying and heating [61]. These researchers observed that tuning the calcination temperature could control the nanorod crystal phases, demonstrated by the formation of anatase and rutile nanorods at low and high calcination temperatures, respectively. In another study, TiO_2–zinc phthalocyanine nanoparticles were obtained by the sol–gel strategy and applied as photosensitizers for cancer photodynamic therapy [62]. Additionally, the hydrolysis and condensation of titanium butoxide with gamma amine butyric acid and mineral acids as the precursors yielded amine-, phosphate-, and sulfate-functionalized TiO_2 nanoparticles in a typical sol–gel synthetic method [63]. These functionalized nanoparticles demonstrated good potential as copper complex drug carriers for cancer chemotherapy.

Utilizing the electrophoretic deposition of the colloidal suspensions of TiO_2 into AAM pores, Lin et al. obtained ordered arrays of TiO_2 nanowires [64]. They employed platinum anode and the AAM with a gold substrate fastened

to copper as the cathode. Making use of a voltage of about 2–5 V, a TiO_2 sol was successfully deposited into the AAM pores. A 5% NaOH dissolution of the AAM template yielded the TiO_2 nanowires, and it was observed that an AAM with long pores was desirable for the preparation of nanowires in favor of nanotubes. In a related study, nanotubes of TiO_2 were synthesized with an AAM template and other organic compounds [65]. Typically, the AAM was dipped into a solution of TTIP and later removed and kept in vacuum to allow the TTIP volume to pull through the template. Then, water vapor hydrolysis in the presence of HCl (24 hours), air drying at ambient temperature, calcination for two hours at 673 K and dissolution of the AAM in 6 M NaOH were conducted to obtain pure TiO_2 nanotubes. In another study, TiO_2 nanotubes were synthesized with a dilute TiF_4 coating of the AAM membranes at time periods of 12–48 hours at 60 °C [66]. The AAM membranes were then removed after the observed formation of the nanotubes. In another experiment by Sugimoto et al., TTIP was mixed with triethanolamine (TEOA) in a sol–gel synthetic strategy, followed by aging for one day at 100 °C and three days at 140 °C [67]. These researchers employed amines (TEOA, diethylenetriamine, ethylenediamine, trimethylamine, and triethylamine) as surfactants and shape controllers for the TiO_2 nanoparticles and observed a morphology change at above pH values of 11 and 9.5 in the presence of TEOA and the other amines, respectively. This control over shape was attributed to the adsorption of the amine shape controllers on the crystal planes of the TiO_2 nanoparticles. Mahshid et al. prepared biphase TiO_2 nanoparticles by the sol–gel method that yielded crystallite sizes between 27 and 107 nm [68]. Hussain et al. also synthesized novel nano-TiO_2 whose size ranged from 10 to 20 nm by the sol–gel technique [69].

In another study, Chong et al. synthesized TiO_2 nanoparticles by the sol–gel method [70]. They hydrolyzed titanium IV butoxide precursor with ethanol, followed by a condensation reaction. Through this first step, it was possible to control the homogeneity and microstructures of the eventually formed TiO_2 crystals. Control of the hydrolysis extent is very crucial in obtaining nano-sized TiO_2. For this purpose, these researchers carried out the hydrolysis in two stages, where the ethanol addition to the titanium IV butoxide precursor was utilized to target the partially hydrolyzed state. This partially hydrolyzed state ensures an improved molecular homogeneity and non-hydrolyzable Ti ligands for enhanced growth of the TiO_2 [71]. The control of the hydrolysis reaction extent was achieved by an acid-mediated hydrolysis with nitric acid, owing to the low range of ethanol functionality in the titanium IV butoxide precursor hydrolysis.

1.3.3 Solvothermal Method

The solvothermal synthetic strategy is closely related to the hydrothermal technique but for the use of non-aqueous solvents in the former [58]. Due to the use of a wide range of organic solvents of appreciably high boiling points in the former, the working temperatures can be elevated way much higher than is attainable in the later [7]. Moreover, the solvothermal method offers intriguing advantages including an improved tuning of morphology, particle size, crystallinity of the

synthesized nanoparticles, and temperature and pressure controls of the solvents used for the synthesis [72]. Additionally, this method provides a versatile route to the synthesis of TiO_2 nanoparticles with improved dispersity and narrow size distribution [7].

The solvothermal synthetic strategy was used for the preparation of TiO_2 nanorods and nanoparticles with or without surfactant mediation [58, 73]. In the light of this, anhydrous toluene was employed at 250 °C for 20 hours to dissolve TTIP, using oleic acid as a surfactant [74]. In a controlled hydrolyzation reaction, redispersible TiO_2 nanorods and nanoparticles were synthesized with $Ti(OC_4H_9)_4$ in the presence of linoleic acid. This reaction was carried out with a catalyst (triethylamine) to aid the inorganic Ti–O–Ti condensation in order to obtain the crystals with consistent morphology [73].

1.3.4 Chemical and Physical Vapor Deposition Method

Vapor deposition can be referred to as the condensation of materials in the vapor phase to solid phase [58]. In the absence of a chemical reaction in the vacuum chamber, the process is termed physical vapor deposition (PVD), otherwise it is termed chemical vapor deposition (CVD) [75]. In a typical CVD process, the deposition reaction is driven by thermal energy that heats the gases present in the coating compartment [7]. Employing TTIP pyrolysis in an atmosphere of oxygen/helium utilizing a liquid precursor, TiO_2 nanoparticles with average sizes below 10 nm were successfully synthesized [76].

Nevertheless, other CVD approaches exist, which include diffusion flame pyrolysis, ultrasonic spray pyrolysis, ultrasonic-assisted hydrolysis, electrostatic spray hydrolysis, laser-induced pyrolysis, and plasma-enhanced CVD (PECVD) [58]. In a typical PECVD, the amorphous TiO_2 nanoparticles are placed on the cold compartments of the reactor at temperatures less than 90 °C as shown in Figure 1.5a [77]. The obtained nanoparticles from PECVD after annealing same at high temperatures usually possess high surface areas (Figure 1.5b,c) [78].

In another experiment employing catalyst- and template-free metal organic CVD (MOCVD), Wu and Yu successfully grew TiO_2 nanorods on fused silica substrates [79]. Typically, O_2/N_2 flow was used to convey titanium acetylacetonate that was vaporizing in the low-temperature region of the furnace (200–230 °C) to the high-temperature region (500–700 °C), resulting in the growth of the TiO_2 nanorods on the substrates directly. The morphology and phase of the nanorods were demonstrated to be tunable with the reaction conditions. To illustrate this, at a pressure of 5 Torr, single-crystalline anatase and rutile nanorods were obtained at 560 and 630 °C, respectively, while at 3.6 Torr, anatase nanowalls comprising of well-aligned nanorods were obtained at 535 °C. The MOCVD method has also been applied using a WC–Co substrate and a TTIP precursor for the successful synthesis of TiO_2 nanorods as reported in a study by Pradhan et al. [80].

Primary PVD methods include ion plating, sputtering, laser surface alloying, thermal deposition, and laser vaporization [7]. The PVD method or thermal deposition has been employed for the synthesis of TiO_2 nanowires [81]. In a typical experiment conducted in a tube furnace, a titanium source (pure

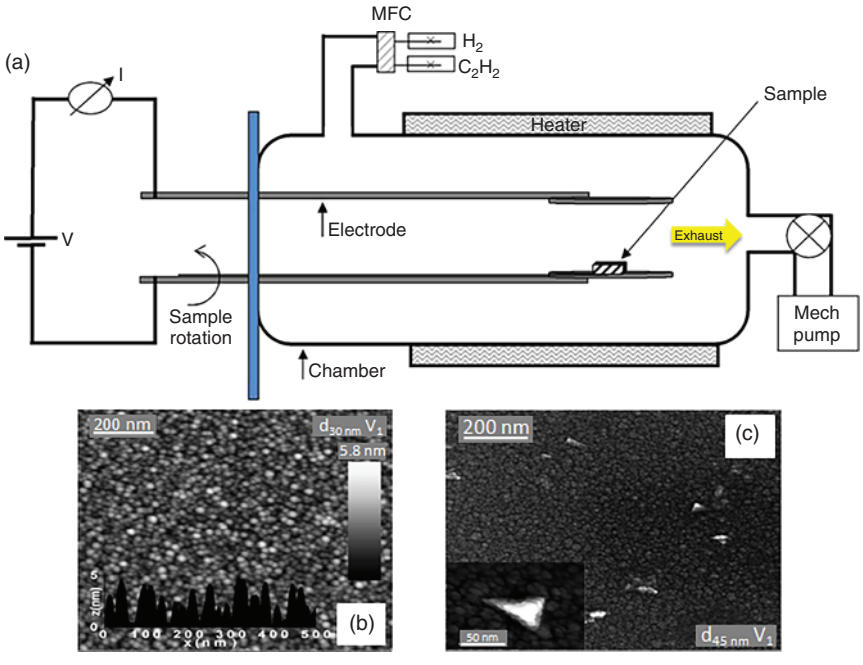

Figure 1.5 (a) Schematic diagram of a typical PECVD. Source: Baghgar et al. 2009 [77]. Reproduced with permission of Institute of Physics. (b) Atomic force. Source: Adapted with permission from Borras et al. 2009 [78]. Copyright American Chemical Society. (c) Scanning electron microscopy (SEM) images of TiO_2 grown by PECVD.

Ti metal) was loaded on a quartz boat, and under an argon atmosphere, the temperature was raised to 850 °C. This was followed by pumping down of the furnace chamber to about 300 Torr with the argon flow rate of 100 sccm for three hours, to obtain fine TiO_2 nanowires. In an alternative route, Wu et al. employed Au as a catalyst and deposited a nanopowder layer of Ti on the substrate, prior to the growth of the TiO_2 nanowires [82].

1.3.5 Thermal Decomposition Method

The thermal decomposition method has been employed in the past decade by various researchers for the synthesis of TiO_2 nanoparticles [83–85]. For instance, the thermal degradation of TTIP vapor at 300 °C, yielded TiO_2 nanoparticles in a study by Moravec et al. [84]. They saturated the carrier gas (dry, particle free, and deoxidized nitrogen) with the TTIP vapor in a saturator that was externally heated. It was observed that the formation of fine TiO_2 nanoparticles was initiated by the heterogeneous decomposition of the TTIP. In another experiment, TiO_2 nanoparticles were obtained by thermal decomposition of titanium (IV) *n*-butoxide in 1,4-butanediol. The reaction was also conducted in an autoclave at 300 °C for two hours at 25 °C. The obtained nanoparticles were further calcined for two hours at 500 °C in a box furnace and were obtained as crystals of anatase TiO_2 nanoparticles with average diameter of 15 nm.

Furthermore, TiO_2 nanoparticles with improved photocatalytic ability were successfully synthesized using the thermal decomposition method by treating the precursor titanyl sulfate with peroxo compounds such as hydrogen peroxide, urea hydrogen peroxide, and ammonium persulfate [86]. Annealing temperatures of 600, 850, and 700 °C were utilized in air at 60 minutes for the hydrogen peroxide, urea hydrogen peroxide, and ammonium persulfate peroxo-containing phases, respectively, to obtain the anatase phase TiO_2 nanoparticles. In a different study, Im et al. synthesized 10 nm-TiO_2 nanoparticles by thermally decomposing metal–organic frameworks (denoted as MIL-125 and MIL-125-NH_2) that contain titanium, for six hours at 350 °C in air [85]. They observed a random aggregation of the nanoparticles within the crystalline particles of the metal–organic framework precursors. These nanoparticles showed capacity for effective decomposition of 4-chlorophenol by photocatalysis.

1.3.6 Oxidation Method

This method involves the direct oxidation of the element titanium by the use of oxidants or anodic reactions to produce the nanoparticles [58]. For instance, using a voltage of 10–20 V and 0.5% hydrogen fluoride, Varghese et al. successfully prepared well-aligned TiO_2 nanotubes [87]. Annealing the anodized plate of titanium at 500 °C for six hours in the presence of oxygen was necessary in obtaining the nanotubes. It was observed that the diameter and length of the nanotubes could be controlled by tuning the applied voltage.

The hydrogen peroxide-induced oxidation of the element titanium was reported to be effective for the synthesis of TiO_2 nanotubes by placing the titanium metal in 50 ml hydrogen peroxide solution (30 wt%) for 72 hours at 353 K [88]. In the oxidative synthesis of TiO_2 nanoparticles, the phase of the products were controlled by adding specific inorganic salts in the preparation process, particularly during the dissolution precipitation [89]. For instance, NaCl is usually added for the generation of rutile phase, and NaF or Na_2SO_4 are required to obtain the anatase phase TiO_2 nanoparticles [90]. Acetone has also been employed as an oxygen source at 850 °C for 90 minutes to obtain well-aligned and highly dense TiO_2 nanorod arrays [91].

Furthermore, TiO_2 nanoparticles can be synthesized by either the wet or dry processes. In the dry process, the vapor phase oxidation of $TiCl_4$ is conducted, which leads to formation of amorphous TiO_2 nanoparticles as shown in Eq. (1.1). This is usually followed by annealing of the synthesized amorphous TiO_2 nanoparticles at different temperatures to obtain desired crystalline phases of anatase or rutile [21].

$$TiCl_4(g) + O_2(g) \rightarrow TiO_2(s) + 2Cl_2(g) \tag{1.1}$$

In the wet process, homogenous products and nanocomposites with complex shapes can be obtained, and there is also the possibility of controlling the stoichiometry. However, the presence of carbon (an impurity in this case), long processing times, and expensive precursors are the major drawbacks of this process [22].

1.4 Applications of TiO_2 Nanoparticles

Due to their fascinating properties, TiO_2 nanoparticles have found vast array of applications such as in nanobiotechnology [92], nanomedicine [14], energy devices [93], soil remediation [94], food [95], healthcare and cosmetic products [96], wastewater treatment [97], and paint [98], paper [99], and plastics productions [100]. Some of these general applications of TiO_2 nanoparticles will be briefly discussed in the following subsections.

1.4.1 Nanobiotechnology

Owing to the increasing difficulty in treating multidrug resistant strains (*Pseudomonas aeruginosa*), there is an urgent need to fabricate new class of antibacterial agents with totally different mode of action and structure from conventional agents [19]. Additionally, multidrug resistant strains have been linked to complications in present-day medicine [101]. These strains have also been identified worldwide as major nosocomial pathogens [102]. The last decade has witnessed various failures in the treatment of animal and human bacterial diseases that have been generally attributed to the strong resistance of bacterial pathogens to conventional drugs [103, 104]. This is mainly due to the ability of these bacterial pathogens to rapidly adapt to new environmental terrains such as antimicrobial molecules presence, consequently increasing the bacterial resistance following the use of antimicrobials [105]. In recent years, a good number of nanoparticles have demonstrated encouraging biological activities, particularly toward bacterial treatment [106]. Among these nanoparticles, nano-TiO_2 has gained attention based on its hydrolysis and oxidative properties [92]. It has also been observed that the biocidal action of nano-TiO_2 is partly a consequence of charge carrier (electron-hole) modulation at the external surface interface of the nanoparticles, giving rise to appreciable antimicrobial capabilities by optimizing the inorganic–organic interfacial contact and inorganic phase dispersions [107–110]. Additionally, nano-TiO_2 has been tipped to outperform metal-based systems and other chemicals such as H_2O_2, NO, and other small molecules due to the intrinsically environmental friendliness and non-contact antimicrobial action of TiO_2–polymer nanocomposites [111, 112]. As such, no release of toxic nanoparticles to the surrounding media (with adverse health effects) occurs in order to obtain the disinfection efficacies [113, 114].

Nano-TiO_2 has also been used for the disinfection of a broad microorganism spectrum [92, 115], but hitherto, the mechanism by which these nanoparticles induce microbial death is poorly understood [116]. Rather, most studies have focused on the alteration of enzyme activities that depend on coenzyme-A [117], hydroxyl radicals-induced DNA damage [118], and the popular oxidative attack by nano-TiO_2 on the inner and outer cell membranes of microorganisms [119, 120]. As regards antibacterial coatings, high density of nano-TiO_2 on the surface enhances the generation of reactive oxygen species (ROS) with resultant increase in antibacterial efficacy [121]. Notwithstanding, several other antimicrobial applications based on the generation of ROS as a mechanism of action

have been documented [115, 122]. These include disinfectants or biocides such as potassium permanganate, ozone, hydrogen peroxide, pancreatic acid, etc. [123]. Some researchers have incorporated these biocides into the nanocomposites of polymers, thereby generating vast antimicrobial materials with wide range of applications such as in biomedicine, packaging, etc. [116, 124–128]. Unfortunately, kinetic and thermodynamic barriers reduce the dispersal of such inorganic (often hydrophilic) nanoparticles (NPs) in the matrices of hydrophobic polymers, thereby posing serious challenges to the development of such materials [116]. However, other approaches that are seemingly more targeted can be considered in order to enhance the generation of ROS, such as the photodynamic inactivation (PDI). A typical PDI entails the excitation of photosensitizer dyes to the long-lived triplet states that then undergo some reactions involving energy transfers to either produce singlet oxygen or the hydroxyl radicals [129, 130]. PDI has therefore been applied with photosensitizers in solution or heterogeneous dyes, wherein the dyes are conjugated to polymer films or other solid supports [131, 132]. For instance, PDI was exploited using the common photosensitizer (methylene blue) that was excited at 660 nm (red light) and potentiated with an inorganic nontoxic salt (potassium iodide) [133]. This gave rise to an increase in the killing of Gram-positive and Gram-negative bacteria by 2-logs. However, a recent report has demonstrated that the antimicrobial photocatalysis of TiO_2 nanoparticles could be potentiated with sodium iodide with a resultant 3-log increase in antimicrobial efficacy [134].

In the light of these, an investigation into the inhibition effectiveness of TiO_2 nanoparticles in combination with active antibiotics of the cell wall (cefotaxime and cefazidime) against *P. aeruginosa* (a multidrug resistant strain) was carried out [19]. The *P. aeruginosa* was isolated from endo-tracheal tract, sputum, pus, and bronchoalveolar lavage. It was observed that upon exposure to UV light for one hour, the TiO_2 nanoparticles demonstrated antimicrobial effect on the nosocomial pathogen at nanoparticle concentrations of 350 mg/ml and higher. Additionally, a 6-log increase in minimum inhibitory concentration values was generated for the cefotaxime against cefazidime.

In a related study, the photocatalytic effect of low-dose UV light-activated TiO_2 nanoparticles on the genome/proteome-wide expression of *P. aeruginosa* was investigated two minutes post treatment [116]. They analyzed and quantified the radical species released from *P. aeruginosa* biofilms and estimated the contribution of such radicals in the damage and ultimate death of cells. It was observed that the photocatalytic action of the TiO_2 nanoparticles triggered a decline in the expression of a large collection of genes/proteins responsible for growth and signaling functions in parallel with the subsequent impacts on coenzyme-independent respiration, cell wall structure, and ion homeostasis. It was also observed that the nano-TiO_2-mediated biocidal action or those of other photoactive nanoparticles were counteracted by the cells as the cells triggered numerous regulatory responses with no significant metabolic function loss within the time scale of the experiment. They also established clear-cut indications of nano-TiO_2 selective catalysis in distinct cell-critical systems. These researchers therefore proposed the combination of biological and chemical methods to tackle the present limitations in understanding the link

between microorganism transport and metabolic properties, and nano-TiO_2 photo-induced biocidal efficacy. This would also benefit the proper definition of the nature of photocatalyzed reactions, the cells that take part in the response, and the degree at which nano-TiO_2 biocidal action could be reversed.

The antimicrobial effect of TiO_2 nanoparticles on another drug-resistant nosocomial pathogen (methicillin-resistant *Staphylococcus aureus*, denoted as MRSA) was demonstrated in a study by Jesline et al. [106]. The MRSA was described as a major nosocomial pathogen linked to an array of infections such as the catheter-related and surgical site infections, bacteremia, soft tissue and skin infection, and pneumonia. They attributed the main contributory factor for pathogen resistance of antibiotics to the formation of biofilms. Additionally, the strong resistance to drugs by MRSA was described by their formation of extracellular polymeric substances consisting of nucleic acids, lipids, and polysaccharides. Importantly, a sessile bacteria that is embedded in an extracellular polymeric substance is capable of withstanding the immune responses from the host and as such becomes less accessible by antibiotics as such drugs experience difficulties in penetrating the biofilm. These researchers monitored the production of biofilms by the MRSA using the culture plate method and thus reported that UV-mediated treatment with TiO_2 nanoparticles significantly suppressed the production of these biofilms. An earlier report also explains that the ability of TiO_2 nanoparticles to decompose organic compounds lies on their constant release of superoxide ions and hydroxyl radicals that is efficient for inhibiting MRSA growth [135]. Furthermore, Chorianopoulos et al. investigated the photocatalytic effect of TiO_2 nanoparticles on the production of biofilms by the *Listeria monocytogenes* bacteria [136]. In that study, various TiO_2 nanoparticles were deposited on stainless steel and glass surfaces in a doctor-blade strategy. These surfaces were irradiated with UV light after the formation of the biofilms. They observed a fast log reduction of the biofilm attributable to the presence of the UV-activated nanoparticles, compared with the control test.

It has also been demonstrated that the addition of an inorganic salt (potassium iodide) significantly increased the photocatalytic effect of TiO_2 nanoparticles on fungi and Gram-positive and Gram-negative bacteria by approximately six logs [115]. The antimicrobial effect was dependent on the intensity of the applied UV light, and the concentrations of the potassium iodide and TiO_2 nanoparticles. They established that the most effective potassium iodide concentration for the enhanced antimicrobial effect was 100 mM. They observed that in the reaction mixture, there was a generation of long-lived antimicrobial species that may probably be iodine and hypoiodite, but more killing was produced by short-lived antibacterial reactive species. Strategically, the iodide quenched the fluorescent probes for singlet oxygen and the hydroxyl radicals. The TiO_2–UV–potassium iodide produced a tri-iodide (whose peak was observed at 350 nm and formed blue compound with starch) but was intensively decreased when the MRSA cells were present.

Nano-TiO_2 has also been used to kill a broad spectrum of bacteria including *Escherichia coli*, *S. aureus*, *Bacteroides fragilis, P. aeruginosa*, and *Enterococcus hirae*, in a study on orthopedic implants infections [137]. In the clinic, the

metal pins used for the application of external fixation devices or skeletal tractions to manage orthopedic fractures are highly susceptible to pin site infections [138]. These fractures most times are associated with bone and wound infections [139]. The high adaptability of bacteria enabling their colonization on damaged tissue cells or "inert" biomaterials surfaces remain the most critical complication in the external fixation strategy for the management of pin tract infection [140]. Notably, the stability of pin–bone interfaces is reduced by the pin tract infection, while an unstable pin–bone-fixator construct may cause half-pin loosening and pin site infections [137]. The colonization of external fixators with bacteria such as *Staphylococcus epidermidis* and *S. aureus* was reported in an earlier study by Collinge et al. [141]. In developed countries, antibiotics are routinely administered to ameliorate these infections, while other common practices include surgical debridement, stabilization, and irrigation, when indicated [138]. Due to the widespread use of antibiotics and the buildup of drug resistance in bacteria, the need to develop alternative means for sterilization cannot be overemphasized. Moreover, the conventional sterilization strategy of wiping is not effective at the long run, time and staff intensive, and cannot be standardized, coupled with the challenges associated with using aggressive chemicals for such practice [142]. For this reason, Tsuang et al. demonstrated that the coating of an orthopedic implant with TiO_2 nanoparticles could reduce bacteria-related colonization of such implants and the associated infections [137]. They observed that almost all the tested bacteria were killed following 50 minutes of UV irradiation of the TiO_2 nanoparticles. Additionally, a decrease in the formation of bacterial colonies on top of the nano-TiO_2-coated metal plates. It was also established that the photokilling of the bacteria followed a two-step decay kinetics, wherein a relatively lower rate was followed by a higher one. However, this was contrary to earlier photokilling kinetic reports that were described by pseudo-first-order reactions [143, 144].

1.4.2 Nanomedicine

Exploiting the optical properties of TiO_2 nanoparticles, some researchers have applied same for *in vitro* and *in vivo* cancer PTT [14, 15]. A recent strategic research demonstrated the use of hydrogenated TiO_2 nanoparticles in cancer PTT, wherein the photothermal ability of the nanoparticles was attributed to their dramatically improved non-radiative recombination [14]. They employed black TiO_2 nanoparticles for the PTT of cancer cells owing to the limitations of white TiO_2 nanoparticles as regards the mutagenicity and shallow penetration of UV light. The hydrogenated TiO_2 nanoparticles were coated with polyethylene glycol (PEG) and were observed to possess good biocompatibility and low toxicity, low cost and simple preparation strategy, and excellent near-infrared (NIR) effect. A better cancer PTT ability triggered by NIR of the hydrogenated TiO_2 nanoparticles was observed as against photodynamic therapy (PDT) of TiO_2 nanoparticles induced by UV light.

In a related study, an NIR-triggered multifunctional nanoplatform comprised of black TiO_2 nanoparticles was successfully and rationally constructed for an effective cancer theranostics [15]. These PEGylated nanoparticles demonstrated

fascinating hemo/histocompatibility, wide absorption range, and high stability and dispersity in aqueous solution. Irradiated by a single NIR laser, these novel multifunctional nanoparticles showed high PDT/PTT synergistic cancer therapeutic efficacy under photoacoustic/infrared thermal imaging. Notably, the obstacles associated with the use of high laser power density, UV light, multi-component nanocomposites, and combination cancer therapy were circumvented by the use of these synthesized novel multifunctional theranostic nanoparticles. Furthermore, these novel multifunctional nanoparticles demonstrated negligible side effects to main tissues and blood in three months of investigation.

The potential of nano-sized TiO_2 as photosensitizers for PDT have indeed been extensively investigated in the last few decades [2, 13, 62]. To this end, photosensitizers based on TiO_2 nanoparticles for cancer PDT were prepared by incorporating zinc phthalocyanine (ZnPc) into the porous networks of the TiO_2 nanoparticles as reported in a study by Lopez et al. [62]. These photosensitizers demonstrated negligible cytotoxicity following the 3-(4,5-dimethylthiazol-2-yl)-2,5-diphenyltetrazolium bromide (MTT) assay on four mammalian cell lines and parasites, namely, human hepatocellular liver carcinoma cells, human-derived fibroblasts, human acute monocytic leukemia cell line, and the African green monkey epithelial cells. The mechanism for cell necrosis following the PDT was determined by the preferential localization of the photosensitizers in target organelles such as lysosomes or mitochondria. Without an external impetus, TiO_2 nanoparticles are excited by UV wavelengths in the region of 320–400 nm, which are harmful to the human body due to the fact that hemoglobin, melanin, and proteins are also excited in this UV range [2]. Taking cognizance of this, Lopez et al. demonstrated that incorporating the ZnPc increases the useful wavelength of the TiO_2 nanoparticles to the visible region, wherein an intercomponent electron transfer is achieved in the molecular semiconductor–semiconductor oxide of the couple [62].

Similarly, ZnPc-integrated TiO_2 nanoparticles have also been synthesized for *in vitro* cancer PDT [145]. It was observed that the toxicity of ZnPc was reduced by the TiO_2 nanoparticles, while the ZnPc–TiO_2 nanoparticles demonstrated good PDT potential when tested differently with human healthy lung cell lines (WI38), hepatocellular carcinoma (HepG2), and colorectal adenocarcinoma tumor (HT29). The ZnPc–TiO_2 nanoparticles were further labeled with ^{131}I radionuclide and it was observed that the ^{131}I–ZnPc–TiO_2 nanoparticles demonstrated good potential for nuclear imaging. Recently, Yurt et al. synthesized Subphthalocyanine (SubPc)-integrated TiO_2 nanoparticles that were also labelled with the ^{131}I radionuclide (denoted as^{131}I–SubPc–TiO_2) [146]. When treated differently with WI38, HepG2, and HT29, these nanoparticles also demonstrated good potential as nuclear imaging and PDT agents.

Upconversion TiO_2 nanoparticles have also been synthesized and applied in the PDT of cancer [147–149]. The upconversion nanoparticles (UCNPs) of $NaYF_4$:Yb^{3+} and Tm^{3+}@$NaGdF_4$:Yb^{3+} were used for the synthesis of UCNP@TiO_2 nanoparticles for the NIR-induced photoactivation of the TiO_2 nanoparticles. The UCNP@TiO_2 nanoparticles generated ROS-induced apoptosis of tumor cells by reducing the mitochondrial membrane potential,

subsequently releasing cytochrome C for the activation of caspase-3. To mitigate the multidrug resistance of breast cancer cells, UCNPs of $NaYF_4$:Yb/Tm-TiO_2 as inorganic photosensitizers loaded with an anticancer drug doxorubicin (DOX) were successfully synthesized and applied for the NIR-induced PDT of breast cancer [149]. By exploiting the upconversion luminescence ability of the $NaYF_4$:Yb/Tm that converts NIR radiation to UV light, the TiO_2 could then generate sufficient ROS for effective PDT with observed low photo-damage and deep penetration. The cellular uptake of these nanoprobes was enhanced by their folic acid functionalization, enabling the accelerated release of DOX in the drug resistant MCF-7/ADR and MCF-7 cells.

Recently, TiO_2 nanoparticles were grafted into and outside UCNP@mesoporous silica (UCNP@$mSiO_2$) nanovehicle [148]. Furthermore, a UV-cleavable derivative linker of *o*-nitrobenzene (TC linker) was employed as a "gate" for the encapsulation of DOX inside the $mSiO_2$. It was reported that upon NIR irradiation, the emitted UV light excited the TiO_2 to afford ROS, caused the photodegradation of the TC linker and also enhanced DOX release for a synergistic PDT and chemotherapy.

Furthermore, TiO_2 nanoparticles have also been applied as drug carriers for cancer chemotherapy. In this regard, the surfaces of TiO_2 nanoparticles were functionalized by phosphate, sulfate, and amine groups in a sol–gel synthetic strategy with titanium butoxide [63]. These functionalized TiO_2 nanoparticles were further loaded with copper complexes to obtain potential drug delivery systems with average sizes of 4–10 nm. Interestingly, the morphology of the functionalized TiO_2 nanoparticles and the structures of the copper complexes remained unchanged after the drug loading. Additionally, cell viability tests using these nanoparticles showed not less than a 90% survival for all the cell lines tested. In another study, the porosity of TiO_2 nanowhiskers (Ws) were exploited for the loading of the anticancer drug daunorubicin (DNR) [150]. These TiO_2 Ws demonstrated good biocompatibility and enhanced photocatalytic ability. On irradiation with UV light, efficient PDT was observed on hepatic carcinoma cells (SMMC-7721) as there was an increase in the intracellular concentration of the DNR that obviously increased its anti-tumor efficacy as shown in Figure 1.6. Moreover, the excellent drug delivery capacity of the TiO_2Ws has been linked to their large surface area and reactivity [2].

Nanoparticles of TiO_2 have also been investigated for their application in sonodynamic cancer therapy as a result of the deep penetration capacity of ultrasound radiation enabling the targeting of deep-seated tumors and other diseases [151]. Prior to the emergence of TiO_2-based sonosensitizers for sonodynamic therapy, most sonosensitizers used for generating ROS on ultrasonic activation were organic compounds such as 5-aminolevulinic acid, phthalocyanines, porphyrin, etc. [152, 153]. To investigate the utility of TiO_2 nanoparticles for sonodynamic therapy, Shen et al. synthesized TiO_2-encapsulated Fe_3O_4 nanoparticles, denoted as TiO_2@Fe_3O_4 [151]. The TiO_2 nanoparticles were employed as both sonosensitizers and as carriers for the loading of DOX. It was observed that the core–shell TiO_2@Fe_3O_4 nanoparticles demonstrated a pH-dependent loading of DOX and its subsequent release to MCF-7 and subline of the ubiquitous keratin-forming tumor (KB) cells. Additionally, ROS were efficiently generated by the

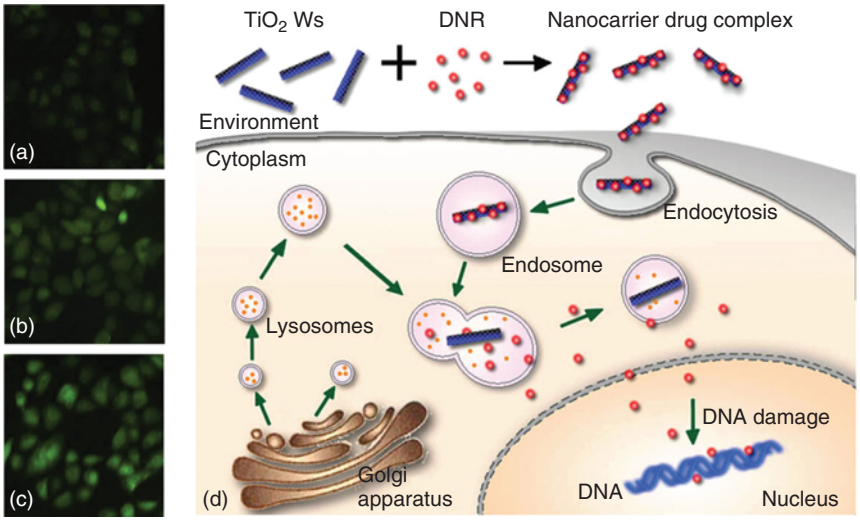

Figure 1.6 Fluorescence microscopic images of the SMMC-7721 cancer cells that were treated with DNR (a), DNR–TiO_2 nanoparticles (b), and DNR–TiO_2Ws (c). (d) Illustration of the possible mechanism for the cellular uptake of TiO_2Ws in the SMMC-7721 cancer cells. Source: Adapted with permission from Li et al. 2009 [150]. Copyright Elsevier Limited.

TiO_2@Fe_3O_4 nanoparticles upon ultrasound irradiation. Owing to the enhanced accumulation of the core–shell nanoparticles in the tumor region and the long-time retention effect, a combinational sonodynamic and chemotherapeutic outcome was observed, with minimal side effects. To illustrate this, they reported that the combination therapy showed an 88.36% inhibitory effect as against 38.91% and 28.36% for sonodynamic therapy and chemotherapy, respectively.

In another study, TiO_2–PEG nanoparticles were successfully synthesized and also applied as sonosensitizers in a combination of photodynamic (PD) and sonodynamic therapies [154]. Upon irradiation of the nanoparticles with 5.0 mW/cm^2 laser, the nanoparticles demonstrated an effective reduction in the viability and membrane integrity of human glioblastoma cells U251. The generation of singlet oxygen alongside other ROS after sonoactivation was utilized for sonodynamic therapy using core–shell TiO_2–polyallylamine micelle nanoparticles in a study by Harada et al. [155]. Their findings are very important and capable of revolutionizing imaging-guided sonodynamic therapy for diseases such as the neoplastic maladies.

In combination with other macromolecules and nanomaterials, nano-sized TiO_2 has been used for the synergistic theranostics of certain diseases [13, 151, 156, 157]. To this end, Zeng et al. synthesized TiO_2–Fe_3O_4 nanocomposites and applied same for the theranostics of neoplastic disease [13]. The TiO_2 nanoparticles in the nanocomposites served as excellent photosensitizers for PDT, while the Fe_3O_4 provided contrast enhancement for MRI. In another experiment, TiO_2 nanoparticles were used in combination with another photosensitizer chlorine e6 to obtain a synergistically enhanced PDT, contrary to those obtained from the individual photosensitizers [156].

Undoubtedly, medical implants have dramatically revolutionized orthopedic surgeries, particularly the endoprosthetics. However, the liberal application of cardiovascular stents and orthopedic implants have been hindered by autoimmune reactions [2]. To this end, Ti and its alloys, especially TiO_2-based nanoparticles have been reported as effective surface coatings for orthopedic implants to mitigate these reactions [158]. Additionally, there are suggestions that TiO_2-based nanoparticles provide safe tissue-recognition scaffolds in endoprosthetic surgeries [159]. To elaborate this, TiO_2 nanotubes were synthesized and used to ameliorate acetabulum hip joint or tibia-tarsal joint fractures in prosthetic articular surgery [160]. The utility of TiO_2 nanotubes in enhancing osteoblast adhesion *in vitro*, strong bone adhesion *in vivo*, and bone mineralization has also been documented [161]. In a pull-out testing after a four-week implantation of TiO_2 nanotubes in rabbit tibias, it was demonstrated that up to a ninefold increase in bone-bonding strength was obtained against the use of TiO_2 grit-blasted surfaces.

1.4.3 Wastewater Treatment

Drinkable and clean water that is free of carcinogenic substances, harmful bacteria, and toxic chemicals is crucial for human health [97]. According to the 2018 World Water Development Report of the United Nations, the past decade has witnessed a 1% yearly rise in global water demand, and it is expected that in 2050, the demand for clean water will increase by about one-third of its present state [162]. Importantly, the high demand for clean water is also increased as a result of its crucial role in industrial processes such as in the production of electronic devices, pharmaceuticals, paints, foods, and other beverages [163–166]. To meet this ever-increasing demand for quality water supply, numerous efforts are made to reclaim wastewaters both from households and industries. Advances in nanotechnology and nanoengineering have demonstrated good promise in achieving marked improvements in the quality of water, aided by nanosorbents [167], nanocatalysts [168], nanoparticle-enhanced filtration [169], and bioactive nanomaterials [170]. Owing to the fact that remarkable changes in the physical and chemical properties and enhancements in the surface-to-volume ratios (increase in surface reactivity) of materials are obtained when they are prepared in nanoscales (1–100 nm), nanotechnology-based materials that reduce the amounts of toxic substances to low levels could appreciably contribute to achieving good standards for water quality and decrease adverse health challenges [171–173]. Various photocatalytic nanomaterials have been investigated in the past decade for their water treatment abilities. These include the nanorods and nanoparticles of zinc oxide [174, 175], nanocubes of silver chloride [176, 177], quantum dots and nanoparticles of bismuth vanadate [178], and cadmium sulfide [179, 180].

In recent times, environmental purification with TiO_2 nanoparticles as a photocatalyst has attracted great attention due to their chemical stability, low pollutant loading, low toxicity, self-cleaning ability, hydrophilicity, and availability at low cost [97]. Specifically, wastewater treatment with TiO_2 nanoparticles has been demonstrated as an effective technique for degrading organic contaminants by

photocatalysis [181]. The pH of the solution has been reported as a crucial parameter in the photocatalytic degradation reactions that take place on the surfaces of the nanoparticles, as it controls the surface charge properties and size of the aggregates formed by the photocatalyst [44, 181]. In this regard, Nasikhudin et al. evaluated the efficacy of TiO_2 nanoparticles for the photodegradation of methylene blue at different pH conditions [44]. They reported that the TiO_2 nanoparticles have the anatase structure with average size of 27 nm. On exposure to UV light, 97% of the methylene blue dye was photodegraded in three hours, while a 15% photodegradation was observed without UV illumination at same time. They attributed the 15% degradation to mere adsorption of methylene blue by the TiO_2, rather than photocatalytic degradation. They also observed that the specific degradation of the methylene blue in acidic (pH 4.1), neutral (pH 7.0), and basic media (pH 9.7) were 40%, 90%, and 97%, respectively, suggesting that a better photodegradation of the organic pollutant occurs in alkaline medium. This was attributed to the abundant hydroxyl groups in basic medium that can react directly with a hole in the TiO_2 nanoparticles, thereby generating -OH radicals.

The effects of varying the precursors and conditions in the sol–gel synthesis of on the photocatalytic activity of TiO_2 nanoparticles for the removal of an organic pollutant was investigated in a study by Behnajady et al. [182]. Particularly, these researchers varied the solvent percent, reflux time and temperature, sol drying method, calcination temperature, and water percent. The organic pollutant (C.I. Acid Red 27) was used as a model textile industry contaminant whose photodegradation was monitored under the irradiation with a UV-C light. These researchers established that the photo-induced degradation of the C.I. Acid Red 27 by the TiO_2 nanoparticles was a function of solvent type, precursor type, and other conditions of the synthesis process. In comparison to the commercial TiO_2 P25, the TiO_2 nanoparticles that were synthesized with titanium (IV) isopropoxide as precursor, methanol as the reflux solvent for three hours at 80 °C, coupled with appropriate thermal drying of the sol, and calcination at 450 °C demonstrated approximately same photocatalytic activity.

Several constraints have limited the utility of nano-TiO_2 for large-scale water treatment: (i) its large band gap (3.2 eV for the anatase phase) limiting its light absorption at the UV region, wherein a small range (3–5%) of the solar spectrum can be used for the activation of the nanoparticles, (ii) the quick e^-/h^+ recombination that occur during the TiO_2 photocatalysis, and (iii) the occurrence of TiO_2 nanoparticles in slurry form during the treatment process, making it particularly difficult to recover and recycle the nanoparticles [183].

Interestingly, recent studies have also shown that embedding an Fe_3O_4 core can improve the magnetic separation of TiO_2 nanoparticles due to the fact that the Fe_3O_4 itself is superparamagnetic at particle sizes less than 20 nm [97, 184–186]. It is worthy of note that this strategy has been employed in numerous studies for the treatment of water and wastewater [187–190]. For instance, Chen and coworkers synthesized Fe_3O_4@TiO_2 nanospheres and tested same for the photodegradation of Rhodamine B (RhB). The nanospheres demonstrated high crystallinity degree and excellent magnetic properties that enabled the recovery of the nanospheres by magnetization. Following UV irradiation of the nanospheres, the intensity of the absorption maximum of RhB at 552 nm decreased with time.

They observed that the UV-induced degradation of the RhB was initially fast and later became slow. Additionally, the Fe_3O_4@TiO_2 nanospheres could not degrade RhB in the dark, confirming that the degradation process was photo-induced. The degradation of RhB was also observed to be very slow in the absence of the photocatalyst. Taken together, the 95% degradation of the RhB dye in 60 minutes recorded with the nanospheres was superior to the 55% degradation recorded with a commercial photocatalyst (P25), thus confirming the excellent synergy between the Fe_3O_4 and TiO_2nanoparticles.

Other researchers have also proposed other strategies to improve the photocatalytic ability of TiO_2 nanoparticles including surface sensitization, inclusion of an inert support, incorporation of metal ion or noble metals, transition and non-metals doping, and synthesizing nanocomposites of other nanomaterials with TiO_2 nanoparticles [183, 191]. For instance, Li et al. reported that TiO_2 nanoparticles can be doped with SiO_2 or alumina to improve its photocatalytic performance, surface area, and/or thermal stability [192]. Nano-TiO_2 can also be anchored onto carbon-based materials including carbon nanotubes (CNTs) [193–195], graphene [196–198], and carbon nanofibers [199], to obtain nanohybrids with improved photocatalytic abilities for wastewater treatment. Carbon-based materials offer suitable anchors for TiO_2 due to their fascinating chemical resistance [200], mechanical [201], thermal [202], electrical [203–205], and optical properties [206, 207], coupled with the fabrication of structures with optimized pore and surface properties [208–210], giving rise to fast charge transfer on the TiO_2/carbon hybrid composites [211, 212]. Carbon-based TiO_2 nanoparticles are not only used for the treatment of wastewater but have also been applied for the production of hydrogen by the photocatalytic water splitting [213–215], antibiotic photocatalyst [216], and photodegradation of biological pollutants [217, 218]. In particular, CNTs and graphene show potential for contributing to the enhancement of the photo-induced activities of TiO_2 nanoparticles, owing to their large surface area, decrease of electron/hole recombination, tuning band gap for visible light catalysis, and excellent active sites [219].

Some mechanisms have been proposed for the photocatalytic behavior of TiO_2/CNTs: first, the nanotubes may behave as photosensitizers by facilitating electron transfers to the surfaces of the TiO_2 nanoparticles, which might be responsible for effectively extending the photocatalytic activity of the TiO_2 to the visible light region [220, 221]. Second, the CNTs can assume the role of an effective electron sink, which is typical of p-type semiconductors [222], and also create a form of Schottky barrier (a space-charge region) at the interface of the TiO_2/CNTs. Irrespective of the fact that TiO_2 exhibits the behavior of typical n-type semiconductors, CNTs cause the movement of photo-induced electrons in the TiO_2 to freely migrate toward the direction of the CNTs, which may possess a lower Fermi level that can be likened to that of a metal [219]. Additionally, some other researchers have proposed a range of hypothesis for the TiO_2/CNTs photocatalytic mechanism [218, 223]. Application of TiO_2/nanocarbon composites in advanced oxidation processes for wastewater treatment may show good self-purification effects in comparison with ozonation and UV light irradiation. On an industrial scale, the nanocomposites are

expected to demonstrate effective wastewater treatment in advanced oxidation technologies due to the ability of the nanocarbon materials to form tight support to immobilize the TiO_2 nanoparticles, thereby inhibiting the nanoparticles loss as the fluid stream flows [224, 225].

In a study by Matsunaga and Inagaki, carbon-coated TiO_2 nanoparticles were synthesized and applied for the photodegradation of methylene blue [226]. Specifically, they mix the powders of anatase TiO_2 and poly(vinyl alcohol) in a 90/10 mass ratio and heated same at various temperatures (500, 600, 700, 800, 900, and 1000 °C) for one hour. They measured the carbon contents in the nanoparticles following combustion of same in air at 800 °C. They observed that the anatase phase of the TiO_2 remained stable up to 700 °C after carbon coating with a slight improvement in crystallinity, while carbon content was 5% by mass. Heat treatment above 800 °C commenced the phase transformation from the anatase to rutile phase with carbon content of 3.6% by mass. A complete phase transformation to the rutile phase was observed at 900 °C heat treatment. At this temperature, the rutile phase was observed to react with the coated carbon, giving rise to a reduced TiO_2 phase identified as Ti_9O_{17} following the X-ray diffraction analysis. The heat treatment up to 1000 °C was dominated by the Ti_9O_{17} with a small carbon content of 1.4 wt%. The methylene blue photodegradation at room temperature and concentration of 1.4×10^5 mol/l under 1 mW/cm^2 UV irradiation was best observed with the carbon-coated TiO_2 nanoparticles after 800 °C heat treatment. They also observed a reduction in the photodegradation rate constant for the methylene blue at temperatures higher than 800 °C, attributed to the dominance of the reduced TiO_2 phase (Ti_9O_{17}). In another study, chitosan–TiO_2 nanocomposite fibers were synthesized and applied for the degradation of organic contaminants in wastewater [227]. Various TiO_2 loadings (1, 5, 10,15, and 20 wt%) were used to understand the effect of varying the concentration of TiO_2 on the photocatalytic property of the nanocomposite fibers. The researchers separately kept each chitosan–TiO_2 nanocomposite fibers formulation in each salt solution of $CuSO_4$, $NiSO_4$, $AgNO_3$, and $CoNO_3$ and observed that the metal ions of the salts (Cu^{2+}, Ni^+, Ag^+, and Co^{2+} ions) were loaded onto the nanocomposite fibers. This led to the reduction of these ions to their corresponding zero-valent metal nanoparticles (ZV-MNPs) such as Cu^0, Ni^0, Ag^0, and Co^0, following a $NaBH_4$ treatment. The ZV-MNPs-templated chitosan–TiO_2 fibers were then applied for the photo-induced degradation of some organic dyestuffs (methyl orange, methylene blue, acridine orange, and congo red) and nitrophenols including 2-nitrophenol, 3-nitrophenol, 4-nitrophenol, and 2,6-dinitrophenol. Among all the tested ZV-MNPs-templated chitosan–TiO_2 fibers, Cu^0 ZV-MNP with 15 wt% TiO_2 demonstrated the highest photocatalytic efficiency for the degradation of the organic dyes and nitrophenols. Moreover, the Cu^0 ZV-MNP-templated fibers could easily be recovered from solution after the photodegradation process by a simple pull-out of the fiber from the medium.

Furthermore, chitosan–TiO_2 nanoparticles were modified with tungstophosphoric acid (TPA) and investigated for their photobleaching activity on an organic dyestuff malachite green in a study by Rengifo-Herrera et al. [228]. Various TPA/TiO_2 to chitosan ratios (10%, 20%, 30%, and 40% w/w) were

employed in the study to determine the effect of varying the ratios on the photobleaching capacity of the photocatalysts. They observed an effective dispersion of the TPA/TiO_2 nanoparticles through the films of the chitosan by scanning electron microscopy that was coupled with energy dispersive X-ray spectroscopy. Additionally, weak interactions between the TPA/TiO_2 nanoparticles and the functional groups on the chitosan by Fourier transform infrared spectroscopy. With respect to the photobleaching of malachite green, the chitosan-TPA/TiO_2 nanoparticles with 30% w/w ratio demonstrated the highest photocatalytic activity upon exposure to UV-A and visible light. The photocatalytic effect observed with this formulation (30% w/w ratio) was higher than that recorded for chitosan films with same amount of the commercial Evonik P25. Particularly, the 30% w/w ratio formulation exhibited an excellent photobleaching performance at irradiation wavelengths above 450 nm that was accompanied by a slight fading of the color of malachite green at wavelengths above 590 nm. After five reuse cycles, the 30% w/w ratio formulation also demonstrated impressive stability and malachite green photobleaching. Notably, as a result of *N*-demethylation oxidative reactions, a hypsochromic shift was observed for the wavelength of maximum absorption for the malachite green. These researchers therefore established that the TPA–modified chitosan–TiO_2 nanoparticles could induce a solid–gas interface photobleaching of malachite green by an oxidative path, following photosensitized and photocatalytic routes.

As rapid industrialization in various countries has expanded the application of numerous synthetic dyestuffs in industrial processes to meet the ever-increasing consumer product demand. Wastewater containing industrial dye stuffs has been reported to be highly refractory due to its high concentration of organic compounds and salts, making it less biodegradable in the environment [229, 230]. In order to save the natural environment and reduce the bioaccumulation of these synthetic dyestuffs, the direct discharge of industrial wastewater to local water treatment plants or environmental waterways should be discouraged [231, 232]. Rather, the on-site pre-treatment of these industrial effluents to ensure that most of the toxic parent synthetic azo-compounds and their intermediates or derivatives are appreciably reduced before discharging same to waterways or local water treatment plants [233]. It has been pointed out in a study by Chong et al. that the main challenges for the application of photocatalytic nanoparticles in advanced industrial dye treatment are to improve the separation and ultimately recover the used photocatalysts as to prevent same from entering the environment [70]. To this end, these researchers synthesized a functional form of TiO_2–zeolite nanocomposites by a modified sol–gel method with titanium IV butoxide as the precursor and applied the nanocomposites for the enhanced treatment of industrial dye-contaminated water and the recovery of the nanocomposites after treatment. They observed that the nanocomposites-enhanced removal of the industrial dye (reactive black 5 dye) followed a pseudo-first-order reaction with a rate constant of 0.042 per minute at low concentration of the dye. This indicated that the TiO_2–zeolite nanocomposites followed an adsorption-oriented industrial dye removal by photocatalytic degradation that could benefit the removal of untreated and trace dye stuffs at the treatment stage of industrial dye wastewater.

Furthermore, it was reported that sustainable and effective treatment of the wastewater from hospitals is often challenging to environmental and wastewater engineers worldwide [234, 235]. This is because such wastewater usually contains pharmaceutical, radioactive, and chemical substances, alongside numerous pathogenic microorganisms [236, 237]. The dominance of pharmaceutical and radioactive compounds in the environment that resulted in the contamination of drinking, surface, and ground waters has been documented in the literature [238–240]. In this regard, the assessment of TiO_2 nanofibers for the treatment and biodegradability enhancement of a pharmaceutical compound (carbamazepine) in a hospital wastewater mimic was conducted in a study by Chong and Jin [56]. The hospital wastewater mimic was prepared by dissolving 5000 µg/l of the carbamazepine in municipal wastewater obtained from a water treatment facility in South Australia, while the TiO_2 nanofibers were synthesized by the hydrothermal method in NaOH, followed by an ion exchange post-synthesis in HCl. They observed that the TiO_2 nanofibers removed 78% of the carbamazepine, 23% phosphate, and 40% chemical oxygen demand (COD) within four hours. Additionally, a shift in the molecular weight of the organic fractions in the synthetic hospital wastewater from >10–1000 to <10 kDa demonstrated that the photocatalytic treatment with the TiO_2 nanofibers could appreciably enhance the biodegradability of the organic compound. Moreover, the nanofibers-mediated photodegradation profile of the carbamazepine at high concentrations in the hospital wastewater mimic was better described by the Langmuir–Hinshelwood kinetics model.

1.4.4 Air Treatment

On the other hand, air pollutants such as the nitrates and sulfur dioxide have potentials for generating persistent negative effects on human and animal health. As it is with water treatment, TiO_2 nanoparticles are the most extensively studied photocatalysts for improved air purification. The photocatalysis of TiO_2 nanoparticles stands tall as one of the various efficient advanced oxidation processes for the decomposition of microbiologically and chemically stable volatile organic compounds (VOCs). Unfortunately, advances in the photocatalysis of these nanoparticles have been significantly hindered by their relatively low surface area and poor adsorption properties for organic compounds [241]. A group of researchers reported an enhancement of the removal of NO using TiO_2 nanoparticles that were coated with carbon [226]. For this purpose, they dissolved 0.03 g of the nanoparticles in acetone under a supersonic vibration. The dissolved nanoparticles were then spread on a filter paper and exposed to an NO-containing air bubbled in a distilled water column with an NO concentration of 0.6 ppm and flow rate of 3 l/min at room temperature. The nanoparticles were illuminated with UV light for 60 minutes and another 30 minutes without illumination for 10 repeated cycles. Two UV lamps with power of 19 W and 158 mm away from the nanoparticles were used for the illumination through quartz glasses whose thickness were 5 mm. Then, the NO concentration in the

gas and that of the reaction product (NO_2) were measured by chemiluminescence at one minute interval. They observed a decrease in the NO concentration in the effluent gas within one minute of UV irradiation. Turning off the UV lamp resulted in a return of the NO concentration to its initial concentration, also within one minute. Additionally, high decomposition of NO, i.e. high photoactivity, was recorded with the carbon-coated TiO_2 nanoparticles calcined at 500 and 600 °C as against those calcined at temperatures between 700 and 1000 °C. This was attributed to the high abundance of anatase TiO_2 obtained at calcination temperatures of 500 and 600 °C, whereas the rutile phase was prominent above those temperatures, i.e. between 700 and 1000 °C. Moreover, a larger decomposition fraction value was observed in the first cycle, followed by a near-constant decomposition from the second cycle onward.

For the purpose of exploiting the high photocatalytic ability of TiO_2 nanoparticles, numerous reactor designs have been developed and tested, including honeycomb [242], carberry type [243], fluidized bed [244], and the multi-tubular type [245]. Most of these reactors employ immobilized TiO_2 on the surfaces of aluminum [243, 246], glass [247, 248], concrete [249], or carbon [250–252]. The first substrate, i.e. aluminum, is one of the most commonly used supporting materials that is mainly attributed to its ability to withstand high temperatures during the calcination process, and its high transparency. Additionally, its design ease, strength, and low price have been reported as factors that have increased the choice of aluminum substrates over others, irrespective of its seldom deactivation effect on the catalyst [253]. The deactivation effect has been attributed to its migration from the support to the catalyst with subsequent Al_2O_3 and $Al(OH)_3$ coexistence [241]. Furthermore, the application of aluminum substrate for most photocatalytic processes with TiO_2 nanoparticles has been suppressed by its sodium content, which is detrimental to TiO_2 photocatalytic property in situations whereby high temperatures are required to treat the deposited film [254, 255]. This drawback can be addressed by introducing amorphous SiO_2 layer barrier between the carrier and the TiO_2 film [256, 257] or employing the mixed film of TiO_2/SiO_2 [258, 259].

In this regard, Šuligoj et al. immobilized TiO_2 nanoparticles on porous SiO_2 substrate and investigated its air-cleaning effect [241]. These researchers used titania in aqueous solutions from two different sources: a TiO_2 sol that was prepared at low temperature at the University of Nova Gorica and a TiO_2 suspension obtained from a producer of TiO_2 at Slovenia, Cinkarna Celje. They also employed two different mesoporous SiO_2 types: SBA-15 that had an ordered arrangement of hexagonal pores and KIL-2 that had a disordered mesoporosity between the particles. These researchers then monitored the adsorption properties, photocatalytic activities, and structural characteristics of the catalysts that were deposited as thin films on aluminum plates. They observed higher air-cleaning and adsorption activities with the TiO_2 produced at Slovenia, Cinkarna Celje. They attributed this to the higher amount of Ti–OH groups on its surface in comparison with the TiO_2 sol prepared at the University of Nova Gorica. Moreover, the introduction of the mesoporous SiO_2 increased the adsorption and photocatalytic activities for both sources of the TiO_2 with the SBA-15 showing enhanced effect than the KIL-2.

In another study, nano-TiO_2 were conjugated with a metal–organic framework, NH_2-UiO-66 and applied for the purification of VOCs [260]. The TiO_2@NH_2-UiO-66 was synthesized by employing the hard–soft acid–base strategy with tunable TiO_2 size and content. It was observed that the TiO_2@NH_2-UiO-66 nanocomposites increased the separation of electrons and holes generated by UV illumination following an appreciable extension of optical absorption in comparison to bare TiO_2. This was also attributed to the intriguing interface contact between the NH_2-UiO-66 and TiO_2. Moreover, an effective diffusion of the VOCs into the pores of the outer NH_2-UiO-66 was enabled by their abundant 3D cavities that were interconnected. This was responsible for the observed high concentration microenvironment of the VOCs around the embedded TiO_2. A significantly enhanced photocatalysis and deactivation resistance in the course of the gaseous styrene photo-induced degradation under visible light irradiation was also observed. This was ascribed to the synergism between the NH_2-UiO-66 and TiO_2. Whereas the photodegradation efficiency for the removal of styrene achieved with bare TiO_2 was 32.5% in 600 minutes, up to a 99% removal ratio and efficient mineralization of the styrene to CO_2 was obtained with the TiO_2@NH_2-UiO-66 nanocomposites that possess 5 wt% TiO_2.

Since the promotion of an air-cleaning TiO_2-based paint (KNOxOUT) by Pacific Paints (Boysen) Philippines, Inc., which has the capacity of cleaning nitrogen oxides (NOx) from automobile emissions [261], research into the utility of TiO_2 nanoparticles for air purification has increased tremendously. Nitrogen oxides are known respiratory irritants and ground-state ozone precursors. For instance, Le et al. recently investigated the air-cleaning ability of a silver nanoparticles-coated air filter with TiO_2 nanoparticles [262]. The nano-TiO_2 with average size of 16–20 nm were prepared by the sol–gel synthetic strategy and placed on a porous quartz tube with a diameter of 74 mm, length of 418 mm, and deposit density of about 16.4 mg/cm^2. The formation of the photocatalytic filter tube by this deposition process was mediated by a poly(methylmethacrylate) layer. Additionally, they synthesized silver nanoparticles with average size of about 20 nm by the aqueous molecular solution method and coated same on a polypropylene pre-filter. They observed that a high VOCs, fungi, and bacteria degradation was obtained with four photocatalytic filter tubes, four UVA lamps operating at 36 W, an electrostatic air filter, and an air cleaner whose capacity was 250 m^3/h. Interestingly, this air-cleaning equipment demonstrated more than 99% killing of the microorganisms after passing air through it. Furthermore, the degradation of various VOCs differed with time. They observed a 43% oxidation of benzene in 150 minutes, and the removal of 80% acetone, 91.6% butanol, and 70.1% diethyl ether in 100, 55, and 120 minutes, respectively, using a 10 m^3 box. These researchers also tested the air-cleaning equipment in practical (real-life) condition at E Hospital, Hanoi, Vietnam. In an intensive care room, 69% and 63% bacteria and fungi, respectively, were killed in six hours using a 125 m^3 box.

Similarly, the sol–gel method was used by Haider et al. to prepare TiO_2 nanoparticles and also investigated same for air purification [263]. They employed a titanium trichloride precursor and calcinations at two temperatures (500 and 900 °C). At 500 °C, the nanoparticles were observed to have the

anatase structure, while a rutile structure was observed for the nanoparticles at 900 °C. Moreover, increasing the calcination temperature consequently increase crystallinity of the product. The indoor and outdoor air-cleaning abilities of the nanoparticles were investigated using glass substrates coated with the nanoparticles. The TiO_2 nanoparticles-coated films exhibited good permeability, optical activity, and a low water contact angle. The aforementioned properties are characteristic of materials applicable as self-cleaning agents. These researchers therefore inferred that the synthesized TiO_2 nanoparticles could be used as surface coating in microbiological sensitive areas such as hospitals and food factories to mitigate air pollution. Notwithstanding the various studies on the utility of TiO_2 nanoparticles for air cleaning, some researchers have reported that the mechanism for this application is still unclear [261, 264].

1.4.5 Energy Devices

The ever-increasing growth in nanoscience and nanotechnology research has showcased new chemical and physical properties of TiO_2 nanoparticles, thereby providing new avenues for developing nano-sized solar cells composed of TiO_2 [38]. In this regard, TiO_2 nanoparticles have been recently synthesized in various forms, wherein their surface areas are maximized to facilitate the interface reaction between the interacting media and the TiO_2 nanoparticles in photovoltaic devices [93]. Surface modification has proven to affect the interfacial energy offset and transport, charge separation, and the recombination processes of TiO_2 nanoparticles [7, 265]. Among the various TiO_2 nanoparticle forms, nanowhiskers have been reported to be the most suitable for the fabrication of solar cells and windscreens due to their enhanced charge transportation [2]. In order to enhance the effective collection of electrons that are injected into the TiO_2 nanoparticles, high electron mobility of the nanoparticles are greatly desired [38].

As a consequence of the exposed surface area and high surface reactivity of TiO_2, it undergoes physical and chemical transformations by its interaction with some environmental factors (sunlight, natural organic matter, ionic species, etc.) in practical applications [93]. This behavior has been attributed to aggregation process where e.g. either the hydroxyl groups on the TiO_2 surface interacts with various components in aqueous medium or pH variation during the photocatalytic process generates particle aggregation [266]. Therefore, an in-depth knowledge of the transformations of TiO_2 nanoparticles in aqueous irradiated suspensions is essential in understanding their photocatalytic behaviors. A general overview of the photocatalytic applications of TiO_2 nanoparticles is presented in Figure 1.7.

It has been reported that the major setback for the use of TiO_2 nanoparticles in semiconductor-based sensing devices is their relative humidity sensitivity, making the response of such sensors in environments with variable humidity to be unreliable [265]. The presence of the hydroxyl groups on the surfaces of these nanoparticles have been attributed to be responsible for these sensitivity variations [266]. The surface chemistry of TiO_2 nanoparticles is rather complex and highly dependent on the preparation route and the crystalline state of the

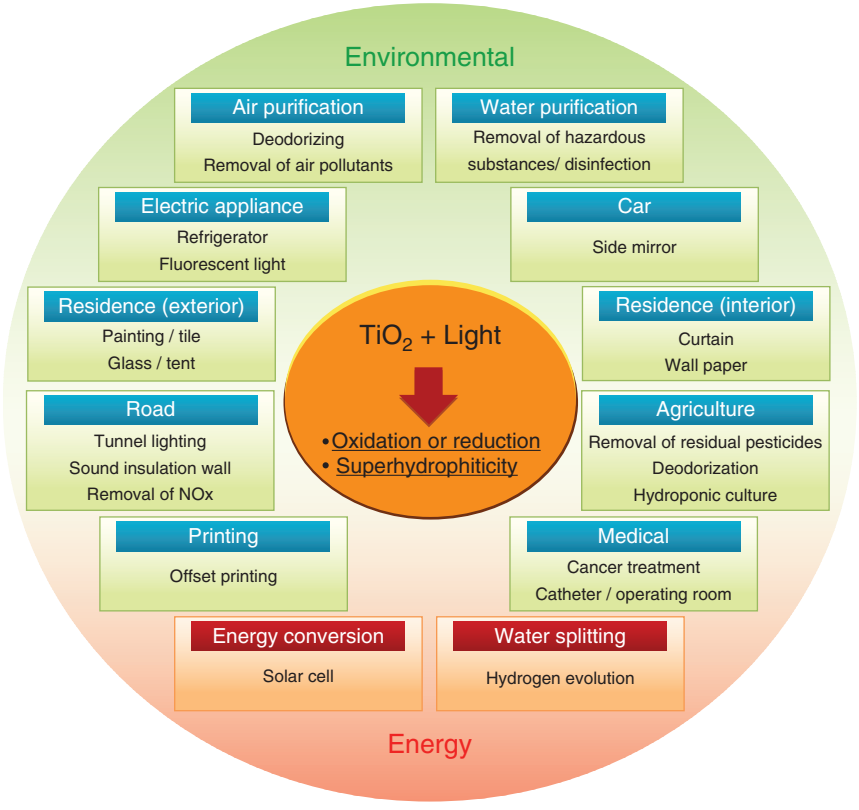

Figure 1.7 Illustration of the general photocatalytic applications of TiO_2 nanoparticles. Source: Adapted with permission from Nakata and Fujishima 2012 [36]. Copyright Elsevier Limited.

nanoparticles [267]. For the purpose of reducing the impact of these hydroxyl groups, surface modification of the TiO_2 nanoparticles were carried out by grafting with hexamethyldisilazane, thereby reducing the density of the hydroxyl groups and the cross-sensitivity of the sensor to humidity [265].

1.4.6 Water Splitting for Hydrogen Production

Chemical fuel production by the conversion of solar energy is regarded as a crucial strategy for ameliorating the present-day world energy challenges [268, 269]. Right from the early discovery of water splitting on an electrode of TiO_2 in 1972 [1], photocatalysis has attracted much interest as a promising technique for the production of environmentally friendly, clean, and low-cost hydrogen (H_2), using the solar energy [270, 271]. For an effective water splitting, titania has proven superior to other oxide semiconductor photocatalysts due to its chemical and biological inertness, environmental friendliness, long-term stability against chemical and photo-corrosion, availability, and cost effectiveness [272–275]. Owing to the fact that bare TiO_2 demonstrates relatively poor photocatalytic behavior, photocatalytic production of H_2 on TiO_2 highly depends on the

amount and nature of cocatalysts [276, 277]. This is due to the fact that TiO_2 is mainly active under UV illumination to overcome the anatase phase band gap (3.2 eV) [278] and exhibits fast e^-/h^+ recombination owing to its high trap states density [279, 280]. It then follows that appropriate band gap engineering is necessary in order to utilize TiO_2 as a semiconductor photocatalyst for enhanced H_2 production by water splitting. Earlier on, some cations such as Ag, Al, Mn, Cr, Fe, V, Sb, Nd, and Ru were employed as dopants for the effective introduction of states into the band gap of TiO_2 [281]. However, Asahi et al. reported that various issues such as enhanced centers for carrier recombination, the importance of a low-cost facility for ion-implantation, and thermal instability present obvious challenges to this technique [282]. These researchers rather suggested that nitrogen doping into the TiO_2 provides an improved avenue for band gap engineering than cationic or anionic doping. Notwithstanding, a later experimental and theoretical study raised some reservations about the suitability of the n-doping technique as the most efficient doping strategy [283]. Moreover, the reported photocatalysis of the n-doped TiO_2 for the photo-induced reduction of water to produce H_2 is relatively low [284].

In order to enhance H_2 production by water splitting with TiO_2 nanoparticles, a group of researchers added platinum (Pt) as a cocatalyst to the nanoparticles and observed an enhanced evolution of H_2 in the presence of some sacrificial reagents [37]. Unfortunately, the scarce nature and high cost of the noble metal Pt poses a challenge on the scalability of this strategy. Park et al. reported the successful synthesis of carbon-doped TiO_2 nanotubes for effective H_2 evolution [275]. The nanotubes were vertically grown and demonstrated high aspect ratios that enabled the photocleavage of water molecules in the presence of white light irradiation. They observed that the synthesized nanotube arrays also demonstrated far much higher water splitting efficiency and photocurrent density on exposure to visible light with wavelength of more than 420 nm in comparison with bare TiO_2 nanotubes. Additionally, the carbon-doped TiO_2 nanotube arrays outperformed the commercial photocatalyst (P-25) with more than 20 times higher photocurrent under visible light irradiation.

In another experiment, Chen et al. demonstrated a conceptually different strategy for the enhancement of solar absorption and its consequent utility for water splitting by black TiO_2 nanocrystals following the introduction of disorder in the nanophase surface layers by hydrogenation [89]. The TiO_2 nanocrystals were prepared with a TTIP precursor in the presence of ethanol, deionized water, an organic template Pluronic F127, and hydrochloric acid. This yielded the nanocrystals that were further calcined for six hours at 500 °C for the purpose of removing the Pluronic F127 and enhance the TiO_2 crystallization. For the purpose of introducing the disorders into the nanophase of the TiO_2, these researchers generated a porous TiO_2 nanocrystals network that was <10 nm and hydrogenated the material. The disorder-engineered nanocrystals demonstrated a shift in the absorption onset from UV to NIR region after the hydrogenation process that was accompanied by a remarkable color change. They also reported that the disorder-engineered nanocrystals showed marked photocatalytic activities such as organic compounds photo-oxidation in water and the evolution of H_2 using sacrificial donor in the presence of solar light.

Particularly, 0.2 mmol H_2 was generated by 0.02 g of the disorder-engineered black nanocrystals in one hour of solar irradiation, i.e. 10 mmol/h for every gram of the black TiO_2 photocatalyst. Notably, the production rate for H_2 reported by these researchers was higher than those of many semiconductor photocatalysts by a magnitude of about 2 orders [271, 285].

In a related experiment by Wang et al., H_2 treatment was demonstrated as an effective and facile technique to enhance the photocatalytic activity of TiO_2 nanowires for H_2 evolution by water splitting, following photoelectrochemical means [286]. These researchers annealed pristine rutile TiO_2 nanowires at different temperatures ranging from 200 to 500 °C in a H_2 atmosphere to successfully synthesize the H_2-treated rutile TiO_2 nanowires, denoted as H : TiO_2 nanowires. They observed that the H : TiO_2 nanowires demonstrated significantly improved photocurrent all through the potential window in comparison with pristine TiO_2 nanowires. More importantly, low photocurrent saturation potentials of −0.6 V versus Ag/AgCl (0.4 V versus reversible hydrogen electrode [RHE]) were obtained with the H : TiO_2 nanowires that show that these nanowires could efficiently separate and transport charges. Additionally, a photocurrent density of about 1.97 mA/cm^2 was achieved with the optimized H : TiO_2 nanowires in 1 M NaOH at −0.6 V versus Ag/AgCl in an imitated solar light illumination from a 150 W Xenon lamp, operating at 100 mW/cm^2, and coupled with a 1.5 G AM filter. The photocurrent density obtained for the H : TiO_2 nanowires corresponds to about 1.63% solar-to-H_2 efficiency. These researchers further established that a solar-to-H_2 efficiency of about 1.1% (best value for TiO_2-based photoanode) could be obtained for the H : TiO_2 nanowires. They achieved this by an integration of the spectrum of incident photon-to-current conversion efficiency (IPCE) of the nanowires with a standard 1.5 G AM solar spectrum, so as to eliminate the discrepancy between solar light and the xenon lamp irradiance. Theoretically, rutile TiO_2 (optical band gap = 3.0 eV) was predicted to afford about 2.25% photoconversion efficiency at the maximum with a 100 mW/cm^2 and 1.5 G irradiation, but the reported efficiency and photocurrent densities for TiO_2-based photoanodes still fall below this theoretical prediction [287]. The enhancement of the photocurrent for the H : TiO_2 nanowires was ascribed to an improvement in the photocatalytic activity of TiO_2 nanoparticles in the UV range as ascertained by IPCE analyses. Furthermore, the H_2 treatment increased the TiO_2 nanowire donor density by a magnitude of 3 orders, through the creation of high oxygen vacancies density that serve as effective electron donors. These researchers also obtained similar photocurrent enhancements with H_2 treated anatase TiO_2 nanotubes.

Differently, mesoporous TiO_2 nanoparticles with regular mesopore and interpenetrated systems have gained recent research interest based on their intriguing properties such as environmental benignity, tunable mesostructures and pore sizes, low cost, excellent optical and electronic properties, high specific surface areas, and good chemical stability [288–290]. Irrespective of their potentials for photoelectrochemical water splitting and application in photovoltaic cells, numerous research have focused on enhancing their photocatalytic activities by enhancing their abilities to absorb solar light, charge separation, and transport [291–293]. Additionally, several strategies such as

band gap engineering, controlling heterojunctions, optimizing exposed facets, and maximizing crystallinity have been employed for the design of performance mesoporous TiO_2 materials with improved performance [294–298]. In this regard, Zhou et al. demonstrated the simple synthesis of mesoporous black TiO_2 nanomaterials with ordered mesostructures, high crystalline anatase walls, and high surface areas [299]. The mesoporous black TiO_2 nanomaterials were synthesized by an evaporation-mediated self-assembly in combination with an encircling process with ethylenediamine. They elaborated the fact that employing a high surface area and thermally stable mesoporous TiO_2 precursor for the hydrogenation is very crucial for the fabrication of the ordered mesoporous nanomaterials. This facilitates the diffusion of H_2 gas into the TiO_2, interaction of H_2 gas with TiO_2 structures, maintains the ordered mesoporous structures, inhibits phase transformation (anatase to rutile), and crystal formation in the hydrogenation process at 500 °C. They observed that the ordered mesoporous nanomaterials possess large pore size of about 9.6 nm, high surface area of about 124 m^2/g, and large pore volume of 0.24 cm^3/g. Notably, an extension of photoactivity (from UV to visible and NIR regions) was observed for the ordered mesoporous nanomaterials. Moreover, the ordered mesoporous nanomaterials demonstrated a substantially high photocatalytic H_2 generation rate (136.2 μmol/h) approximately two times higher than the observed rate for pristine ordered mesoporous TiO_2.

Furthermore, it has been reported that the addition of a layered structure of molybdenum disulfide (MoS_2) could enhance the production of H_2 by photocatalysis with TiO_2 [300]. This may have been guided by the progress made so far on H_2 evolution with MoS_2 as an electrocatalyst [301–304]. However, the potential of MoS_2 as a cocatalyst for the evolution of H_2 by photocatalysis has only gained sporadic attention, irrespective of the high activities demonstrated by this cocatalyst in heterogeneous catalysis for H_2 production [305–307]. In a bid to exploit the potential of MoS_2 to combine with TiO_2 nanocrystals and enhance H_2 production, Xiang et al. investigated the synergistic effect of the cocatalysts MoS_2 and graphene on the photocatalytic activity of TiO_2. Graphene has also been reported in other studies as a promising cocatalyst for the evolution of H_2 by photocatalysis due to its intriguing electron mobility and specific surface area [308–311]. Leveraging the intriguing properties of graphene and MoS_2 as cocatalysts, their composite nanomaterial with TiO_2 nanocrystals were prepared following a facile two-step hydrothermal strategy employing tetrabutylorthotitanate as the precursor for TiO_2 and thiourea, graphene oxide, and sodium molybdate as precursors for the graphene/MoS_2hybrid. The TiO_2/graphene/MoS_2 nanocomposite exhibited a quantum efficiency of 9.7% under a UV irradiation of 365 nm. Additionally, a high rate for the production of H_2 (165.3 μmol/h) was obtained with the nanocomposite when the composition of the graphene/MoS_2 cocatalyst was 0.5 wt% and the graphene composition in this cocatalyst was 5.0 wt%. The high photocatalytic activity observed with the nanocomposite arose from the synergistic effect of the graphene and MoS_2 in the hybrid cocatalyst, serving as source of sites for adsorption and an electron collector, respectively.

1.4.7 Food and Cosmetics

Indeed, advances in nanoscience and nanotechnology have markedly provided benefits to various fields, including the food and cosmetic industries [312]. As such, some nanomaterials, particularly TiO_2 nanoparticles have been widely applied in food processing, packaging, nutrition, and healthcare products [313–315]. For instance, the application of TiO_2 nanoparticles in food packaging was investigated by using same as a material for the disinfection of *L. monocytogenes* biofilm-contaminated packaging surfaces [136]. It was observed that the nanoparticles decreased the formation of the biofilms by 3 log CFU/cm^2 following UV irradiation for 90 minutes.

In a related experiment, TiO_2 nanoparticles were coated on a food packaging film (low density polyethylene) and their capacity to inactivate *E. coli* was investigated under fluorescent and UV lights [316]. Under UV light, the antimicrobial effect of the nanoparticles was higher than that which was observed under fluorescent light and depended on the concentration of the nanoparticles and exposure time. Recently, Xie and Hung embedded TiO_2 nanoparticles in the biodegradable film of cellulose acetate and irradiated same with a 1.3 mW/cm^2 intensity UV light for two hours [95]. They observed that the nanoparticle-embedded film demonstrated a 1.69 log CFU/ml decrease in the growth of *E. coli*, suggesting the potential use of this film as an antibacterial food packaging material. Additionally, nano-sized TiO_2 has long been used as a food flavor enhancer and colorant in diary and confectionary products, seeds, beverages, toothpastes, and some medications [317–319].

On the other hand, TiO_2 nanoparticles are extensively used as inorganic UV absorbers in sunscreen products, enabling the application of an optically transparent film on the human skin [315, 320]. The addition of TiO_2 nanoparticles in sunscreen products has been reported to prevent skin irritation and the disruption of the endocrine system [321]. Various researchers have also quantified the amounts of these nanoparticles as useful components of sunscreen products [96, 320–322]. In the light of this, Lewicka et al. determined the elemental composition, shape, dimension, surface area, and crystal phase of TiO_2 nanoparticles in commercial sunscreen products [320]. They observed that the products contained mainly rutile nanocrystals with near-spherical or needle-like shapes and average size of about 25 nm. Similarly, Lu et al. observed anatase and rutile TiO_2 nanoparticles (~24 nm) with spherical and needle-like shapes, respectively, in commercial sunscreen samples [321]. Weir et al. also determined the presence of TiO_2 nanoparticles in various brands of commercial personal care products [96]. They reported that about 10% of TiO_2 nanoparticles by weight was found in sunscreens, while shaving creams, deodorants, and shampoos contained about 0.1 μg/mg.

In another study, Jaroenworaluck et al. synthesized silica-coated TiO_2 nanoparticles and characterized same for application in sunscreen products [315]. They observed that the non-crystalline nano-sized silica coating enhanced the UV absorption capacity of the TiO_2 nanoparticles, thereby suggesting their potential utility in enhancing the efficacy of sunscreen products.

1.4.8 Soil Remediation

The application of TiO_2 nanoparticles in agriculture is relatively new and as such requires more exploration following the gains that have already been made from the use of these nanoparticles for pesticide degradation, residue detection, and plant protection [323]. There are various interesting reports on the remediation of contaminated soil with nano-TiO_2, especially for the UV-mediated degradation of soil organic pollutants [5, 324]. Notably, environmental weathering processes including biodegradation, dissolution, and volatilization generally remove the more bioavailable and lighter hydrocarbons, while the recalcitrant and less bioavailable heavy hydrocarbons (HHCs) are left behind. Common biodegradation strategies such as slurry bioreactors and land farming have been employed to remove these HHCs from the soil [325–327]. However, these strategies are characterized by slow degradation with about two- to six-month timeframes of remediation [94]. This has been attributed to the recalcitrant structures and low biodegradabilities of the HHCs. Additionally, in some instances, depending on the nature of soil and the conditions therein, good standards for soil cleanup may not be obtained using bioremediation as a single technology. Therefore, an integration of bioremediation with advanced oxidation processes could afford less expensive and scalable enhancement of HHCs bioavailability with a consequent increase in processing capacities and treatment rates [328–330].

Nano-TiO_2 and its derivatives have also been investigated for their abilities to clean up other organic pollutants by the photocatalytic oxidation process as demonstrated in the photodegradation of diphenylarsinic acid (DPAA) using TiO_2 nanoparticles [331]. DPAA is usually formed from the leakages of arsenic weapons and pose adverse health effects to humans. Unfortunately, strategies for their remediation are still scarce. These researchers firstly studied the DPAA degradation pathway and identified arsenate as the final product. For the purpose of optimizing operational parameters for the effective removal of the DPAA including TiO_2 nanoparticles dosage, light intensity, irradiation time, and soil–water ratio, the researchers advantageously conducted 9 experiments following an orthogonal array experimental design $L_9(3)^4$, as against the conventional 81 experiments required in a one-factor-at-a-time design. They therefore reported that the optimal conditions for the treatment of 4 g contaminated soil with 20 mg/kg DPAA was 5% TiO_2 nanoparticles, light intensity of 40 mW/cm^2, irradiation time of three hours, and a soil–water ratio of 1 : 10. They observed that the aforementioned parameters yielded an 82.7% removal efficiency of the DPAA. The researchers further validated this method in nine different soil samples but changed the irradiation time to 1.5 hours and obtained removal efficiencies of 57.0–78.6%. Additionally, they observed that the removal efficiencies negatively correlated with pH, phosphorus content, electrical conductivity, and organic matter content. Furthermore, the generation of hydroxyl radicals by the TiO_2 nanoparticles as monitored by electron spin resonance (ESR) were found to be affected by the soil properties.

Wang et al. also applied the photocatalysis of TiO_2 nanoparticles in combination with nonthermal discharge plasma for the removal of *p*-nitrophenol from contaminated soil [332]. Nitrophenols are biorefractory and toxic organic

compounds that are extensively used as intermediates and raw materials for the production of pharmaceuticals, pigments, wood preservatives, dyes, rubber chemicals, pesticides, and explosives [333]. Notably, three of these nitrophenols (2,4-dinitrophenol, 2-nitrophenol, and 4-nitrophenol) had earlier been listed as priority pollutants in the US Environmental Protection Agency (USEPA) list [334]. In the study conducted on the removal of *p*-nitrophenol, Wang et al. envisaged that the photocatalysis of the TiO_2 nanoparticles could be driven by pulsed discharge plasma [332]. They reported that up to 88% of the *p*-nitrophenol was successfully removed in 10 minutes by employing this process. Enhancing the pulsed discharge voltage was also found to increase the removal efficiency of the pollutant. These researchers monitored the mineralization of the pollutant and the formation of intermediates by UV–vis spectroscopic analysis, denitrification, COx selectivity analysis, and total organic carbon. Following these techniques, they identified some intermediates, mainly benzoquinone, benzo[d][1, 2, 3]-trioxole, hydroquinone, phenol, acetic acid, NO^{2-}, NO^{3-}, formic acid, oxalic acid, and catechol. The generation of these major intermediates demonstrated the enhanced effect of the TiO_2 catalytic pulsed discharge plasma system. When compared with the plasma system alone, it was observed that the enhancements in pollutant mineralization and degradation were achieved with the generation of increased amounts of active species such as H_2O_2 and O_3 in the TiO_2 catalytic pulsed discharge plasma system.

1.4.9 Pesticides Removal

Among the organic contaminants, pesticides (insecticides, fungicides, and herbicides), i.e. formulations with wide structural variety and usually applied to targets in the field or household to achieve intended efficacy to certain fungal diseases, weeds and pests, form a large portion of these pollutants [22]. Although pesticides are used in agriculture mainly to boost crop yield, excessive usage of same may lead to adverse effects to humans and the environment at large [323]. Moreover, repeated and indiscriminate applications of pesticides causes an accumulation of pesticide residues in the area of application and biota [335]. There are numerous reports on pesticide contamination of air, land, and aquatic environments and as such pose serious treats to humans, non-target plant species, terrestrial organisms, and aquatic life [331, 336, 337]. As a consequence, tangible efforts have been made in developing appropriate strategies for the removal of these noxious chemicals and possibly destroy the bio-recalcitrant organic pollutants [335]. For this purpose, photocatalysis with semiconductors has gained meaningful research interest as a favorable strategy to remedy the problems associated with pesticide residue accumulation in the environment [338, 339]. For the past decade, TiO_2 nanoparticles have been widely investigated as photocatalytic semiconductors for the efficient degradation of pesticides [339]. Numerous research have also been conducted in order to modify TiO_2 nanoparticles for enhanced photodegradation outcomes [335, 340–342]. Following a UV light-induced photocatalytic process and TiO_2 nanoparticles, various pesticides have been reportedly degraded [343, 344].

Specifically, unmodified and modified TiO_2 nanoparticles have been used to degrade some pesticides such as imidacloprid [5], methamidophos [336], chlorfenapyr [337], atrazine [345], chlorotoluron [346], cinosulfuron [347], Diuron [324], chlorpyrifos [344], etc. For instance, Ahmari et al. demonstrated that the UV irradiation of TiO_2 nanoparticles was capable of eliminating imidacloprid in less than two hours [5]. Imidacloprid, an organic pesticide composed of nitramide, dihydroimidazole, and pyridinium attacks the central nervous system of insects, even though it poses less toxicity to humans. In order to irradiate the imidacloprid suspension and the TiO_2 nanoparticles, a UV lamp placed in a reactor was used. The reactor also comprised of a coaxial cylinder whose inner cylinder uniformly rotated at constant speed. These researchers operated the reactor in two modes; batch and continuous. In the continuous mode, the nano-TiO_2 was adequately deposited on a textile base due to the passage of the pesticide suspension through the reactor. Changes in the concentration of the pesticide was determined by UV–vis spectroscopy. They observed that the exposure of the pollutant to the nano-TiO_2 photocatalyst was increased as a consequence of the reactor design strategy with an inner rotating cylinder. This obviously caused an increase in the rate of mass transfer. Additionally, they observed that the efficiency of the irradiation increased as a result of small gap between the cylinders, thus allowing the contact between the light source and a small suspension volume.

This reactor design was also employed in another study for the removal of linear alkyl benzene sulfonate (LAS) from solution using TiO_2 nanoparticles [348]. LAS is a widely used nonionic surfactant for the production of detergents. The pollutant suspension and the TiO_2 nanoparticles were incorporated into the reactor and the changes in pollutant concentration were determined by UV–vis spectroscopy. It was reported that at high LAS concentrations, UV irradiation of the TiO_2 nanoparticles outperformed activated nano-TiO_2, whereas at low concentrations of LAS, the time required to attain pollutant elimination was markedly reduced. In another experiment, Affam and Chaudhuri investigated the degradation of three pesticides including chlorpyrifos, chlorothalonil, and cypermethrin with TiO_2 nanoparticles that was irradiated with a UVA light source at 365 nm [344]. They further determined the degradation enhancement and biodegradability index, i.e. the ratio of biological oxygen demand (BOD_5) to chemical oxygen demand (COD), following the addition of hydrogen peroxide. After 300 minutes of UVA irradiation of the TiO_2 nanoparticles (1.5 g/l) at pH 6, the removal of total oxygen demand (TOC) and COD were 8.45% and 25.95%, respectively. Following the UVA irradiation of the TiO_2 nanoparticles (1.5 g/l) in the presence of hydrogen peroxide (100 mg/l) at pH 6 for 300 minutes, the TOC and COD removal were 21.54 and 53.62, respectively. This was accompanied with an increase in biodegradability index up to 0.26. Mineralization was also observed, which was evidenced by an increase in nitrate-nitrogen from 0.70 to 13.80 mg/l and a corresponding decrease in ammonia-nitrogen from 22.00 to 7.80 mg/l in 300 minutes. They also observed that the pesticides degradation followed the pseudo-first-order kinetics with rate constants of 0.0008 and 0.0025 per minute for the removal of TOC and COD, respectively.

Žabar et al. also studied the photodegradation of imidacloprid and thiamethoxam using a photoreactor equipped with six polychromatic fluorescent lamps and glass slides immobilized with TiO_2 [349]. They observed the photodegradation of the pesticides within two hours of UV irradiation. The degradation processes were also described to follow the first-order kinetics. Additionally, the imidacloprid and thiamethoxam degradation was monitored by high performance liquid chromatography, and the mineralization efficiency was determined by measuring the total organic carbon. However, the mineralization rate was low with values of $19.1\% \pm 0.2$ and $14.4\% \pm 2.9\%$ for imidacloprid and thiamethoxam, respectively, showing that various transformation products were rather formed. These researchers further analyzed the accruing transformation products, which led to the first ever discovery of the compound clothianidin. In another study, Zhang et al. investigated the photodegradation of 4,4′-biphenol with TiO_2 nanoparticles in the presence of cyclodextrins. For the purpose of inducing the photodegradation by UV irradiation, a metal halide lamp operating at 250 W and a wavelength of 365 nm was used as the light source. They further investigated the inclusion complex of the cyclodextrins with the 4,4′-biphenol, and the adsorption of 4,4′-biphenol on the TiO_2 surface in the presence and absence of the cyclodextrins. They observed that the photocatalytic reaction was dominated by the inclusion complex behaviors of cyclodextrins with the 4,4′-biphenol. However, a large inclusion constant of 5600 per molar of 4,4′-biphenol with β-cyclodextrin accompanied with an increase in the adsorption on the TiO_2 surface resulted in an enhanced photodegradation. Conversely, an opposite effect was observed with α-cyclodextrin that was attributed to a small inclusion constant of 355 per molar.

The mechanism, degradation performance, and technical feasibility of aqueous imidacloprid were investigated in a different study by Malato et al. [350]. They utilized two photocatalytic systems on a pilot scale, since it is possible to employ natural UV light. For this purpose, homogeneous and heterogeneous photocatalysis using photo-Fenton reaction and TiO_2, respectively, were studied. The utility of equivalent field conditions and pilot scale enabled proper comparison of the toxicity and mineralization extents, and the transformation products obtained from the mineralization processes of both systems. It was observed that <2.0 mg/l (95%) mineralization was attained after 450 minutes with the TiO_2 and 250 minutes with photo-Fenton reaction. This demonstrated that the total organic carbon disappears slower (~2.4 times) with the TiO_2 than the photo-Fenton reaction. In a related study, Agüera et al. oxidized imidacloprid in water at a concentration of 50 mg/l using TiO_2 in conjunction with formulating agents [351]. The oxidized solutions were analyzed complementarily with liquid chromatography (LC)-atmospheric pressure chemical ionization (APCI)-mass spectroscopy (MS) and GC-Ion Trap-MS employing either chemical ionization (CI) or electron ionization (EI) as the ionization modes. The complementary analysis provided an avenue for adequate evaluation and confirmation of the pesticide decay and the existence of accruing degradation products. Whereas the LC-APCI-MS technique provided adequate monitoring of the imidacloprid and a degradation product (6-chloronicotinic acid) in the course of the degradation, the Gas chromatography–mass spectroscopy (GC–MS) technique enabled the

detection of five other degradation products. Unequivocally, three of these five degradation products were identified. Furthermore, other complementary analytical techniques including ion chromatography and total organic carbon were employed to evaluate the degree of mineralization. They observed that after irradiating the TiO_2 with UV light for 450 minutes, both the pesticide and its degradation products were not detected. Interestingly, a near-total mineralization was recorded after the irradiation for 700 minutes.

Higarashi and Jardim reported that Diuron in 4 cm of contaminated top soil was degraded by TiO_2 nanoparticles in a UV radiation intensity-dependent degradation rate [324]. Herbicides such as Diuron belong to a class of pesticides with wide application in agriculture. Owing to their high vapor pressure and lipid affinity, and low biodegradability, these haloaromatic pesticides are generally considered as persistent chemicals. Unfortunately, if they are accidentally or uncontrollably disposed in the soil, they stand a high chance of posing adverse health risks to humans. These researchers spiked soil samples with Diuron concentrations of 10, 50, and 100 mg/kg, loaded the soil samples with various TiO_2 concentrations (0%, 0.1%, 0.5%, 1%, and 2% w/w), and then exposed them to solar light (average intensity = 2 mW/cm at 365 nm, 47 W and 22 S). They observed that both the TiO_2 and Diuron concentrations negligibly affected the photodegradation kinetics that was largely dependent on the intensity of the radiation. These researchers further evaluated the effects of water and $Ca(OH)_2$ on the photo-induced degradation process. They also reported that the addition of water increased the degradation rate of the Diuron. On the other hand, pH increase following the addition of $Ca(OH)_2$ had no effect of the degradation rates. Additionally, the photocatalytic degradation of the pesticide obtained by combining the solar light with TiO_2 was demonstrated to be efficient.

Furthermore, the photocatalytic degradation of melathion by WO_3-modified TiO_2 nanoparticles was investigated in a study by Ramos-Delgado et al. [340]. The TiO_2 nanoparticles were synthesized by the sol–gel synthetic technique using tetrabutylorthotitanate and ammonium *p*-tungstate at a pH of 3. The TiO_2 nanoparticles were then modified with two different WO_3 percentages, i.e. 2 and 5 wt% in the presence of 2-butanol and an aging time of 48 hours. Structural analysis of the WO_3/TiO_2 photocatalysts demonstrated the dispersion of the WO_3 on the TiO_2 surface with particle sizes of 19.4 and 25.6 nm for the 2% and 5% WO_3 percentages, respectively. They also reported the 2% WO_3/TiO_2 photocatalytic formulation showed the best degradation effect, evidenced by the 76% total organic carbon reduction after 300 minutes of UV irradiation. Meanwhile, this was compared with those of bare TiO_2 and 5% WO_3/TiO_2 photocatalytic formulation that exhibited 47% and 28% mineralization, respectively. The researchers therefore established a long-term stability of the 2% WO_3/TiO_2 photocatalytic formulation following numerous successive cycles obtained in ascertaining the efficacy of the formulation after repeated use.

In a related study, nano-TiO_2 also prepared by the sol–gel synthetic technique was sulfate-modified and investigated for the degradation of methyl orange [338]. In that study, tetraisopropylorthotitanate was used as the starting material and the synthesized TiO_2 nanoparticles were promoted with different weight percentages (2.0, 2.5, 3.0, and 3.5 wt%) of sulfate, following an incipient wetness

impregnation strategy. They observed the mesoporous nature of the synthesized TiO_2 nanoparticles and established the fact that sulfate modification of the nanoparticles could reduce phase transformation and enhance the thermal stability of the nano-TiO_2. Additionally, the sulfate modification was found to decrease the crystal size and enhance the surface area of the TiO_2 nanoparticles. With respect to the degradation of the organic dyestuff, the researchers observed that the degradation efficiency obtained using the 2.5 wt% sulfate loading (61%) was about two times more than that achieved with unmodified nano-TiO_2 (33%). Moreover, the degradation profile was best described by a first-order kinetics.

1.4.10 Paint and Paper Productions

Owing to its light-scattering ability, TiO_2 stands as the most widely used white pigment in the paint and paper industries [98]. The utility of TiO_2 in the paint industry dates back to the late 1920s when the anatase phase was more dominant. In the 1940s, industrialists commenced the use of the rutile phase but with no surface treatments [352]. Today, the surface-treated rutile phase forms have practically replaced the earlier forms.

It has been demonstrated that an aged paint leachate contained appreciable amounts of TiO_2 nanoparticles [353]. The leachate was employed to investigate the phytotoxicity of TiO_2 nanoparticles to lettuce leaves by foliar exposure. Although no acute phytotoxicity was observed, TiO_2 nanoparticles were internalized in the leaves and all types of tissues of the lettuce plant, thus showcasing these nanoparticles as active components of paints. Furthermore, Kaegi et al. reported that TiO_2 nanoparticles are components of both new and aged facade paints [354]. They used a centrifugation-based sample preparation technique to recover about 20–300 nm of the nanoparticles, also emphasizing their utility in paint production. Elsewhere, the environmental fate of TiO_2 nanoparticles was investigated by comparing the impacts of pristine TiO_2 nanoparticles and those released from a TiO_2 nanoparticles-containing paint [355]. By shaking an aged paint powder in water, 580 μg/l of TiO_2 nanoparticles (average diameter of 200–300 nm) were obtained, demonstrating the actual incorporation of these nanoparticles in paint production.

In the papermaking industry, fillers are normally used to enhance the optical properties, printing quality, writability, environmental friendliness, sheet formation, and dimensional stability of papers [356]. This has increased the general interest of papermaking industries to enhance the filler contents of papers [357]. Notwithstanding, it is also very important to overcome the major drawbacks associated with the use of mineral fillers, which includes the reduction of fiber-to-fiber bonding. Obviously, the fiber-to-fiber bonding reduction induces a subsequent decrease in the strength properties of the paper and additional challenges such as dusting, white waters circulation, and retention [358]. These fillers such as TiO_2 nanoparticles, calcium carbonate, talc, and kaolin are usually mixed with the pure fiber pulp to produce the paper sheets [359]. Importantly, TiO_2 nanoparticles have been employed as fillers largely due to their fascinating refractive index, insolubility in acidic and alkaline solutions, and high

degree of whiteness [360]. To this end, Tao et al. prepared novel $CaCO_3$@TiO_2 core–shell nanoparticles and applied same as fillers in paper production [356]. They employed carbonization as a process to obtain $CaCO_3$ and the relatively cheap inorganic titanium sulfate as a precursor for the TiO_2 nanoparticles. It was observed that the $CaCO_3$@TiO_2 showed higher UV absorption capacity than either components. Additionally, the $CaCO_3$@TiO_2 filler-containing paper demonstrated a 3% improved whiteness (73.80%) than pure fiber paper (70.35%) but comparable with that of TiO_2 nanoparticle-incorporated paper (73.16%).

In a related study, Adel et al. also prepared uncoated and chitosan-coated $CaCO_3$@TiO_2 core–shell nanoparticles as fillers and coats, respectively, in paint production [99]. They also observed that the $CaCO_3$@TiO_2 nanoparticles demonstrated improved photo-stabilization of the paper after exposure to UV light. Moreover, an enhanced thermal stability of the paper was achieved by incorporating the chitosan-coated core–shell nanoparticles. This corroborates earlier reports on the improvements of TiO_2 thermal stability [227], mechanical property [361], and biodegradability following incorporation with chitosan [362]. Undoubtedly, these improvements can be attributed to the widely reported fascinating biodegradability of chitosan [227, 363, 364]. In another experiment, novel antifungal nanocomposites synthesized by incorporating chitosan and TiO_2 nanoparticles into carboxymethyl cellulose polymeric membrane were tested for their capacity to preserve the carboxymethyl cellulose in paper-art-works [365]. They investigated the antifungal activity of the nanocomposites on two commonly found fungi species in library materials: *Aspergillus niger* and *Aspergillus flavus*. They observed that the yellow color and adherence of the carboxymethyl cellulose adhesive of the paper was preserved due to the presence of the TiO_2 and chitosan nanoparticles.

1.5 Conclusion

Indeed, TiO_2 nanoparticles have been demonstrated to possess low production cost, thin film transparency, chemical and mechanical stability, bio- and chemical inertness, high light conversion efficiency, hydrophilicity, and corrosion resistance. Taking advantage of some specific properties such as their exceptional photocatalytic ability, biocompatibility, low toxicity, and production costs, these nanoparticles have been successfully applied in nanomedicine and nanobiotechnology. Interestingly, these nanoparticles can be synthesized by a wide range of methods including hydrothermal, sol–gel, thermal decomposition, vapor deposition, micelle and inverse micellar, oxidation, sonochemical, microwave-assisted, and electrodeposition methods. The vast array of synthetic methods for these nanoparticles has dramatically increased their utility in various other aspects including wastewater treatment, soil remediation, energy devices, food, cosmetics, paints, paper, antiseptics, and printing inks. Taken together, we envisage the emergence of new applications for these nanoparticles, compensating the ever-increasing research into the exploitation of their fascinating properties.

Acknowledgments

The authors would like to thank the continuous support by National Key R&D Program of China (2018YFC0910601, 2019YFA0405603), Natural Science Foundation of China (31971292, U1432114 to Aiguo Wu and 8161101589, 81950410638 to M. Zubair Iqbal), Zhejiang Province Financial Supporting (2017C03042, LY18H180011), and the Science & Technology Bureau of Ningbo City (2015B11002,2017C110022). Furthermore, the authors also acknowledge Shanghai Synchrotron Radiation Facility at Line BL15U (No. h15sr0021) for X-ray fluorescence imaging and National Synchrotron Radiation Laboratory in Hefei for soft X-ray imaging (No. 2016-HLS-PT-002193). Ozioma Udochukwu Akakuru also appreciates the Chinese Academy of Sciences (CAS) and The World Academy of Sciences (TWAS) for the award of the CAS-TWAS President's Fellowship (2017A8017422001) for PhD studies.

References

1 Fujishima, A. and Honda, K. (1972). Electrochemical photolysis of water at a semiconductor electrode. *Nature* 238: 37–38.
2 Rehman, F.U., Zhao, C., Jiang, H., and Wang, X. (2016). Biomedical applications of nano-titania in theranostics and photodynamic therapy. *Biomaterials Science* 4: 40–54.
3 Alivisatos, A.P. (1996). Semiconductor clusters, nanocrystals, and quantum dots. *Science* 271: 933.
4 Barnard, A.S., Erdin, S., Lin, Y. et al. (2006). Modeling the structure and electronic properties of TiO_2 nanoparticles. *Physical Review B* 73: 205405.
5 Ahmari, H., Heris, S.Z., and Khayyat, M.H. (2018). The effect of titanium dioxide nanoparticles and UV irradiation on photocatalytic degradation of Imidaclopride. *Environmental Technology* 39: 536–547.
6 Shehap, A.M. and Akil, D.S. (2016). Structural and optical properties of TiO_2 nanoparticles/PVA for different composites thin films. *International Journal of Nanoelectronics and Materials* 9: 17–36.
7 Chen, X. and Mao, S.S. (2007). Titanium dioxide nanomaterials: synthesis, properties, modifications, and applications. *Chemical Reviews* 107: 2891–2959.
8 Choi, H.C., Jung, Y.M., and Kim, S.B. (2005). Size effects in the Raman spectra of TiO_2 nanoparticles. *Vibrational Spectroscopy* 37: 33–38.
9 Li, Y., Zhang, S., Yu, Q., and Yin, W. (2007). The effects of activated carbon supports on the structure and properties of TiO_2 nanoparticles prepared by a sol–gel method. *Applied Surface Science* 253: 9254–9258.
10 Camps, I., Borlaf, M., Colomer, M.T. et al. (2017). Structure-property relationships for Eu doped TiO_2 thin films grown by a laser assisted technique from colloidal sols. *RSC Advances* 7: 37643–37653.
11 Trujillo-Navarrete, B., del Pilar Haro-Vázquez, M., Félix-Navarro, R.M. et al. (2017). Effect of Nd^{3+} doping on structure, microstructure, lattice distortion

and electronic properties of TiO_2 nanoparticles. *Journal of Rare Earths* 35: 259–270.

12 Çeşmeli, S. and Biray Avci, C. (2018). Application of titanium dioxide (TiO_2) nanoparticles in cancer therapies. *Journal of Drug Targeting* 27: 762–766.

13 Zeng, L., Ren, W., Xiang, L. et al. (2013). Multifunctional Fe_3O_4–TiO_2 nanocomposites for magnetic resonance imaging and potential photodynamic therapy. *Nanoscale* 5: 2107–2113.

14 Ren, W., Yan, Y., Zeng, L. et al. (2015). A near infrared light triggered hydrogenated black TiO_2 for cancer photothermal therapy. *Advanced Healthcare Materials* 4: 1526–1536.

15 Mou, J., Lin, T., Huang, F. et al. (2016). Black titania-based theranostic nanoplatform for single NIR laser induced dual-modal imaging-guided PTT/PDT. *Biomaterials* 84: 13–24.

16 Gomes, S.I.L., Roca, C.P., von der Kammer, F. et al. (2018). Mechanisms of (photo)toxicity of TiO_2 nanomaterials (NM103, NM104, NM105): using high-throughput gene expression in *Enchytraeus crypticus*. *Nanoscale* 10: 21960–21970.

17 Skocaj, M., Filipic, M., Petkovic, J., and Novak, S. (2011). Titanium dioxide in our everyday life; is it safe? *Radiology and Oncology* 45: 227–247.

18 Govindasamy, G., Murugasen, P., and Sagadevan, S. (2016). Investigations on the synthesis, optical and electrical properties of TiO_2 thin films by chemical bath deposition (CBD) method. *Materials Research* 19: 413–419.

19 Arora, B., Murar, M., and Dhumale, V. (2015). Antimicrobial potential of TiO_2 nanoparticles against MDR *Pseudomonas aeruginosa*. *Journal of Experimental Nanoscience* 10: 819–827.

20 Mo, S.-D. and Ching, W.Y. (1995). Electronic and optical properties of three phases of titanium dioxide: rutile, anatase, and brookite. *Physical Review B* 51: 13023–13032.

21 Hoang, V.V., Zung, H., and Trong, N.H.B. (2007). Structural properties of amorphous TiO_2 nanoparticles. *The European Physical Journal D* 44: 515–524.

22 Gupta, S.M. and Tripathi, M. (2011). A review of TiO_2 nanoparticles. *Chinese Science Bulletin* 56: 1639.

23 Simons, P.Y. and Dachille, F. (1967). The structure of TiO_2II, a high-pressure phase of TiO_2. *Acta Crystallographica* 23: 334–336.

24 Latroche, M., Brohan, L., Marchand, R., and Tournoux, M. (1989). New hollandite oxides: TiO_2(H) and $K_{0.06}TiO_2$. *Journal of Solid State Chemistry* 81: 78–82.

25 Kingon, A.I., Maria, J.-P., and Streiffer, S.K. (2000). Alternative dielectrics to silicon dioxide for memory and logic devices. *Nature* 406: 1032–1038.

26 Li, W., Ni, C., Lin, H. et al. (2004). Size dependence of thermal stability of TiO_2 nanoparticles. *Journal of Applied Physics* 96: 6663–6668.

27 Dambournet, D., Belharouak, I., and Amine, K. (2010). Tailored preparation methods of TiO_2 anatase, rutile, brookite: mechanism of formation and electrochemical properties. *Chemistry of Materials* 22: 1173–1179.

28 Selloni, A. (2008). Anatase shows its reactive side. *Nature Materials* 7: 613.

29 Tripathi, A.K., Singh, M.K., Mathpal, M.C. et al. (2013). Study of structural transformation in TiO_2 nanoparticles and its optical properties. *Journal of Alloys and Compounds* 549: 114–120.

30 Arbiol, J., Cerdà, J., Dezanneau, G. et al. (2002). Effects of Nb doping on the TiO_2 anatase-to-rutile phase transition. *Journal of Applied Physics* 92: 853–861.

31 Zhang, Q., Gao, L., and Guo, J. (2000). Effects of calcination on the photocatalytic properties of nanosized TiO_2 powders prepared by $TiCl_4$ hydrolysis. *Applied Catalysis B* 26: 207–215.

32 Christy, P.D., Jothi, N.S.N., Melikechi, N., and Sagayaraj, P. (2009). Synthesis, structural and optical properties of well dispersed anatase TiO_2 nanoparticles by non-hydrothermal method. *Crystal Research and Technology* 44: 484–488.

33 Auvinen, S., Alatalo, M., Haario, H. et al. (2011). Size and shape dependence of the electronic and spectral properties in TiO_2 nanoparticles. *The Journal of Physical Chemistry C* 115: 8484–8493.

34 Shaikh, S.F., Mane, R.S., Min, B.K. et al. (2016). D-sorbitol-induced phase control of TiO_2 nanoparticles and its application for dye-sensitized solar cells. *Scientific Reports* 6: 20103.

35 Fujishima, A., Zhang, X., and Tryk, D.A. (2008). TiO_2 photocatalysis and related surface phenomena. *Surface Science Reports* 63: 515–582.

36 Nakata, K. and Fujishima, A. (2012). TiO_2 photocatalysis: design and applications. *Journal of Photochemistry and Photobiology C* 13: 169–189.

37 Carp, O., Huisman, C.L., and Reller, A. (2004). Photoinduced reactivity of titanium dioxide. *Progress in Solid State Chemistry* 32: 33–177.

38 Bai, Y., Mora-Seró, I., De Angelis, F. et al. (2014). Titanium dioxide nanomaterials for photovoltaic applications. *Chemical Reviews* 114: 10095–10130.

39 Gogos, A., Knauer, K., and Bucheli, T.D. (2012). Nanomaterials in plant protection and fertilization: current state, foreseen applications, and research priorities. *Journal of Agricultural and Food Chemistry* 60: 9781–9792.

40 Kumar, S.G. and Devi, L.G. (2011). Review on modified TiO_2 photocatalysis under UV/visible light: selected results and related mechanisms on interfacial charge carrier transfer dynamics. *The Journal of Physical Chemistry A* 115: 13211–13241.

41 Ikeda, K., Sakai, H., Baba, R. et al. (1997). Photocatalytic reactions involving radical chain reactions using microelectrodes. *The Journal of Physical Chemistry B* 101: 2617–2620.

42 Löberg, J., Perez Holmberg, J., Mattisson, I. et al. (2013). Electronic properties of TiO_2 nanoparticles films and the effect on apatite-forming ability. *International Journal of Dentistry* 2013: 139615.

43 Park, J.Y. and Davies, J.E. (2000). Red blood cell and platelet interactions with titanium implant surfaces. *Clinical Oral Implants Research* 11: 530–539.

44 Nasikhudin, E.P., Diantoro, M., Kusumaatmaja, A., and Triyana, K. (2018). Study on photocatalytic properties of TiO_2 nanoparticle in various pH condition. *Journal of Physics: Conference Series* 1011: 012069.

45 Tański, T., Matysiak, W., and Krzemiński, Ł. (2017). Analysis of optical properties of TiO_2 nanoparticles and PAN/TiO_2 composite nanofibers. *Materials and Manufacturing Processes* 32: 1218–1224.

46 Feng, X., Zhai, J., and Jiang, L. (2005). The fabrication and switchable superhydrophobicity of TiO_2 nanorod films. *Angewandte Chemie International Edition* 44: 5115–5118.

47 Chae, S.Y., Park, M.K., Lee, S.K. et al. (2003). Preparation of size-controlled TiO_2 nanoparticles and derivation of optically transparent photocatalytic films. *Chemistry of Materials* 15: 3326–3331.

48 Yang, Z., Choi, D., Kerisit, S. et al. (2009). Nanostructures and lithium electrochemical reactivity of lithium titanites and titanium oxides: a review. *Journal of Power Sources* 192: 588–598.

49 Dawson, G., Chen, W., Zhang, T. et al. (2010). A study on the effect of starting material phase on the production of trititanate nanotubes. *Solid State Sciences* 12: 2170–2176.

50 Yan, J., Feng, S., Lu, H. et al. (2010). Alcohol induced liquid-phase synthesis of rutile titania nanotubes. *Materials Science and Engineering B* 172: 114–120.

51 Mozia, S. (2010). Application of temperature modified titanate nanotubes for removal of an azo dye from water in a hybrid photocatalysis-MD process. *Catalysis Today* 156: 198–207.

52 Bavykin, D.V., Parmon, V.N., Lapkin, A.A., and Walsh, F.C. (2004). The effect of hydrothermal conditions on the mesoporous structure of TiO_2 nanotubes. *Journal of Materials Chemistry* 14: 3370–3377.

53 Viet, P.V., Hieu, L.V., and Thi, C.M. (2016). The directed preparation of TiO_2 nanotubes film on FTO substrate via hydrothermal method for gas sensing application. *AIMS Materials Science* 3: 460–469.

54 Zhang, Y.X., Li, G.H., Jin, Y.X. et al. (2002). Hydrothermal synthesis and photoluminescence of TiO_2 nanowires. *Chemical Physics Letters* 365: 300–304.

55 Zhang, Q. and Gao, L. (2003). Preparation of oxide nanocrystals with tunable morphologies by the moderate hydrothermal method: insights from rutile TiO_2. *Langmuir* 19: 967–971.

56 Chong, M.N. and Jin, B. (2012). Photocatalytic treatment of high concentration carbamazepine in synthetic hospital wastewater. *Journal of Hazardous Materials* 199–200: 135–142.

57 Cao, X., Jing, W., Xing, W. et al. (2011). Fabrication of a visible-light response mesoporous TiO_2 membrane with superior water permeability via a weak alkaline sol–gel process. *Chemical Communications* 47: 3457–3459.

58 Chen, X. (2009). Titanium dioxide nanomaterials and their energy applications. *Chinese Journal of Catalysis* 30: 839–851.

59 Bessekhouad, Y., Robert, D., and Weber, J.V. (2003). Synthesis of photocatalytic TiO_2 nanoparticles: optimization of the preparation conditions. *Journal of Photochemistry and Photobiology A* 157: 47–53.

60 Wang, C., Deng, Z.-X., Zhang, G. et al. (2002). Synthesis of nanocrystalline TiO_2 in alcohols. *Powder Technology* 125: 39–44.

61 Miao, L., Tanemura, S., Toh, S. et al. (2004). Heating-sol–gel template process for the growth of TiO_2 nanorods with rutile and anatase structure. *Applied Surface Science* 238: 175–179.

62 Lopez, T., Ortiz, E., Alvarez, M. et al. (2010). Study of the stabilization of zinc phthalocyanine in sol–gel TiO_2 for photodynamic therapy applications. *Nanomedicine: Nanotechnology, Biology, and Medicine* 6: 777–785.

63 López, T., Ortiz, E., Guevara, P. et al. (2014). Physicochemical characterization of functionalized-nanostructured-titania as a carrier of copper complexes for cancer treatment. *Materials Chemistry and Physics* 146: 37–49.

64 Lin, Y., Wu, G.S., Yuan, X.Y. et al. (2003). Fabrication and optical properties of TiO_2 nanowire arrays made by sol gel electrophoresis deposition into anodic alumina membranes. *Journal of Physics* 15: 2917–2922.

65 Lee, S., Jeon, C., and Park, Y. (2004). Fabrication of TiO_2 tubules by template synthesis and hydrolysis with water vapor. *Chemistry of Materials* 16: 4292–4295.

66 Liu, S.M., Gan, L.M., Liu, L.H. et al. (2002). Synthesis of single-crystalline TiO_2 nanotubes. *Chemistry of Materials* 14: 1391–1397.

67 Sugimoto, T., Zhou, X., and Muramatsu, A. (2003). Synthesis of uniform anatase TiO_2 nanoparticles by gel–sol method. 3. Formation process and size control. *Journal of Colloid and Interface Science* 259: 43–52.

68 Mahshid, S., Askari, M., Sasani Ghamsari, M. et al. (2009). Mixed-phase TiO_2 nanoparticles preparation using sol–gel method. *Journal of Alloys and Compounds* 478: 586–589.

69 Hussain, M., Ceccarelli, R., Marchisio, D.L. et al. (2010). Synthesis, characterization, and photocatalytic application of novel TiO_2 nanoparticles. *Chemical Engineering Journal* 157: 45–51.

70 Chong, M.N., Tneu, Z.Y., Poh, P.E. et al. (2015). Synthesis, characterisation and application of TiO_2–zeolite nanocomposites for the advanced treatment of industrial dye wastewater. *Journal of the Taiwan Institute of Chemical Engineers* 50: 288–296.

71 Chong, M.N. and Jin, B. (2012). Sol–gel synthesis of inorganic mesostructured composite photocatalyst for water purification: an insight into the synthesis fundamentals, reaction, and binding mechanisms. *Synthesis and Reactivity in Inorganic, Metal-Organic, and Nano-Metal Chemistry* 42: 68–75.

72 Ranga Rao, A. and Dutta, V. (2007). Low-temperature synthesis of TiO_2 nanoparticles and preparation of TiO_2 thin films by spray deposition. *Solar Energy Materials and Solar Cells* 91: 1075–1080.

73 Li, X.L., Peng, Q., Yi, J.X. et al. (2006). Near monodisperse TiO_2 nanoparticles and nanorods. *Chemistry (Weinheim an der Bergstrasse, Germany)* 12: 2383–2391.

74 Kim, C.-S., Moon, B.K., Park, J.-H. et al. (2003). Solvothermal synthesis of nanocrystalline TiO_2 in toluene with surfactant. *Journal of Crystal Growth* 257: 309–315.

75 Ayllón, J.A., Figueras, A., Garelik, S. et al. (1999). Preparation of TiO_2 powder using titanium tetraisopropoxide decomposition in a plasma enhanced

chemical vapor deposition (PECVD) reactor. *Journal of Materials Science Letters* 18: 1319–1321.

76 Seifried, S., Winterer, M., and Hahn, H. (2000). Nanocrystalline titania films and particles by chemical vapor synthesis. *Chemical Vapor Deposition* 6: 239–244.

77 Baghgar, M., Abdi, Y., and Arzi, E. (2009). Fabrication of low-pressure field ionization gas sensor using bent carbon nanotubes. *Journal of Physics D* 42: 135502.

78 Borras, A., Sanchez-Valencia, J.R., Widmer, R. et al. (2009). Growth of crystalline TiO_2 by plasma enhanced chemical vapor deposition. *Crystal Growth and Design* 9: 2868–2876.

79 Wu, J.-J. and Yu, C.-C. (2004). Aligned TiO_2 nanorods and nanowalls. *The Journal of Physical Chemistry B* 108: 3377–3379.

80 Pradhan, S.K., Reucroft, P.J., Yang, F., and Dozier, A. (2003). Growth of TiO_2 nanorods by metalorganic chemical vapor deposition. *Journal of Crystal Growth* 256: 83–88.

81 Xiang, B., Zhang, Y., Wang, Z. et al. (2005). Field-emission properties of TiO_2 nanowire arrays. *Journal of Physics D* 38: 1152–1155.

82 Wu, J.-M., Shih, H.C., and Wu, W.-T. (2005). Electron field emission from single crystalline TiO_2 nanowires prepared by thermal evaporation. *Chemical Physics Letters* 413: 490–494.

83 Ritala, M., Leskela, M., Niinisto, L., and Haussalo, P. (1993). Titanium isopropoxide as a precursor in atomic layer epitaxy of titanium dioxide thin films. *Chemistry of Materials* 5: 1174–1181.

84 Moravec, P., Smolík, J., and Levdansky, V.V. (2001). Preparation of TiO_2 fine particles by thermal decomposition of titanium tetraisopropoxide vapor. *Journal of Materials Science Letters* 20: 2033–2037.

85 Im, J.H., Kang, E., Yang, S.J. et al. (2014). Simple preparation of anatase titanium dioxide nanoparticles by heating titanium–organic frameworks. *Bulletin of the Korean Chemical Society* 35: 2477–2480.

86 Savinkina, E.V., Obolenskaya, L.N., Kuzmicheva, G.M. et al. (2018). Effects of peroxo precursors and annealing temperature on properties and photocatalytic activity of nanoscale titania. *Journal of Materials Research* 33: 1422–1432.

87 Varghese, O.K., Gong, D., Paulose, M. et al. (2011). Crystallization and high-temperature structural stability of titanium oxide nanotube arrays. *Journal of Materials Research* 18: 156–165.

88 Kim, H., Noh, K., Choi, C. et al. (2011). Extreme superomniphobicity of multiwalled 8 nm TiO_2 nanotubes. *Langmuir* 27: 10191–10196.

89 Chen, X., Liu, L., Yu, P.Y., and Mao, S.S. (2011). Increasing solar absorption for photocatalysis with black hydrogenated titanium dioxide nanocrystals. *Science* 331: 746.

90 Wu, J.M., Zhang, T.W., Zeng, Y.W. et al. (2005). Large-scale preparation of ordered titania nanorods with enhanced photocatalytic activity. *Langmuir* 21: 6995–7002.

91 Peng, X. and Chen, A. (2004). Aligned TiO_2 nanorod arrays synthesized by oxidizing titanium with acetone. *Journal of Materials Chemistry* 14: 2542–2548.

92 Maness, P.C., Smolinski, S., Blake, D.M. et al. (1999). Bactericidal activity of photocatalytic TiO_2 reaction: toward an understanding of its killing mechanism. *Applied and Environmental Microbiology* 65: 4094–4098.

93 Carbajo, J., Tolosana-Moranchel, A., Casas, J.A. et al. (2018). Analysis of photoefficiency in TiO_2 aqueous suspensions: effect of titania hydrodynamic particle size and catalyst loading on their optical properties. *Applied Catalysis B* 221: 1–8.

94 Yang, Y., Javed, H., Zhang, D. et al. (2017). Merits and limitations of TiO_2-based photocatalytic pretreatment of soils impacted by crude oil for expediting bioremediation. *Frontiers of Chemical Science and Engineering* 11: 387–394.

95 Xie, J. and Hung, Y.-C. (2018). UV-A activated TiO_2 embedded biodegradable polymer film for antimicrobial food packaging application. *LWT* 96: 307–314.

96 Weir, A., Westerhoff, P., Fabricius, L. et al. (2012). Titanium dioxide nanoparticles in food and personal care products. *Environmental Science and Technology* 46: 2242–2250.

97 Ahmed, S.N. and Haider, W. (2018). Heterogeneous photocatalysis and its potential applications in water and wastewater treatment: a review. *Nanotechnology* 29: 342001.

98 Karlsson, M.C.F., Álvarez-Asencio, R., Bordes, R. et al. (2018). Characterization of paint formulated using secondary TiO_2 pigments recovered from waste paint. *Journal of Coatings Technology and Research* 16: 607–617.

99 Adel, A.M., Ahmed, N.M., Diab, M.A., and Selim, M.M. (2016). The influence of TiO_2/CC core/shell pigments on the properties of paper sheets. *Powder Technology* 291: 437–447.

100 Carneiro, J.O., Teixeira, V., Portinha, A. et al. (2007). Iron-doped photocatalytic TiO_2 sputtered coatings on plastics for self-cleaning applications. *Materials Science and Engineering B* 138: 144–150.

101 Obritsch, M.D., Fish, D.N., MacLaren, R., and Jung, R. (2005). Nosocomial infections due to multidrug-resistant *Pseudomonas aeruginosa*: epidemiology and treatment options. *Pharmacotherapy* 25: 1353–1364.

102 Mesaros, N., Nordmann, P., Plesiat, P. et al. (2007). *Pseudomonas aeruginosa*: resistance and therapeutic options at the turn of the new millennium. *Clinical Microbiology and Infection* 13: 560–578.

103 Gottlieb, T. and Nimmo, G.R. (2011). Antibiotic resistance is an emerging threat to public health: an urgent call to action at the Antimicrobial Resistance Summit 2011. *The Medical Journal of Australia* 194: 281–283.

104 Davies, J. and Davies, D. (2010). Origins and evolution of antibiotic resistance. *Microbiology and Molecular Biology Reviews* 74: 417–433.

105 Falagas, M.E. and Bliziotis, I.A. (2007). Pandrug-resistant Gram-negative bacteria: the dawn of the post-antibiotic era? *International Journal of Antimicrobial Agents* 29: 630–636.

106 Jesline, A., John, N.P., Narayanan, P.M. et al. (2015). Antimicrobial activity of zinc and titanium dioxide nanoparticles against biofilm-producing methicillin-resistant *Staphylococcus aureus*. *Applied Nanoscience* 5: 157–162.

107 Hamming, L.M., Qiao, R., Messersmith, P.B., and Brinson, L.C. (2009). Effects of dispersion and interfacial modification on the macroscale properties of TiO_2 polymer matrix nanocomposites. *Composites Science and Technology* 69: 1880–1886.

108 Kubacka, A., Ferrer, M., and Fernández-García, M. (2012). Kinetics of photocatalytic disinfection in TiO_2-containing polymer thin films: UV and visible light performances. *Applied Catalysis B* 121–122: 230–238.

109 Kubacka, A., Serrano, C., Ferrer, M. et al. (2007). High-performance dual-action polymer-TiO_2 nanocomposite films via melting processing. *Nano Letters* 7: 2529–2534.

110 Kubacka, A., Ferrer, M., Cerrada, M.L. et al. (2009). Boosting TiO_2-anatase antimicrobial activity: polymer-oxide thin films. *Applied Catalysis B* 89: 441–447.

111 Josset, S., Keller, N., Lett, M.-C. et al. (2008). Numeration methods for targeting photoactive materials in the UV-A photocatalytic removal of microorganisms. *Chemical Society Reviews* 37: 744–755.

112 Wiener, J., Quinn, J.P., Bradford, P.A. et al. (1999). Multiple antibiotic–resistant *Klebsiella* and *Escherichia coli* in nursing homes. *Journal of the American Medical Association* 281: 517–523.

113 AshaRani, P.V., Low Kah Mun, G., Hande, M.P., and Valiyaveettil, S. (2009). Cytotoxicity and genotoxicity of silver nanoparticles in human cells. *ACS Nano* 3: 279–290.

114 Llorens, A., Lloret, E., Picouet, P.A. et al. (2012). Metallic-based micro and nanocomposites in food contact materials and active food packaging. *Trends in Food Science and Technology* 24: 19–29.

115 Huang, Y.-Y., Choi, H., Kushida, Y. et al. (2016). Broad-spectrum antimicrobial effects of photocatalysis using titanium dioxide nanoparticles are strongly potentiated by addition of potassium iodide. *Antimicrobial Agents and Chemotherapy* 60: 5445.

116 Kubacka, A., Diez, M.S., Rojo, D. et al. (2014). Understanding the antimicrobial mechanism of TiO_2-based nanocomposite films in a pathogenic bacterium. *Scientific Reports* 4: 4134.

117 Matsunaga, T., Tomoda, R., Nakajima, T., and Wake, H. (1985). Photoelectrochemical sterilization of microbial cells by semiconductor powders. *FEMS Microbiology Letters* 29: 211–214.

118 Gogniat, G. and Dukan, S. (2007). TiO_2 photocatalysis causes DNA damage via Fenton reaction-generated hydroxyl radicals during the recovery period. *Applied and Environmental Microbiology* 73: 7740–7743.

119 Foster, H.A., Ditta, I.B., Varghese, S., and Steele, A. (2011). Photocatalytic disinfection using titanium dioxide: spectrum and mechanism of antimicrobial activity. *Applied Microbiology and Biotechnology* 90: 1847–1868.

120 Kiwi, J. and Nadtochenko, V. (2005). Evidence for the mechanism of photocatalytic degradation of the bacterial wall membrane at the TiO_2 interface by ATR-FTIR and laser kinetic spectroscopy. *Langmuir* 21: 4631–4641.

121 Amézaga-Madrid, P., Nevárez-Moorillón, G.V., Orrantia-Borunda, E., and Miki-Yoshida, M. (2002). Photoinduced bactericidal activity against *Pseudomonas aeruginosa* by TiO_2 based thin films. *FEMS Microbiology Letters* 211: 183–188.

122 Vatansever, F., de Melo, W.C.M.A., Avci, P. et al. (2013). Antimicrobial strategies centered around reactive oxygen species – bactericidal antibiotics, photodynamic therapy, and beyond. *FEMS Microbiology Reviews* 37: 955–989.

123 Maillard, J.-Y. (2002). Bacterial target sites for biocide action. *Journal of Applied Microbiology* 92: 16S–27S.

124 Rai, M., Yadav, A., and Gade, A. (2009). Silver nanoparticles as a new generation of antimicrobials. *Biotechnology Advances* 27: 76–83.

125 Noimark, S., Dunnill, C.W., Wilson, M., and Parkin, I.P. (2009). The role of surfaces in catheter-associated infections. *Chemical Society Reviews* 38: 3435–3448.

126 Appendini, P. and Hotchkiss, J.H. (2002). Review of antimicrobial food packaging. *Innovative Food Science & Emerging Technologies* 3: 113–126.

127 Duncan, T.V. (2011). Applications of nanotechnology in food packaging and food safety: barrier materials, antimicrobials and sensors. *Journal of Colloid and Interface Science* 363: 1–24.

128 Dunlop, P.S.M., Sheeran, C.P., Byrne, J.A. et al. (2010). Inactivation of clinically relevant pathogens by photocatalytic coatings. *Journal of Photochemistry and Photobiology A* 216: 303–310.

129 Yin, R., Agrawal, T., Khan, U. et al. (2015). Antimicrobial photodynamic inactivation in nanomedicine: small light strides against bad bugs. *Nanomedicine (London, England)* 10: 2379–2404.

130 Hamblin, M.R. and Hasan, T. (2004). Photodynamic therapy: a new antimicrobial approach to infectious disease? *Photochemical & Photobiological Sciences* 3: 436–450.

131 McCoy, C.P., O'Neil, E.J., Cowley, J.F. et al. (2014). Photodynamic antimicrobial polymers for infection control. *PLoS One* 9: e108500.

132 Bezman, S.A., Burtis, P.A., Izod, T.P.J., and Thayer, M.A. (1978). Photodynamic inactivation of *E. coli* by rose bengal immobilized on polystyrene beads. *Photochemistry and Photobiology* 28: 325–329.

133 Vecchio, D., Gupta, A., Huang, L. et al. (2015). Bacterial photodynamic inactivation mediated by methylene blue and red light is enhanced by synergistic effect of potassium iodide. *Antimicrobial Agents and Chemotherapy* 59: 5203–5212.

134 Wu, X., Huang, Y.-Y., Kushida, Y. et al. (2016). Broad-spectrum antimicrobial photocatalysis mediated by titanium dioxide and UVA is potentiated by addition of bromide ion via formation of hypobromite. *Free Radical Biology and Medicine* 95: 74–81.

135 Shah, M.S.A.S., Nag, M., Kalagara, T. et al. (2008). Silver on PEG-PU-TiO_2 polymer nanocomposite films: an excellent system for antibacterial applications. *Chemistry of Materials* 20: 2455–2460.

136 Chorianopoulos, N.G., Tsoukleris, D.S., Panagou, E.Z. et al. (2011). Use of titanium dioxide (TiO_2) photocatalysts as alternative means for *Listeria*

monocytogenes biofilm disinfection in food processing. *Food Microbiology* 28: 164–170.

137 Tsuang, Y.-H., Sun, J.-S., Huang, Y.-C. et al. (2008). Studies of photokilling of bacteria using titanium dioxide nanoparticles. *Artificial Organs* 32: 167–174.

138 Gosselin, R.A., Roberts, I., and Gillespie, W.J. (2004). Antibiotics for preventing infection in open limb fractures. *The Cochrane Database of Systematic Reviews* https://doi.org/10.1002/14651858.CD003764.pub2.

139 Lethaby, A., Temple, J., and Santy-Tomlinson, J. (2013). Pin site care for preventing infections associated with external bone fixators and pins. *The Cochrane Database of Systematic Reviews* https://doi.org/10.1002/14651858.CD004551.pub3.

140 Bosetti, M., Masse, A., Tobin, E., and Cannas, M. (2002). Silver coated materials for external fixation devices: *in vitro* biocompatibility and genotoxicity. *Biomaterials* 23: 887–892.

141 Collinge, C.A., Goll, G., Seligson, D., and Easley, K.J. (1994). Pin tract infections: silver vs uncoated pins. *Orthopedics* 17: 445–448.

142 Kühn, K.P., Chaberny, I.F., Massholder, K. et al. (2003). Disinfection of surfaces by photocatalytic oxidation with titanium dioxide and UVA light. *Chemosphere* 53: 71–77.

143 Watts, R.J., Kong, S., Orr, M.P. et al. (1995). Photocatalytic inactivation of coliform bacteria and viruses in secondary wastewater effluent. *Water Research* 29: 95–100.

144 Wei, C., Lin, W.Y., Zainal, Z. et al. (1994). Bactericidal activity of TiO_2 photocatalyst in aqueous media: toward a solar-assisted water disinfection system. *Environmental Science and Technology* 28: 934–938.

145 Yurt, F., Ince, M., Colak, S.G. et al. (2017). Investigation of *in vitro* PDT activities of zinc phthalocyanine immobilised TiO_2 nanoparticles. *International Journal of Pharmaceutics* 524: 467–474.

146 Yurt, F., Sarı, F.A., Ince, M. et al. (2018). Photodynamic therapy and nuclear imaging activities of SubPhthalocyanine integrated TiO_2 nanoparticles. *Journal of Photochemistry and Photobiology A* 367: 45–55.

147 Hou, Z., Zhang, Y., Deng, K. et al. (2015). UV-emitting upconversion-based TiO_2 photosensitizing nanoplatform: near-infrared light mediated *in vivo* photodynamic therapy via mitochondria-involved apoptosis pathway. *ACS Nano* 9: 2584–2599.

148 Tong, R., Lin, H., Chen, Y. et al. (2017). Near-infrared mediated chemo/photodynamic synergistic therapy with DOX-UCNPs@mSiO_2/TiO_2-TC nanocomposite. *Materials Science & Engineering C, Materials for Biological Applications* 78: 998–1005.

149 Zeng, L., Pan, Y., Tian, Y. et al. (2015). Doxorubicin-loaded $NaYF_4$:Yb/Tm-TiO_2 inorganic photosensitizers for NIR-triggered photodynamic therapy and enhanced chemotherapy in drug-resistant breast cancers. *Biomaterials* 57: 93–106.

150 Li, Q., Wang, X., Lu, X. et al. (2009). The incorporation of daunorubicin in cancer cells through the use of titanium dioxide whiskers. *Biomaterials* 30: 4708–4715.

151 Shen, S., Wu, L., Liu, J. et al. (2015). Core-shell structured Fe_3O_4@TiO_2-doxorubicin nanoparticles for targeted chemo-sonodynamic therapy of cancer. *International Journal of Pharmaceutics* 486: 380–388.

152 Yumita, N., Iwase, Y., Nishi, K. et al. (2012). Involvement of reactive oxygen species in sonodynamically induced apoptosis using a novel porphyrin derivative. *Theranostics* 2: 880–888.

153 Wang, P., Xiao, L., Wang, X. et al. (2010). Sonodynamic effects of protoporphyrin IX disodium salt on Ehrlich ascetic tumor cells. *Ultrasonics* 50: 634–638.

154 Yamaguchi, S., Kobayashi, H., Narita, T. et al. (2011). Sonodynamic therapy using water-dispersed TiO_2-polyethylene glycol compound on glioma cells: comparison of cytotoxic mechanism with photodynamic therapy. *Ultrasonics Sonochemistry* 18: 1197–1204.

155 Harada, A., Ono, M., Yuba, E., and Kono, K. (2013). Titanium dioxide nanoparticle-entrapped polyion complex micelles generate singlet oxygen in the cells by ultrasound irradiation for sonodynamic therapy. *Biomaterials Science* 1: 65–73.

156 Yoshikazu, T., Mao, Y., Norimichi, K., and Tsutomu, M. (2006). Anticancer effect of dye-sensitized TiO_2 nanocrystals by polychromatic visible light irradiation. *Chemistry Letters* 35: 496–497.

157 Saeed, M., Iqbal, M.Z., Ren, W. et al. (2019). Tunable fabrication of new theranostic Fe_3O_4-black TiO_2 nanocomposites: dual wavelength stimulated synergistic imaging-guided phototherapy in cancer. *Journal of Materials Chemistry B* 7: 210–223.

158 Feng, B., Weng, J., Yang, B.C. et al. (2003). Characterization of surface oxide films on titanium and adhesion of osteoblast. *Biomaterials* 24: 4663–4670.

159 Tautzenberger, A., Kovtun, A., and Ignatius, A. (2012). Nanoparticles and their potential for application in bone. *International Journal of Nanomedicine* 7: 4545–4557.

160 Sul, Y.T. (2010). Electrochemical growth behavior, surface properties, and enhanced in vivo bone response of TiO_2 nanotubes on microstructured surfaces of blasted, screw-shaped titanium implants. *International Journal of Nanomedicine* 5: 87–100.

161 Bjursten, L.M., Rasmusson, L., Oh, S. et al. (2010). Titanium dioxide nanotubes enhance bone bonding *in vivo*. *Journal of Biomedical Materials Research Part A* 92: 1218–1224.

162 UNESCO (2018). The United Nations World Water Development Report 2018: Nature-Based Solutions for Water.

163 Kirby, R.M., Bartram, J., and Carr, R. (2003). Water in food production and processing: quantity and quality concerns. *Food Control* 14: 283–299.

164 Compton, M., Willis, S., Rezaie, B., and Humes, K. (2018). Food processing industry energy and water consumption in the Pacific northwest. *Innovative Food Science & Emerging Technologies* 47: 371–383.

165 Valta, K., Kosanovic, T., Malamis, D. et al. (2015). Overview of water usage and wastewater management in the food and beverage industry. *Desalination and Water Treatment* 53: 3335–3347.

166 Ölmez, H. (2013). Water consumption, reuse and reduction strategies in food processing. In: *Sustainable Food Processing* (eds. B.K. Tiwari, T. Norton and N.M. Holden), 401–434. USA: John Wiley and Sons Ltd.

167 Khajeh, M., Laurent, S., and Dastafkan, K. (2013). Nanoadsorbents: classification, preparation, and applications (with emphasis on aqueous media). *Chemical Reviews* 113: 7728–7768.

168 Sadjadi, S. (2014). Nanocatalytic wastewater treatment system for the removal of toxic organic compounds. In: *Nanomaterials for Environmental Protection* (eds. B.I. Kharisov, O.V. Kharissova and D. HVR), 401–427. USA: John Wiley and Sons Ltd.

169 Papageorgiou, S.K., Katsaros, F.K., Favvas, E.P. et al. (2012). Alginate fibers as photocatalyst immobilizing agents applied in hybrid photocatalytic/ultrafiltration water treatment processes. *Water Research* 46: 1858–1872.

170 Veréb, G., Manczinger, L., Oszkó, A. et al. (2013). Highly efficient bacteria inactivation and phenol degradation by visible light irradiated iodine doped TiO_2. *Applied Catalysis B: Environmental* 129: 194–201.

171 Liu, Y., Li, J., Qiu, X., and Burda, C. (2006). Novel TiO_2 nanocatalysts for wastewater purification: tapping energy from the sun. *Water Science and Technology* 54: 47–54.

172 Likodimos, V., Han, C., Pelaez, M. et al. (2013). Anion-doped TiO_2 nanocatalysts for water purification under visible Light. *Industrial and Engineering Chemistry Research* 52: 13957–13964.

173 Anjum, M., Miandad, R., Waqas, M. et al. (2016). Remediation of wastewater using various nano-materials. *Arabian Journal of Chemistry* https://doi.org/10.1016/j.arabjc.2016.10.004.

174 Rodríguez, J., Paraguay-Delgado, F., López, A. et al. (2010). Synthesis and characterization of ZnO nanorod films for photocatalytic disinfection of contaminated water. *Thin Solid Films* 519: 729–735.

175 Rajendran, S., Khan, M.M., Gracia, F. et al. (2016). Ce^{3+}-ion-induced visible-light photocatalytic degradation and electrochemical activity of ZnO/CeO_2 nanocomposite. *Scientific Reports* 6: 31641.

176 Shu, J., Wang, Z., Xia, G. et al. (2014). One-pot synthesis of AgCl@Ag hybrid photocatalyst with high photocatalytic activity and photostability under visible light and sunlight irradiation. *Chemical Engineering Journal* 252: 374–381.

177 Yang, S.-F., Niu, C.-G., Huang, D.-W. et al. (2017). $SrTiO_3$ nanocubes decorated with Ag/AgCl nanoparticles as photocatalysts with enhanced visible-light photocatalytic activity towards the degradation of dyes, phenol and bisphenol A. *Environmental Science: Nano* 4: 585–595.

178 Das, T., Rocquefelte, X., Laskowski, R. et al. (2017). Investigation of the optical and excitonic properties of the visible light-driven photocatalytic $BiVO_4$ material. *Chemistry of Materials* 29: 3380–3386.

179 Yue, Z., Liu, A., Zhang, C. et al. (2017). Noble-metal-free hetero-structural CdS/Nb_2O_5/N-doped-graphene ternary photocatalytic system as visible-light-driven photocatalyst for hydrogen evolution. *Applied Catalysis B: Environmental* 201: 202–210.

180 Zhu, Y., Wang, Y., Chen, Z. et al. (2015). Visible light induced photocatalysis on CdS quantum dots decorated TiO_2 nanotube arrays. *Applied Catalysis A: General* 498: 159–166.

181 Carbajo, J., Bahamonde, A., and Faraldos, M. (2017). Photocatalyst performance in wastewater treatment applications: towards the role of TiO_2 properties. *Molecular Catalysis* 434: 167–174.

182 Behnajady, M.A., Eskandarloo, H., Modirshahla, N., and Shokri, M. (2011). Investigation of the effect of sol–gel synthesis variables on structural and photocatalytic properties of TiO_2 nanoparticles. *Desalination* 278: 10–17.

183 Kanakaraju, D. and Wong, S.P. (2018). Photocatalytic efficiency of TiO_2-biomass loaded mixture for wastewater treatment. *Journal of Chemistry* 2018: 14.

184 Yang, X., Chen, W., Huang, J. et al. (2015). Rapid degradation of methylene blue in a novel heterogeneous Fe_3O_4 @rGO@TiO_2-catalyzed photo-Fenton system. *Scientific Reports* 5: 10632.

185 Mascolo, M.C., Pei, Y., and Ring, T.A. (2013). Room temperature co-precipitation synthesis of magnetite nanoparticles in a large pH window with different bases. *Materials (Basel)* 6: 5549–5567.

186 Upadhyay, S., Parekh, K., and Pandey, B. (2016). Influence of crystallite size on the magnetic properties of Fe_3O_4 nanoparticles. *Journal of Alloys and Compounds* 678: 478–485.

187 Chen, Y., Yuan, T., Wang, F. et al. (2016). Magnetically separable Fe_3O_4@TiO_2 nanospheres: preparation and photocatalytic activity. *Journal of Materials Science* 27: 9983–9988.

188 Han, L., Li, Q., Chen, S. et al. (2017). A magnetically recoverable Fe_3O_4-NH_2-Pd sorbent for capture of mercury from coal derived fuel gas. *Scientific Reports* 7: 7448.

189 Bagbi, Y., Sarswat, A., Mohan, D. et al. (2017). Lead and chromium adsorption from water using L-cysteine functionalized magnetite (Fe_3O_4) nanoparticles. *Scientific Reports* 7: 7672.

190 Han, S., Yu, H., Yang, T. et al. (2017). Magnetic activated-ATP@Fe_3O_4 nanocomposite as an efficient Fenton-like heterogeneous catalyst for degradation of ethidium bromide. *Scientific Reports* 7: 6070.

191 Fagan, R., McCormack, D.E., Dionysiou, D.D., and Pillai, S.C. (2016). A review of solar and visible light active TiO_2 photocatalysis for treating bacteria, cyanotoxins and contaminants of emerging concern. *Materials Science in Semiconductor Processing* 42: 2–14.

192 Li, C.-C., Chang, S.-J., and Tai, M.-Y. (2010). Surface chemistry and dispersion property of TiO_2 nanoparticles. *Journal of the American Ceramic Society* 93: 4008–4010.

193 Cong, Y., Li, X., Qin, Y. et al. (2011). Carbon-doped TiO_2 coating on multiwalled carbon nanotubes with higher visible light photocatalytic activity. *Applied Catalysis B* 107: 128–134.

194 Jeon, S., Yun, J., Lee, Y.-S., and Kim, H.-I. (2012). Preparation of poly(vinyl alcohol)/poly(acrylic acid)/TiO_2/carbon nanotube composite nanofibers and their photobleaching properties. *Journal of Industrial and Engineering Chemistry* 18: 487–491.

195 Chen, J., Li, G., Huang, Y. et al. (2012). Optimization synthesis of carbon nanotubes-anatase TiO_2 composite photocatalyst by response surface methodology for photocatalytic degradation of gaseous styrene. *Applied Catalysis B* 123–124: 69–77.

196 Yang, M.-Q., Zhang, N., and Xu, Y.-J. (2013). Synthesis of fullerene–, carbon nanotube–, and graphene–TiO_2 nanocomposite photocatalysts for selective oxidation: a comparative study. *ACS Applied Materials & Interfaces* 5: 1156–1164.

197 Perera, S.D., Mariano, R.G., Vu, K. et al. (2012). Hydrothermal synthesis of graphene-TiO_2 nanotube composites with enhanced photocatalytic activity. *ACS Catalysis* 2: 949–956.

198 Williams, G., Seger, B., and Kamat, P.V. (2008). TiO_2-graphene nanocomposites. UV-assisted photocatalytic reduction of graphene oxide. *ACS Nano* 2: 1487–1491.

199 Baek, M.-H., Jung, W.-C., Yoon, J.-W. et al. (2013). Preparation, characterization and photocatalytic activity evaluation of micro- and mesoporous TiO_2/spherical activated carbon. *Journal of Industrial and Engineering Chemistry* 19: 469–477.

200 Politano, A. and Chiarello, G. (2013). Quenching of plasmons modes in air-exposed graphene-Ru contacts for plasmonic devices. *Applied Physics Letters* 102: 201608.

201 Ahmed, K., Nizami, S.S., and Raza, N.Z. (2013). Characteristics of natural rubber hybrid composites based on marble sludge/carbon black and marble sludge/rice husk derived silica. *Journal of Industrial and Engineering Chemistry* 19: 1169–1176.

202 Nardecchia, S., Carriazo, D., Ferrer, M.L. et al. (2013). Three dimensional macroporous architectures and aerogels built of carbon nanotubes and/or graphene: synthesis and applications. *Chemical Society Reviews* 42: 794–830.

203 Meng, L.-Y. and Park, S.-J. (2013). Influence of carbon nanofibers on electrochemical properties of carbon nanofibers/glass fibers composites. *Current Applied Physics* 13: 640–644.

204 Kim, K.-S. and Park, S.-J. (2012). Electrochemical performance of graphene/carbon electrode contained well-balanced micro- and mesopores by activation-free method. *Electrochimica Acta* 65: 50–56.

205 Kim, K.-S. and Park, S.-J. (2012). Synthesis and electrochemical performance of well-balanced mesopore/micropore contained carbons by activation-free method. *Electrochemistry Communications* 22: 89–92.

206 De Volder, M.F.L., Tawfick, S.H., Baughman, R.H., and Hart, A.J. (2013). Carbon nanotubes: present and future commercial applications. *Science* 339: 535–539.

207 Li, L., Wu, G., Yang, G. et al. (2013). Focusing on luminescent graphene quantum dots: current status and future perspectives. *Nanoscale* 5: 4015–4039.

208 Min, Y., He, G., Li, R. et al. (2013). Doping nitrogen anion enhanced photocatalytic activity on TiO_2 hybridized with graphene composite under solar light. *Separation and Purification Technology* 106: 97–104.

209 Lee, S.-Y. and Park, S.-J. (2011). Preparation and characterization of ordered porous carbons for increasing hydrogen storage behaviors. *Journal of Solid State Chemistry* 184: 2655–2660.

210 Kim, K.-S. and Park, S.-J. (2012). High electrochemical performance of carbon black-bonded carbon nanotubes for electrode materials. *Materials Research Bulletin* 47: 4146–4150.

211 Park, S.-J., Jung, Y., and Kim, S. (2012). Effect of fluorine–oxygen mixed gas treated graphite fibers on electrochemical behaviors of platinum–ruthenium nanoparticles toward methanol oxidation. *Journal of Fluorine Chemistry* 144: 124–129.

212 Kim, S., Cho, M.-H., Lee, J.-R., and Park, S.-J. (2006). Influence of plasma treatment of carbon blacks on electrochemical activity of Pt/carbon blacks catalysts for DMFCs. *Journal of Power Sources* 159: 46–48.

213 Yang, N., Liu, Y., Wen, H. et al. (2013). Photocatalytic properties of graphdiyne and graphene modified TiO_2: from theory to experiment. *ACS Nano* 7: 1504–1512.

214 Ng, Y.H., Ikeda, S., Matsumura, M., and Amal, R. (2012). A perspective on fabricating carbon-based nanomaterials by photocatalysis and their applications. *Energy & Environmental Science* 5: 9307–9318.

215 Chu, D., Yuan, X., Qin, G. et al. (2008). Efficient carbon-doped nanostructured TiO_2 (anatase) film for photoelectrochemical solar cells. *Journal of Nanoparticle Research* 10: 357–363.

216 Brunet, L., Lyon, D.Y., Hotze, E.M. et al. (2009). Comparative photoactivity and antibacterial properties of C_{60} fullerenes and titanium dioxide nanoparticles. *Environmental Science and Technology* 43: 4355–4360.

217 Sigmund, W., Yuh, J., Park, H. et al. (2006). Processing and structure relationships in electrospinning of ceramic fiber systems. *Journal of the American Ceramic Society* 89: 395–407.

218 Woan, K., Pyrgiotakis, G., and Sigmund, W. (2009). Photocatalytic carbon-nanotube–TiO_2 composites. *Advanced Materials* 21: 2233–2239.

219 Lee, S.-Y. and Park, S.-J. (2013). TiO_2 photocatalyst for water treatment applications. *Journal of Industrial and Engineering Chemistry* 19: 1761–1769.

220 Ou, Y., Lin, J., Fang, S., and Liao, D. (2006). MWNT–TiO_2:Ni composite catalyst: a new class of catalyst for photocatalytic H_2 evolution from water under visible light illumination. *Chemical Physics Letters* 429: 199–203.

221 Akhavan, O., Abdolahad, M., Abdi, Y., and Mohajerzadeh, S. (2009). Synthesis of titania/carbon nanotube heterojunction arrays for photoinactivation of *E. coli* in visible light irradiation. *Carbon* 47: 3280–3287.

222 Chen, Y., Crittenden, J.C., Hackney, S. et al. (2005). Preparation of a novel TiO_2-based p–n junction nanotube photocatalyst. *Environmental Science and Technology* 39: 1201–1208.

223 Luo, Y., Heng, Y., Dai, X. et al. (2009). Preparation and photocatalytic ability of highly defective carbon nanotubes. *Journal of Solid State Chemistry* 182: 2521–2525.

224 Ewa, K. and Sven, R. (2010). Photoreactors for wastewater treatment: a review. *Recent Patents on Engineering* 4: 242–266.

225 Mozia, S. (2010). Photocatalytic membrane reactors (PMRs) in water and wastewater treatment. A review. *Separation and Purification Technology* 73: 71–91.

226 Matsunaga, T. and Inagaki, M. (2006). Carbon-coated anatase for oxidation of methylene blue and NO. *Applied Catalysis B: Environmental* 64: 9–12.

227 Ali, F., Khan, S.B., Kamal, T. et al. (2018). Chitosan-titanium oxide fibers supported zero-valent nanoparticles: highly efficient and easily retrievable catalyst for the removal of organic pollutants. *Scientific Reports* 8: 6260.

228 Rengifo-Herrera, J.A., Marín-Silva, D.A., Mendoza-Portillo, E. et al. (2018). Chitosan films containing TiO_2 nanoparticles modified with tungstophosphoric acid for the photobleaching of malachite green in solid-gas interfaces upon different wavelengths. *Molecular Catalysis* 448: 1–9.

229 Alinsafi, A., Khemis, M., Pons, M.N. et al. (2005). Electro-coagulation of reactive textile dyes and textile wastewater. *Chemical Engineering and Processing* 44: 461–470.

230 Vimonses, V., Lei, S., Jin, B. et al. (2009). Adsorption of congo red by three Australian kaolins. *Applied Clay Science* 43: 465–472.

231 Sial, R.A., Chaudhary, M.F., Abbas, S.T. et al. (2006). Quality of effluents from Hattar Industrial Estate. *Journal of Zhejiang University Science B* 7: 974–980.

232 Phiri, O., Mumba, P., Moyo, B.H.Z., and Kadewa, W. (2005). Assessment of the impact of industrial effluents on water quality of receiving rivers in urban areas of Malawi. *International Journal of Environmental Science and Technology* 2: 237–244.

233 Ahmad, M., Bajahlan, A.S., and Hammad, W.S. (2008). Industrial effluent quality, pollution monitoring and environmental management. *Environmental Monitoring and Assessment* 147: 297–306.

234 Oyekale, A.S. and Oyekale, T.O. (2017). Healthcare waste management practices and safety indicators in Nigeria. *BMC Public Health* 17: 740.

235 Ali, M. and Kuroiwa, C. (2009). Status and challenges of hospital solid waste management: case studies from Thailand, Pakistan, and Mongolia. *Journal of Material Cycles and Waste Management* 11: 251–257.

236 Emmanuel, E., Perrodin, Y., Keck, G. et al. (2005). Ecotoxicological risk assessment of hospital wastewater: a proposed framework for raw effluents discharging into urban sewer network. *Journal of Hazardous Materials* 117: 1–11.

237 Verlicchi, P., Galletti, A., Petrovic, M., and Barceló, D. (2010). Hospital effluents as a source of emerging pollutants: an overview of micropollutants and sustainable treatment options. *Journal of Hydrology* 389: 416–428.

238 Putschew, A., Wischnack, S., and Jekel, M. (2000). Occurrence of triiodinated X-ray contrast agents in the aquatic environment. *Science of the Total Environment* 255: 129–134.

239 Sacher, F., Lange, F.T., Brauch, H.J., and Blankenhorn, I. (2001). Pharmaceuticals in groundwaters analytical methods and results of a monitoring program in Baden-Wurttemberg, Germany. *Journal of Chromatography A* 938: 199–210.

240 Anderson, P.D., D'Aco, V.J., Shanahan, P. et al. (2004). Screening analysis of human pharmaceutical compounds in U.S. surface waters. *Environmental Science and Technology* 38: 838–849.

241 Šuligoj, A., Štangar, U.L., and Tušar, N.N. (2014). Photocatalytic air-cleaning using TiO_2 nanoparticles in porous silica substrate. *Chemical Papers* 68: 1265–1272.

242 Taranto, J., Frochot, D., and Pichat, P. (2009). Photocatalytic air purification: comparative efficacy and pressure drop of a TiO_2-coated thin mesh and a honeycomb monolith at high air velocities using a 0.4 m^3 close-loop reactor. *Separation and Purification Technology* 67: 187–193.

243 Tasbihi, M., Kete, M., Raichur, A.M. et al. (2012). Photocatalytic degradation of gaseous toluene by using immobilized titania/silica on aluminum sheets. *Environmental Science and Pollution Research* 19: 3735–3742.

244 Prieto, O., Fermoso, J., and Irusta, R. (2007). Photocatalytic degradation of toluene in air using a fluidized bed photoreactor. *International Journal of Photoenergy* 2007: 8.

245 Adams, M., Skillen, N., McCullagh, C., and Robertson, P.K.J. (2013). Development of a doped titania immobilised thin film multi tubular photoreactor. *Applied Catalysis B* 130–131: 99–105.

246 Tasbihi, M., Štangar, U.L., Černigoj, U., and Kogej, K. (2009). Low-temperature synthesis and characterization of anatase TiO_2 powders from inorganic precursors. *Photochemical & Photobiological Sciences* 8: 719–725.

247 Zita, J., Krýsa, J., Černigoj, U. et al. (2011). Photocatalytic properties of different TiO_2 thin films of various porosity and titania loading. *Catalysis Today* 161: 29–34.

248 Arıer, Ü.Ö.A. and Tepehan, F.Z. (2011). Influence of heat treatment on the particle size of nanobrookite TiO_2 thin films produced by sol–gel method. *Surface and Coatings Technology* 206: 37–42.

249 Folli, A., Pade, C., Hansen, T.B. et al. (2012). TiO_2 photocatalysis in cementitious systems: insights into self-cleaning and depollution chemistry. *Cement and Concrete Research* 42: 539–548.

250 Fu, P., Luan, Y., and Dai, X. (2004). Preparation of activated carbon fibers supported TiO_2 photocatalyst and evaluation of its photocatalytic reactivity. *Journal of Molecular Catalysis A* 221: 81–88.

251 Ye, S.-Y., Li, M.-B., Song, X.-L. et al. (2011). Enhanced photocatalytic decomposition of gaseous ozone in cold storage environments using a TiO_2/ACF film. *Chemical Engineering Journal* 167: 28–34.

252 Ye, S.-Y., Tian, Q.-M., Song, X.-L., and Luo, S.-C. (2009). Photoelectrocatalytic degradation of ethylene by a combination of TiO_2 and activated carbon felts. *Journal of Photochemistry and Photobiology A* 208: 27–35.

253 Chen, S.-Z., Zhang, P.-Y., Zhu, W.-P. et al. (2006). Deactivation of TiO_2 photocatalytic films loaded on aluminium: XPS and AFM analyses. *Applied Surface Science* 252: 7532–7538.

254 Novotna, P., Krysa, J., Maixner, J. et al. (2010). Photocatalytic activity of sol–gel TiO_2 thin films deposited on soda lime glass and soda lime

glass precoated with a SiO_2 layer. *Surface and Coatings Technology* 204: 2570–2575.

255 Černigoj, U., Štangar, U.L., Trebše, P. et al. (2006). Photocatalytically active TiO_2 thin films produced by surfactant-assisted sol–gel processing. *Thin Solid Films* 495: 327–332.

256 Zita, J., Krýsa, J., and Mills, A. (2009). Correlation of oxidative and reductive dye bleaching on TiO_2 photocatalyst films. *Journal of Photochemistry and Photobiology A* 203: 119–124.

257 Štangar, U.L., Černigoj, U., Trebše, P. et al. (2006). Photocatalytic TiO_2 coatings: effect of substrate and template. *Monatshefte für Chemie / Chemical Monthly* 137: 647–655.

258 Novotná, P., Zita, J., Krýsa, J. et al. (2008). Two-component transparent TiO_2/SiO_2 and TiO_2/PDMS films as efficient photocatalysts for environmental cleaning. *Applied Catalysis B* 79: 179–185.

259 Çamurlu, H.E., Kesmez, Ö., Burunkaya, E. et al. (2012). Sol–gel thin films with anti-reflective and self-cleaning properties. *Chemical Papers* 66: 461–471.

260 Yao, P., Liu, H., Wang, D. et al. (2018). Enhanced visible-light photocatalytic activity to volatile organic compounds degradation and deactivation resistance mechanism of titania confined inside a metal-organic framework. *Journal of Colloid and Interface Science* 522: 174–182.

261 Burton, A. (2012). Titanium dioxide photocleans polluted air. *Environmental Health Perspectives* 120 https://doi.org/10.1289/ehp.120-a229.

262 Le, T.S., Dao, T.H., Nguyen, D.C. et al. (2015). Air purification equipment combining a filter coated by silver nanoparticles with a nano-TiO_2 photocatalyst for use in hospitals. *Advances in Natural Sciences* 6: 015016.

263 Haider, A., Al-Anbari, R., Kadhim, G., and Jameel, Z. (2018). Synthesis and photocatalytic activity for TiO_2 nanoparticles as air purification. *MATEC Web of Conferences* 162: 05006.

264 Shah, S.N.A., Shah, Z., Hussain, M., and Khan, M. (2017). Hazardous effects of titanium dioxide nanoparticles in ecosystem. *Bioinorganic Chemistry and Applications* 2017: 12.

265 Baraton, M.-I. and Merhari, L. (2004). Surface chemistry of TiO_2 nanoparticles: influence on electrical and gas sensing properties. *Journal of the European Ceramic Society* 24: 1399–1404.

266 Liu, X., Chen, G., Keller, A.A., and Su, C. (2013). Effects of dominant material properties on the stability and transport of TiO_2 nanoparticles and carbon nanotubes in aquatic environments: from synthesis to fate. *Environmental Science* 15: 169–189.

267 Juhasz, G. (2018). Electrochemical properties of anatase-type TiO_2 nanoparticles with different morphology. *ECS Transactions* 85: 3–10.

268 Hou, Y., Abrams, B.L., Vesborg, P.C. et al. (2011). Bioinspired molecular co-catalysts bonded to a silicon photocathode for solar hydrogen evolution. *Nature Materials* 10: 434–438.

269 Paracchino, A., Laporte, V., Sivula, K. et al. (2011). Highly active oxide photocathode for photoelectrochemical water reduction. *Nature Materials* 10: 456–461.

270 Maeda, K., Xiong, A., Yoshinaga, T. et al. (2010). Photocatalytic overall water splitting promoted by two different cocatalysts for hydrogen and oxygen evolution under visible light. *Angewandte Chemie International Edition* 49: 4096–4099.

271 Kudo, A. and Miseki, Y. (2009). Heterogeneous photocatalyst materials for water splitting. *Chemical Society Reviews* 38: 253–278.

272 Liu, S., Yu, J., and Jaroniec, M. (2011). Anatase TiO_2 with dominant high-energy {001} facets: synthesis, properties, and applications. *Chemistry of Materials* 23: 4085–4093.

273 Yu, J., Qi, L., and Jaroniec, M. (2010). Hydrogen production by photocatalytic water splitting over Pt/TiO_2 nanosheets with exposed (001) facets. *The Journal of Physical Chemistry C* 114: 13118–13125.

274 Ksibi, M., Rossignol, S., Tatibouët, J.-M., and Trapalis, C. (2008). Synthesis and solid characterization of nitrogen and sulfur-doped TiO_2 photocatalysts active under near visible light. *Materials Letters* 62: 4204–4206.

275 Park, J.H., Kim, S., and Bard, A.J. (2006). Novel carbon-doped TiO_2 nanotube arrays with high aspect ratios for efficient solar water splitting. *Nano Letters* 6: 24–28.

276 Yu, J. and Ran, J. (2011). Facile preparation and enhanced photocatalytic H_2-production activity of $Cu(OH)_2$ cluster modified TiO_2. *Energy & Environmental Science* 4: 1364–1371.

277 Murdoch, M., Waterhouse, G.I., Nadeem, M.A. et al. (2011). The effect of gold loading and particle size on photocatalytic hydrogen production from ethanol over Au/TiO_2 nanoparticles. *Nature Chemistry* 3: 489–492.

278 Zuo, F., Wang, L., Wu, T. et al. (2010). Self-doped Ti^{3+} enhanced photocatalyst for hydrogen production under visible light. *Journal of the American Chemical Society* 132: 11856–11857.

279 Li, Y. and Zhang, J.Z. (2010). Hydrogen generation from photoelectrochemical water splitting based on nanomaterials. *Laser & Photonics Reviews* 4: 517–528.

280 Walter, M.G., Warren, E.L., McKone, J.R. et al. (2010). Solar water splitting cells. *Chemical Reviews* 110: 6446–6473.

281 Justicia, I., Ordejón, P., Canto, G. et al. (2002). Designed self-doped titanium oxide thin films for efficient visible-light photocatalysis. *Advanced Materials* 14: 1399–1402.

282 Asahi, R., Morikawa, T., Ohwaki, T. et al. (2001). Visible-light photocatalysis in nitrogen-doped titanium oxides. *Science* 293: 269–271.

283 Thompson, T.L. and Yates, J.T. (2006). Surface science studies of the photoactivation of TiO_2 - new photochemical processes. *Chemical Reviews* 106: 4428–4453.

284 Kim, H.G., Hwang, D.W., and Lee, J.S. (2004). An undoped, single-phase oxide photocatalyst working under visible light. *Journal of the American Chemical Society* 126: 8912–8913.

285 Chen, X., Shen, S., Guo, L., and Mao, S.S. (2010). Semiconductor-based photocatalytic hydrogen generation. *Chemical Reviews* 110: 6503–6570.

286 Wang, G., Wang, H., Ling, Y. et al. (2011). Hydrogen-treated TiO_2 nanowire arrays for photoelectrochemical water splitting. *Nano Letters* 11: 3026–3033.

287 Murphy, A.B., Barnes, P.R.F., Randeniya, L.K. et al. (2006). Efficiency of solar water splitting using semiconductor electrodes. *International Journal of Hydrogen Energy* 31: 1999–2017.

288 Bian, Z., Tachikawa, T., Zhang, P. et al. (2014). Au/TiO_2 superstructure-based plasmonic photocatalysts exhibiting efficient charge separation and unprecedented activity. *Journal of the American Chemical Society* 136: 458–465.

289 Crossland, E.J., Noel, N., Sivaram, V. et al. (2013). Mesoporous TiO_2 single crystals delivering enhanced mobility and optoelectronic device performance. *Nature* 495: 215–219.

290 Crepaldi, E.L., GJAA, S.-I., Grosso, D. et al. (2003). Controlled formation of highly organized mesoporous titania thin films: from mesostructured hybrids to mesoporous nanoanatase TiO_2. *Journal of the American Chemical Society* 125: 9770–9786.

291 Vivero-Escoto, J.L., Chiang, Y.D., Wu, K., and Yamauchi, Y. (2012). Recent progress in mesoporous titania materials: adjusting morphology for innovative applications. *Science and Technology of Advanced Materials* 13: 013003.

292 Zhou, W. and Fu, H. (2013). Mesoporous TiO_2: preparation, doping, and as a composite for photocatalysis. *ChemCatChem* 5: 885–894.

293 Li, W., Wu, Z., Wang, J. et al. (2014). A perspective on mesoporous TiO_2 materials. *Chemistry of Materials* 26: 287–298.

294 Joo, J.B., Zhang, Q., Dahl, M. et al. (2012). Control of the nanoscale crystallinity in mesoporous TiO_2 shells for enhanced photocatalytic activity. *Energy & Environmental Science* 5: 6321–6327.

295 Zhou, W., Sun, F., Pan, K. et al. (2011). Well-ordered large-pore mesoporous anatase TiO_2 with remarkably high thermal stability and improved crystallinity: preparation, characterization, and photocatalytic performance. *Advanced Functional Materials* 21: 1922–1930.

296 Liu, G., Zhao, Y., Sun, C. et al. (2008). Synergistic effects of B/N doping on the visible-light photocatalytic activity of mesoporous TiO_2. *Angewandte Chemie International Edition* 47: 4516–4520.

297 Li, H., Bian, Z., Zhu, J. et al. (2007). Mesoporous Au/TiO_2 nanocomposites with enhanced photocatalytic activity. *Journal of the American Chemical Society* 129: 4538–4539.

298 Zhang, R., Tu, B., and Zhao, D. (2010). Synthesis of highly stable and crystalline mesoporous anatase by using a simple surfactant sulfuric acid carbonization method. *Chemistry A European Journal* 16: 9977–9981.

299 Zhou, W., Li, W., Wang, J.-Q. et al. (2014). Ordered mesoporous black TiO_2 as highly efficient hydrogen evolution photocatalyst. *Journal of the American Chemical Society* 136: 9280–9283.

300 Xiang, Q., Yu, J., and Jaroniec, M. (2012). Synergetic effect of MoS_2 and graphene as cocatalysts for enhanced photocatalytic H_2 production activity of TiO_2 nanoparticles. *Journal of the American Chemical Society* 134: 6575–6578.

301 Hinnemann, B., Moses, P.G., Bonde, J. et al. (2005). Biomimetic hydrogen evolution: MoS_2 nanoparticles as catalyst for hydrogen evolution. *Journal of the American Chemical Society* 127: 5308–5309.

302 Li, Y., Wang, H., Xie, L. et al. (2011). MoS_2 nanoparticles grown on graphene: an advanced catalyst for the hydrogen evolution reaction. *Journal of the American Chemical Society* 133: 7296–7299.

303 Karunadasa, H.I., Montalvo, E., Sun, Y. et al. (2012). A molecular MoS_2 edge site mimic for catalytic hydrogen generation. *Science* 335: 698–702.

304 Bonde, J., Moses, P.G., Jaramillo, T.F. et al. (2009). Hydrogen evolution on nano-particulate transition metal sulfides. *Faraday Discussions* 140: 219–231.

305 Jaramillo, T.F., Jorgensen, K.P., Bonde, J. et al. (2007). Identification of active edge sites for electrochemical H_2 evolution from MoS_2 nanocatalysts. *Science* 317: 100–102.

306 Kanda, S., Akita, T., Fujishima, M., and Tada, H. (2011). Facile synthesis and catalytic activity of MoS_2/TiO_2 by a photodeposition-based technique and its oxidized derivative MoO_3/TiO_2 with a unique photochromism. *Journal of Colloid and Interface Science* 354: 607–610.

307 Zong, X., Yan, H., Wu, G. et al. (2008). Enhancement of photocatalytic H_2 evolution on CdS by loading MoS_2 as cocatalyst under visible light irradiation. *Journal of the American Chemical Society* 130: 7176–7177.

308 Xiang, Q., Yu, J., and Jaroniec, M. (2011). Enhanced photocatalytic H_2-production activity of graphene-modified titania nanosheets. *Nanoscale* 3: 3670–3678.

309 Lightcap, I.V., Kosel, T.H., and Kamat, P.V. (2010). Anchoring semiconductor and metal nanoparticles on a two-dimensional catalyst mat. Storing and shuttling electrons with reduced graphene oxide. *Nano Letters* 10: 577–583.

310 Liang, Y., Li, Y., Wang, H. et al. (2011). Co_3O_4 nanocrystals on graphene as a synergistic catalyst for oxygen reduction reaction. *Nature Materials* 10: 780–786.

311 Li, Q., Guo, B., Yu, J. et al. (2011). Highly efficient visible-light-driven photocatalytic hydrogen production of CdS-cluster-decorated graphene nanosheets. *Journal of the American Chemical Society* 133: 10878–10884.

312 Chen, H., Zhao, R., Wang, B. et al. (2017). The effects of orally administered Ag, TiO_2 and SiO_2 nanoparticles on gut microbiota composition and colitis induction in mice. *NanoImpact* 8: 80–88.

313 Singh, P.K., Jairath, G., and Ahlawat, S.S. (2016). Nanotechnology: a future tool to improve quality and safety in meat industry. *Journal of Food Science and Technology* 53: 1739–1749.

314 Sadeghi, R., Rodriguez, R.J., Yao, Y., and Kokini, J.L. (2017). Advances in nanotechnology as they pertain to food and agriculture: benefits and risks. *Annual Review of Food Science and Technology* 8: 467–492.

315 Jaroenworaluck, A., Sunsaneeyametha, W., Kosachan, N., and Stevens, R. (2006). Characteristics of silica-coated TiO_2 and its UV absorption for sunscreen cosmetic applications. *Surface and Interface Analysis* 38: 473–477.

316 Othman, S.H., Abd Salam, N.R., Zainal, N. et al. (2014). Antimicrobial activity of TiO_2 nanoparticle-coated film for potential food packaging applications. *International Journal of Photoenergy* 2014: 6.

317 Manesh, R.R., Grassi, G., Bergami, E. et al. (2018). Co-exposure to titanium dioxide nanoparticles does not affect cadmium toxicity in radish seeds (*Raphanus sativus*). *Ecotoxicology and Environmental Safety* 148: 359–366.

318 Feizi, H., Rezvani Moghaddam, P., Shahtahmassebi, N., and Fotovat, A. (2012). Impact of bulk and nanosized titanium dioxide (TiO_2) on wheat seed germination and seedling growth. *Biological Trace Element Research* 146: 101–106.

319 Dudefoi, W., Moniz, K., Allen-Vercoe, E. et al. (2017). Impact of food grade and nano-TiO_2 particles on a human intestinal community. *Food and Chemical Toxicology* 106: 242–249.

320 Lewicka, Z.A., Benedetto, A.F., Benoit, D.N. et al. (2011). The structure, composition, and dimensions of TiO_2 and ZnO nanomaterials in commercial sunscreens. *Journal of Nanoparticle Research* 13: 3607.

321 Lu, P.-J., Huang, S.-C., Chen, Y.-P. et al. (2015). Analysis of titanium dioxide and zinc oxide nanoparticles in cosmetics. *Journal of Food and Drug Analysis* 23: 587–594.

322 Labille, J., Feng, J., Botta, C. et al. (2010). Aging of TiO_2 nanocomposites used in sunscreen. Dispersion and fate of the degradation products in aqueous environment. *Environmental Pollution* 158: 3482–3489.

323 Wang, Y., Sun, C., Zhao, X. et al. (2016). The application of nano-TiO_2 photo semiconductors in agriculture. *Nanoscale Research Letters* 11: 529.

324 Higarashi, M.M. and Jardim, W.F. (2002). Remediation of pesticide contaminated soil using TiO_2 mediated by solar light. *Catalysis Today* 76: 201–207.

325 Robles-González, I.V., Fava, F., and Poggi-Varaldo, H.M. (2008). A review on slurry bioreactors for bioremediation of soils and sediments. *Microbial Cell Factories* 7: 5.

326 Tomei, M.C. and Daugulis, A.J. (2013). Ex situ bioremediation of contaminated soils: an overview of conventional and innovative technologies. *Critical Reviews in Environmental Science and Technology* 43: 2107–2139.

327 Kuyukina, M.S., Ivshina, I.B., Ritchkova, M.I. et al. (2003). Bioremediation of crude oil-contaminated soil using slurry-phase biological treatment and land farming techniques. *Soil and Sediment Contamination* 12: 85–99.

328 Nogueira, A.A., Bassin, J.P., Cerqueira, A.C., and Dezotti, M. (2016). Integration of biofiltration and advanced oxidation processes for tertiary treatment of an oil refinery wastewater aiming at water reuse. *Environmental Science and Pollution Research International* 23: 9730–9741.

329 Kyriacou, A., Lasaridi, K.E., Kotsou, M. et al. (2005). Combined bioremediation and advanced oxidation of green table olive processing wastewater. *Process Biochemistry* 40: 1401–1408.

330 Rubalcaba, A., Suarez-Ojeda, M.E., Stuber, F. et al. (2007). Phenol wastewater remediation: advanced oxidation processes coupled to a biological treatment. *Water Science and Technology* 55: 221–227.

331 Wang, A.N., Teng, Y., Hu, X.F. et al. (2016). Diphenylarsinic acid contaminated soil remediation by titanium dioxide (P25) photocatalysis: degradation pathway, optimization of operating parameters and effects of soil properties. *The Science of the Total Environment* 541: 348–355.

332 Wang, T.C., Lu, N., Li, J., and Wu, Y. (2011). Plasma-TiO_2 catalytic method for high-efficiency remediation of *p*-nitrophenol contaminated soil in pulsed discharge. *Environmental Science and Technology* 45: 9301–9307.

333 Uberoi, V. and Bhattacharya, S.K. (1997). Toxicity and degradability of nitrophenols in anaerobic systems. *Water Environment Research* 69: 146–156.

334 Zhao, Q., Liu, X., Sun, M. et al. (2015). Natural kaolin derived stable SBA-15 as a support for Fe/BiOCl: a novel and efficient Fenton-like catalyst for the degradation of 2-nitrophenol. *RSC Advances* 5: 36948–36956.

335 Ahmed, S., Rasul, M.G., Brown, R., and Hashib, M.A. (2011). Influence of parameters on the heterogeneous photocatalytic degradation of pesticides and phenolic contaminants in wastewater: a short review. *Journal of Environmental Management* 92: 311–330.

336 Dai, K., Peng, T., Chen, H. et al. (2008). Photocatalytic degradation and mineralization of commercial methamidophos in aqueous titania suspension. *Environmental Science and Technology* 42: 1505–1510.

337 Cao, Y., Yi, L., Huang, L. et al. (2006). Mechanism and pathways of chlorfenapyr photocatalytic degradation in aqueous suspension of TiO_2. *Environmental Science and Technology* 40: 3373–3377.

338 Parida, K.M., Sahu, N., Biswal, N.R. et al. (2008). Preparation, characterization, and photocatalytic activity of sulfate-modified titania for degradation of methyl orange under visible light. *Journal of Colloid and Interface Science* 318: 231–237.

339 Guan, H., Chi, D., Yu, J., and Li, X. (2008). A novel photodegradable insecticide: preparation, characterization and properties evaluation of nano-imidacloprid. *Pesticide Biochemistry and Physiology* 92: 83–91.

340 Ramos-Delgado, N.A., Gracia-Pinilla, M.A., Maya-Treviño, L. et al. (2013). Solar photocatalytic activity of TiO_2 modified with WO_3 on the degradation of an organophosphorus pesticide. *Journal of Hazardous Materials* 263: 36–44.

341 Leghari, S.A.K., Sajjad, S., Chen, F., and Zhang, J. (2011). WO_3/TiO_2 composite with morphology change via hydrothermal template-free route as an efficient visible light photocatalyst. *Chemical Engineering Journal* 166: 906–915.

342 Attarchi, N., Montazer, M., and Toliyat, T. (2013). $Ag/TiO_2/\beta$-CD nano composite: preparation and photo catalytic properties for methylene blue degradation. *Applied Catalysis A: General* 467: 107–116.

343 Zhang, X., Wu, F., Wang, Z. et al. (2009). Photocatalytic degradation of 4,4′-biphenol in TiO_2 suspension in the presence of cyclodextrins: a trinity integrated mechanism. *Journal of Molecular Catalysis A* 301: 134–139.

344 Affam, A.C. and Chaudhuri, M. (2013). Degradation of pesticides chlorpyrifos, cypermethrin and chlorothalonil in aqueous solution by TiO_2 photocatalysis. *Journal of Environmental Management* 130: 160–165.

345 Konstantinou, I.K., Sakellarides, T.M., Sakkas, V.A., and Albanis, T.A. (2001). Photocatalytic degradation of selected s-triazine herbicides and organophosphorus insecticides over aqueous TiO_2 suspensions. *Environmental Science and Technology* 35: 398–405.

346 Parra, S., Olivero, J., and Pulgarin, C. (2002). Relationships between physicochemical properties and photoreactivity of four biorecalcitrant phenylurea herbicides in aqueous TiO_2 suspension. *Applied Catalysis B* 36: 75–85.

347 Vulliet, E., Emmelin, C., Chovelon, J.-M. et al. (2002). Photocatalytic degradation of sulfonylurea herbicides in aqueous TiO_2. *Applied Catalysis B* 38: 127–137.

348 Ahmari, H., Zeinali Heris, S., and Hassanzadeh Khayyat, M. (2016). Photo catalytic degradation of linear alkylbenzene sulfonic acid. *Research on Chemical Intermediates* 42: 6587–6606.

349 Žabar, R., Komel, T., Fabjan, J. et al. (2012). Photocatalytic degradation with immobilised TiO_2 of three selected neonicotinoid insecticides: imidacloprid, thiamethoxam and clothianidin. *Chemosphere* 89: 293–301.

350 Malato, S., Caceres, J., Aguera, A. et al. (2001). Degradation of imidacloprid in water by photo-Fenton and TiO_2 photocatalysis at a solar pilot plant: a comparative study. *Environmental Science and Technology* 35: 4359–4366.

351 Agüera, A., Almansa, E., Malato, S. et al. (1998). Evaluation of photocatalytic degradation of imidacloprid in industrial water by GC-MS and LC-MS. *Analusis* 26: 245–250.

352 Siddle, G.R. (1975). The prospects for titanium dioxide in the paint industry. *Pigment & Resin Technology* 4: 4–12.

353 Larue, C., Castillo-Michel, H., Sobanska, S. et al. (2014). Fate of pristine TiO_2 nanoparticles and aged paint-containing TiO_2 nanoparticles in lettuce crop after foliar exposure. *Journal of Hazardous Materials* 273: 17–26.

354 Kaegi, R., Ulrich, A., Sinnet, B. et al. (2008). Synthetic TiO_2 nanoparticle emission from exterior facades into the aquatic environment. *Environmental Pollution* 156: 233–239.

355 Al-Kattan, A., Wichser, A., Zuin, S. et al. (2014). Behavior of TiO_2 released from nano-TiO_2-containing paint and comparison to pristine nano-TiO_2. *Environmental Science and Technology* 48: 6710–6718.

356 Tao, H., He, Y., and Zhao, X. (2015). Preparation and characterization of calcium carbonate–titanium dioxide core–shell ($CaCO_3$@TiO_2) nanoparticles and application in the papermaking industry. *Powder Technology* 283: 308–314.

357 Shen, J., Song, Z., Qian, X., and Liu, W. (2009). Modification of papermaking grade fillers: a brief review. 4: 20.

358 Shen, J., Song, Z., Qian, X., and Yang, F. (2010). Carboxymethyl cellulose/alum modified precipitated calcium carbonate fillers: preparation and their use in papermaking. *Carbohydrate Polymers* 81: 545–553.

359 Zhang, Y., Liu, Y., Ge, C. et al. (2009). Evolution mechanism of alumina nanofilms on rutile TiO_2 starting from sodium metaaluminate and the pigmentary properties. *Powder Technology* 192: 171–177.

360 Lu, Z., Ren, M., Yin, H. et al. (2009). Preparation of nanosized anatase TiO_2-coated kaolin composites and their pigmentary properties. *Powder Technology* 196: 122–125.

361 Amin, K.A.M. and Panhuis, M.I. (2012). Reinforced materials based on chitosan, TiO_2 and Ag composites. *Polymers* 4: 590–599.

362 Kavitha, K., Prabhu, M., Rajendran, V. et al. (2013). Optimization of nano-titania and titania–chitosan nanocomposite to enhance biocompatibility. *Current Nanoscience* 9: 308–317.

363 Akakuru, O.U., Louis, H., Uwaoma, R. et al. (2019). Novel highly-swellable and pH-responsive slow release formulations of clotrimazole with chitosan-g-PEG/starch microparticles. *Reactive and Functional Polymers* 135: 32–43.

364 Akakuru, O.U., Louis, H., Akakuru, O.C., and Eno, E.A. (2019). Facile fabrication of pH-responsive and swellable slow release microparticles of chlorpheniramine maleate with chitosan-starch matrices and their crosslinks. *International Journal of Polymeric Materials and Polymeric Biomaterials*: 1–15. https://doi.org/10.1080/00914037.2018.1563084.

365 Ariafar, A.A., Afsharpour, M., and Samanian, K. (2018). Use of TiO_2/chitosan nanoparticles for enhancing the preservative effects of carboxymethyl cellulose in paper-art-works against biodeterioration. *International Biodeterioration & Biodegradation* 131: 67–77.